Volume II
Appendix D.19

Qualification and Interpretation of Sensor Data from STS-107

This appendix provides a thorough review of the Modular Auxiliary Data System (MADS) recorder and sensor operation and an analysis of the data that was gathered from the MADS system and used during the investigation.

This appendix also contains several draft recommendations that were reviewed by the Board. Several of these were adopted and are included in their final form in Volume I. The conclusions drawn in this report do not necessarily reflect the conclusions of the Board; when there is a conflict, the statements in Volume I of the Columbia Accident Investigation Board Report take precedence.

THIS PAGE INTENTIONALLY LEFT BLANK

Qualification and Interpretation of Sensor Data from STS-107

Submitted by Prof. R. B. Darling, Ph.D., P.E.,
University of Washington, Department of Electrical Engineering, June 26, 2003

INTRODUCTION

The first indications of problems with the space shuttle orbiter *Columbia*, flight mission STS-107, during its re-entry on February 1, 2003, were provided by telemetry data that revealed numerous sensors on board the spacecraft had either malfunctioned or recorded a path of propagating destruction through the left wing areas. In the aftermath of the accident, during the ground search over Northern Texas, the OEX flight data recorder was recovered, miraculously intact, and it provided a wealth of additional sensor readings which have proven invaluable to reconstructing the events of the accident. In order to better understand the information provided by these two sources of data, and to provide practical working limits on the extent to which events can be inferred from them, an analysis of the sensor instrumentation systems on the *Columbia* and of the telemetry and recorded data that they provided was undertaken. This work was carried out under the direction of the independent Columbia Accident Investigation Board (CAIB) over the period of March 15 through June 15, 2003. Close support for this work was provided by the *Columbia* Task Force (CTF) at NASA which provided access to raw data, databases, briefings, technical specifications, and specific requests for information.

This report is organized into two main sections: first, an analytical description of the instrumentation system and its operational behavior, and second, an analysis of the unusual events and time correlations on the STS-107 mission. The description of the instrumentation systems follows the same order as the signal flow, starting with the various sensors themselves, proceeding though the wiring to the data acquisition hardware, onward to the data recorder or the telemetry communication links, and finally to the ground where the raw data is extracted and calibrated. The analysis of the anomalous events and time correlations first examines various groups of sensors within the telemetry data and then groups of sensors within the data that came from the OEX recorder. Finally, the report closes with some overall conclusions and recommendations.

As with all efforts to reconstruct a past series of events, numerous hypotheses are put forward to explain the circumstances. This report does not attempt to present any such hypothesis, nor to judge one as being more plausible than any other. Rather, the purpose of this report is to provide a factual basis upon which specific hypotheses can be anchored, and of equal importance, to limit the degree to which conclusions can be logically drawn. It is a natural tendency of human nature to find one minor fact and to over extend its implications. In the present case, there may be a tendency to take a one bit change from one sensor at one point in time and proclaim an entirely new scenario from it. While the one bit may support a new hypothesis, the remaining hundreds of sensors and thousands of time slices may not. In assessing the worth of various hypothetical scenarios for the *Columbia* accident, it is important to not use isolated fragments of the sensor data to support one or more pet hypotheses, but rather to use all of the sensor data collectively to uniformly critique all of the hypotheses. A single instrument does not convey the music of an orchestra, and the same is true for the sensor systems of the *Columbia*.

LINK-WISE ANALYSIS

SENSORS

Resistance-Temperature Detector (RTD) Temperature Sensors

These temperature sensors are described in drawing no. ME449-0160, which can be found in the Shuttle Drawing System (SDS) database. Ten different dash numbers are in use, -0001 through -0010, each comprising a chemically pure platinum (Pt) sensing element that is bonded onto an insulating carrier substrate. These sensors are designed to operate under normal conditions from –320°F to +500°F or up to +2000°F, depending upon the dash number. Each is configured with #30 gauge solid copper leads that are nickel plated and Teflon insulated. Higher temperature sensors have fiberglass insulation on the lead wires. The sensors are connected

by three leads, brown on one end for the (+) lead, and two white leads on the other end for (–) and ground. The sensors are designed to measure surface temperatures and are typically adhesively bonded onto the mechanical component to be measured, using either tape or RTV-560, a silicone rubber adhesive and potting compound. The lead wires from the sensor are connected to the main general purpose instrumentation wiring harnesses by means of crimp-type splices.

Platinum is a near-refractory metal and has a melting point of 1769°C (3216°F). Cold-drawn copper lead wires have a melting point of 1083°C (1981°F). Failure modes for the sensor would thus be most likely associated with debonding or adhesive release, rather than direct melting of the metallic electrical components. This depends greatly upon the specifics of each sensor installation, but should be consistent with their highest temperature of intended use.

Each sensor has a nominal resistance of 100±0.25 Ω at 0°C (32°F), except for a few which have nominal resistances of 500 and 1380 Ω. Self heating effects with up to 5 mW of electrical power produce less than 0.5°F rise in temperature. The thermal time constant for each of these sensors is less than 0.5 seconds due to their small thermal mass. A two-lead plus ground configuration is used to connect each RTD to the data acquisition system. Thus, the series resistance of the wiring harnesses does add directly to the net measured resistance of the RTD. However, 100 ft. of #24 gauge solid copper wire has a series resistance of only 2.567 Ω, and any fixed offset in nominal resistance is removed using the 0^{th} polynomial coefficient of the calibration curve. The temperature rise of the Pt sensing element produces an increase in its electrical resistance, given by the temperature coefficient of resistivity (TCR) of Pt that is $\alpha = 0.0039\ °C^{-1}$. Platinum is used for RTDs because its TCR remains fairly linear and stable over a wide temperature range. A temperature rise of 900°F = 500°C would thus change the resistance of a nominal 100 Ω Pt RTD to 295 Ω. The slight nonlinearity in the TCR versus temperature of Pt is modeled by the Callendar-Van Dusen equation. When this nonlinearity is taken in account, laboratory grade Pt RTDs can readily measure temperatures to an absolute accuracy of 0.01°C. This type of RTD and this type of nonlinear correction are not used on the Space Shuttle Orbiter (SSO) instrumentation. The inherent accuracy of the SSO Pt RTD systems is estimated to be 2-3°F. The RTD sensors were supplied by Rosemount, Minneapolis, MN, and by RdF Corporation, Hudson, NH. Rosemount has since been bought by BF Goodrich Aircraft Sensors Division. Both vendors supplied parts with serial number traceability.

Thermocouple (TC) Temperature Sensors

Thermocouple temperature sensors are described in drawing no. ME449-0204, and two different dash numbers are used. Type I (dash no. -0001) are chromel-alumel thermocouples, known in industry as Type-K, and are used to measure temperatures in the range of –250°F to +2300°F. Type II (dash no. -0002) are platinum alloy (87% Pt, 13% Rh)-platinum thermocouples, known in industry as Type-R, and are used to measure temperatures in the range of –65°F to +3000°F. Both types are welded beads between two wires of the different materials. The wire diameter is specified to be 0.010", which equivalent to #30 gauge. The two wires do not have any insulation, only short colored tape bands to indicate the lead polarity; yellow(+)/red(–) for type K; black(+)/red(–) for type R. The higher temperature capable Type-II (Type R) thermocouples are used for all temperature measurements on the lower outer skin of the wings and fuselage, the outer surface of the heat tiles. Bond line temperature measurements on the inner side of the heat tiles typically use the lower temperature capable Type-I (Type K) thermocouples. The total weight of each sensor is specified to be less than 0.2 ounces, so this will give the thermocouples a thermal time constant of less than one second. Thermocouples were supplied by Templine Co., Torrance, CA, and later by Tayco Engineering, Inc., Long Beach, CA. Both vendors supplied lot traceable calibration.

Chromel is a 80% Ni, 20% Cr alloy, also commonly known as nichrome, and has a melting point of 1400°C (2552°F). Alumel is a 96% Ni, 2% Mn, 2% Al alloy that is produced by the Hastelloy Company. Its melting point is approximately the same as for chromel. Both pure platinum and its rhodium alloy (87% Pt, 13% Rh) have approximately the same melting point of 1769°C (3216°F). All of the thermocouple metals have sufficiently high melting points that they should not have been destroyed by direct heating of the orbiter during re-entry. Each of the materials is also fairly inert so that chemical reactions with the hot gases impacting on the orbiter surfaces should not have caused any unusual etching or corrosion. Failure modes for the thermocouples would more likely arise from mechanical stresses which either broke the welds, wires, or splices, or which pinched the leads together to cause them to short at a location below the weld bead. If thermocouple wires short together downstream of the weld bead sensing point, the effect is simply to move the sensing point to the location of the short. If the short opens at a later time, the sensing point returns to the original weld bead.

The installation of the thermocouple temperature sensors on the outer surfaces of the heat tiles is a complex procedure. A chosen heat tile has an approximately 2" long slot cut into its center and the thermocouple lead wires are fed through with a needle such that the thermocouple weld bead lies coincident with the outer surface. The heat tile is then glazed in its usual manner, and the glazing seals the slot and encapsulates the thermocouple weld bead into the outer surface. On the underside of the heat tile, two small wells are cut into the tile in which insulated thermocouple extension wire is crimp spliced, and the two wells are then back filled with RTV-560. The tile is then mounted onto the orbiter surface in the usual manner with the two thermocouple extension wires running along the vehicle bond line, and out from the bottom edge of the heat tile. An adjacent heat tile is used as the location where the thermocouple extension wires are fed through a grommet into the interior of the vehicle. After the wires have been spliced together, the adjacent heat tile is mounted in the usual manner to close up the connections. About 12" of thermocouple wire runs directly along the bond line of the vehicle, sandwiched between the heat tile and the metal surface paneling. Once inside the vehicle, the thermocouple extension wire is crimp spliced to the thermocouple reference junction (TRJ). Although the grommet through the

metal surface paneling provides a smoothed edge, severe mechanical trauma to this point could cause the insulation on the thermocouple extension wire to be cut, shorting the thermocouple wires to the aluminum metal panel, the grommet, or to each other. Another failure mode is through direct mechanical abrasion or impact to the outer surface of the heat tile where the thermocouple weld bead is located. Past flight history on the OV-102 has indicated that these thermocouple installations have been quite robust with no direct failures from mechanical sources having been reported.

Direct heating of the thermocouple wires will increase their series resistance, similar to the effects in an RTD; however, the thermocouple has a low impedance of 25 Ω or less which works into a high impedance bridge circuit. Hence, heating effects which change the resistance of the wires have an insignificant effect on the measured reading. Thermocouples directly measure the temperature difference between two junctions, the sensing junction and the reference junction. For this reason, thermocouple extension wires are made of the same metals as the original wires themselves. The transition from these special metals to the copper of the wiring harnesses occurs at the thermocouple reference junction (TRJ). The signal voltage that appears between the two copper wires is termed the Seebeck voltage, and it is roughly proportional to the temperature difference between the two junctions and the Seebeck coefficient for the thermocouple pair. For Type K thermocouples, this relationship is fairly linear over a wide range; however, for Type R thermocouples, the relationship has a significant parabolic bow. Calibration for the Type K thermocouples is essentially first order (linear), while calibration for the Type R thermocouples is necessarily second order (parabolic). With this level of calibration, the temperature measurements produced by the thermocouple systems should have 5-7°F accuracy.

Thermocouple temperature transducers refer to a prepackaged thermocouple probe in which a bead-type thermocouple junction and its leads are encased in either a stainless steel or inconel sheath. The interior of the probe is filled with a MgO insulation. These are described in drawing no. ME449-0169. Ten different dash numbers are listed and correspond to different probe lengths (12, 20, and 36 inches), thermocouple types (K or R), sheath material (inconel, stainless steel, or Pt-Rh alloy), and connector fitting (none, pipe thread, or strain relief plate with Teflon sleeve). Type VI covering dash numbers -0008, -0009, and -0010, are assemblies with 3, 2, and 1 sheathed probes, respectively. The probes are collected together into a common connector shell, and each has pre-attached inconel mounting lugs welded to the probe sheath. All of the probes are ungrounded. Type K are specified for ±2°F accuracy; type R are specified for ±10°F accuracy. The fast responding types have thermal time constants of less than 0.1 seconds, while the others have thermal time constants of less than 5.0 seconds. Sensor resistance is specified to be less than 25 Ω with an insulation resistance of greater than 50 MΩ. Operating lifetime is specified to be greater than 5000 hours. These probes appear to be used rather infrequently in the orbiter and only for a few single-point specialized applications, such as the TPS and ambient gas temperature sensing in potentially explosive environments.

Standard Pressure Sensors

Standard low, medium, and high pressure sensors are described in drawing no. ME449-0177. A total of 129 different dash numbers are detailed; however, only two of these, -2101 and -2108 are absolute pressure sensors with a range of 0-15 psia, of the type that were used for OEX aerodynamic measurements on the wing outer surfaces. Both of these are rated as having a 25 psia proof pressure and a 45 psia burst pressure. All of the pressure sensors in this family are strain-gauge diaphragm types and consist of cylindrical metal housing with a threaded tubulation to connect to the pressure sensing port and a multi-pin connector on the other end from which the strain gauge bridge leads are connected into the instrumentation wiring harness. The great majority of all 129 of these sensors are absolute pressure sensors and have a sealed reference vacuum chamber on one side of the diaphragm. For a 0-15 psi absolute pressure sensor, the diaphragm is maximally deflected at sea level pressure of about 14.7 psi, and then becomes neutral (undeflected) as the absolute pressure drops to zero to match the sealed vacuum reference chamber. Each of the strain gauge bridges is excited by a +10.000±0.001 VDC regulated power supply and outputs a maximum signal of 30 mV at full scale deflection. The output impedance of the strain gauge bridge is nominally 2000 Ω. Most of these sensors were manufactured by Schlumberger, Statham Transducer Division, Oxnard, CA.

The pressure measurements recorded in the OEX data were aerodynamic measurements of absolute pressure on the R and L wings. The sensors for these measurements were installed according to six installation drawings: V070-192151, V070-192146, V070-192145, V070-192131, V070-192130, and V070-192134. All of these are 0-15 psia measurements, except for V070-192146 locations which are 0-16 psia measurements that are taken by miniature pressure sensors, described below. The pressure sensing ports were all located on either the center of a specific heat tile, or within the upper wing surface FRSI material. The installation of the pressure ports into the heat tiles was, like the thermocouple installations, rather complex. Each tile with a pressure measurement had a hole drilled through it and Pyrex or Vycor tube was press fitted into the tile to provide a sealed bore. The backside of the tile was milled out to provide a cavity for sealing the backside of the glass tube to a grommet in the metal bond-line skin. The tile was mounted using the usual RTV-560 and a special ring of RTV was created to form the gasket between the glass tube in the tile and the grommet in the metal bond line skin. On the inside of the wing metal skin, a port fitting block was installed into the wing at the time of the wing's manufacture that provided a connection point between the wing grommet and the tubulation of the pressure sensor that was screwed into the port block. The ports were arranged typically along constant Y planes of both wings to provide lateral pressure profiles across the wing versus time.

Of the 181 total aerodynamic absolute pressure measurements recorded in the MADS/OEX data, 55 of these were sensors that were known to be bad prior to the launch. These bad sensors were most likely the result of age and continued stress on the sealed vacuum reference chamber which would

introduce first an offset into the data, and later a permanent OSL condition, since the sensor was designed to measure diaphragm deflections in only one direction. The specifications for the pressure sensors note that they only have a 10 year shelf life, and the orbiter was over 22 years old. The age of the vehicle and the continual one atmosphere of static pressure against the diaphragm is probably responsible for the high fraction of these which went bad prior to the launch of STS-107. Failure modes for absolute pressure sensors are either a slow, gradual leak rate over time into the reference vacuum chamber, or a catastrophic leak which may immediately add a one atmosphere offset to the reading. In all cases, the sensor reads lower pressures as the reference vacuum chamber pressure increases due to leaks.

Miniature Pressure Sensors

The miniature pressure sensors are described in drawing no. ME449-0219. They consist of two types, a Type-I in which the pressure sensing port lies parallel to the body of the sensor, and a Type-II in which the pressure port is the axial end of a nozzle coming out of the body. There are 12 dash numbers, -0001 through -0006 are 0-15 through 0-20 psia range sensors of Type-I, and -0007 through -0012 are 0-15 through 0-20 psia range sensors of Type-II, respectively. All of these devices are excited by a +5.000±0.001 VDC regulated power supply and produce 15 mV full scale output from the strain gauge bridge. All four legs of the strain gauge bridge are contained within the body of the sensor and a temperature compensation module is also included, usually within the overall sensor body. These sensors are probably micromachined silicon strain gauges and diaphragms, due to their size, and were manufactured by Kulite Semiconductor Products, Ridgefield, NJ. These miniature pressure sensors were used mainly for the smaller installation areas within the FRSI material on the upper surface of each wing. All of these devices were 0-16 psia range sensors and are shown in installation drawing no. V070-192146. These devices were also absolute pressure sensors, so all of the preceding comments on the standard pressure sensors also apply to these. The Kulite pressure sensors are generally remarked to be more fragile than the larger Statham types.

Strain Gauge Sensors

The strain gauge sensors are described in drawing no. ME449-0141, and 40 different dash numbers are used to enumerate the many different geometrical permutations that are used. The strain gauges can be configured as single, double, or triple sensors, involving two, three, four, or six leads. Single devices measure uniaxial strain along only one direction. Double devices measure either coarse and fine uniaxial strain along one direction, or more commonly, biaxial strain along two orthogonal directions. Triple devices, sometimes known as strain gauge rosettes, have three devices oriented at 0°, 45°, and 90°, through which the two uniaxial strains can be directly measured, e.g. ε_x and ε_y, and the in-plane shear strain can then also be computed from the set of all three readings, e.g. τ_{xy}. Double and triple strain gauges can be recognized by their different measurement system IDs (MSID) having identical (X, Y, Z) coordinate locations on the vehicle, and are usually denoted by A,B or A,B,C suffixes.

The strain gauge itself is a thin-film metal serpentine pattern composed of either a nickel or copper alloy. The strain effectively changes only the geometrical aspect ratio of the equivalent resistor, not the resistivity of the thin film metal, so each strain gauge has a gauge factor that is very close to the theoretical ideal of 2.00, or equivalently, $\Delta R/R = 2.00*\varepsilon$. The great majority of the various dash numbers have a nominal resistance of R = 1000±0.8% Ω. The thin film metal serpentine pattern is printed onto a carrier material of either glass fiber reinforced epoxy-phenolic resin, or Q or E grades of polyimide film. Wires from each strain gauge element are crimp spliced into the instrumentation wiring harnesses and then run back to the central data acquisition system at which point they are handled by a special strain gauge signal conditioner (SGSC).

All of the strain gauges are specified to be self-temperature compensated (STC) types. This means that the strain gauge is configured for each measurement point so that the entire bridge circuit is located at the sensing site. Each resistor in the bridge is constructed in a similar manner and has the same nominal resistance; thus, each leg of the bridge will experience close to the same variations in temperature with resistance. The thin-film metal serpentine resistors will have, taken by themselves, TCRs in the range of 3500 to 4300 ppm/°C, similar to most metals. Balancing four of these together in a bridge reduces the overall TCR of the bridge to typically a few ppm/°C. The strain gauges are specified to be temperature compensated to better than 13 ppm/°F, 6 ppm/°F, and 0 ppm/°F. The "0 ppm/°F" is most likely interpreted to mean less than 0.5 ppm/°F. The Wheatstone bridge resistances are thus temperature compensated very closely; however, like any strain gauge, the gauge factor itself is not temperature compensated. Unlike a silicon resistor strain gauge, the metal film resistor strain gauges produce a gauge factor that is due to only geometrical changes rather than a combination of geometry and resistivity changes that a silicon resistor strain gauge would respond to. The gauge factor is specified to vary not more than 0.85% per 100°F over a temperature range of –200 to +500°F. For a metal film resistor strain gauge, the gauge factor is extremely temperature independent, and usually not a significant influence on the measurement. Due to the high heat that most of these sensors would have experienced during normal operation and during the accident, the effects of temperature on the strain gauges are of great importance to understanding and correctly interpreting the sensor data. The design of the strain gauge sensors appears to have reduced the temperature sensitivity to a negligible level, and the output from the strain gauges can safely be interpreted as actual mechanical strain, as opposed to a combination of strain and temperature effects on the sensor itself.

In terms of environmental ruggedness and reliability, the strain gauges are quite hearty. They are specified to have a shelf life of 5 years, isolation resistances of greater than 300 MΩ, specified operation over 10^{-10} torr to 15 psia, and remain capable of indicating strains over the range of ±10,000 μin/in (±1% elongation) over their full lifespan. Most measurements are designed to record over a range of ±1000 μin/in, and are thus well within the mechanical elasticity of the strain gauge itself. The specified temperature range for operation is –250 to +350°F. The strain gauges were originally

procured from Micro-Measurements, Raleigh, NC, but the vendor was later changed to Vishay, Measurements Group, Wendell, NC. Gauges are tracked by lot number, and each is supplied with a calibration curve of apparent strain over a temperature range of –300 to +500°F and gauge factor versus temperature over a temperature range of –200 to +500°F.

Piezoelectric and Low Frequency Accelerometers

Piezoelectric accelerometers are described in drawing no. ME449-0150. Six different dash numbers are described, -0001 for Type I, up through -0006 for Type VI. Types I, III, and V are compression types of nominally 2000 pF capacitance, while Types II, IV, and VI are ring shear types with nominal capacitances of 900 pF, 400 pF, and 770 pF. Types I, III, and V are packaged as a 5/8" hexagonal body that mounts on a #10-32 threaded stud. The bodies are roughly an inch tall. Type II have a 0.600" dia. × 0.350" tall cylindrical body. Type IV are a smaller 3/8" hexagonal body, and Type VI are 0.375" dia. × 0.220" tall cylindrical body. Each had a proprietary Endevco coaxial connector fitted to the body. The charge sensitivity for each of the six types is 11.5±0.4, 10.5±1.0, 11.5±0.4, 2.8±0.2, 11.5±0.5, and 3.071±0.180 pC/g at 100 Hz. The frequency response range of each of the six types is 20-2000, 2-50, 20-2000, 20-2000, 1.5-50, and 1.5-10 Hz. Transverse sensitivity is typically limited to 2-3% of the primary axis sensitivity. The response is linear with acceleration to within 1 % error. Each of the six types is specified to have a shelf life of 5 years and an operating service life of at least 2000 hours. These accelerometers were supplied by Endevco, San Juan Capistrano, CA, and were supplied with serial number traceability.

Linear, low-frequency accelerometers are described in drawing no. ME449-0163. Two dash numbers are described, -0001 and -0002; Type I have a temperature range of –65 to +250°F, and Type II have a temperature range of –400 to +350°F. The body is a 0.750" hex, 1.000" tall, and mounts with a ¼"-28/#10-32 threaded stud. A proprietary coaxial connector is fitted to one face of the hexagon base. These devices measure accelerations of 2 to 10 g over a frequency range of 1.5 to 50 Hz. The capacitance is nominally 1000 pF. Charge sensitivity is 11.5±0.2 pC/g at 50 Hz and an amplitude of ±10 g at 70±10°F. These accelerometers are also specified to have a shelf life of 5 years and an operational service life of at least 2000 hours. These accelerometers were supplied by Gulton Industries, Inc., Costa Mesa, CA, and were supplied with serial number traceability.

Both of these accelerometer types are used with a FDM signal conditioner to supply wide-band data measurements. Coaxial cable is run all the way from the sensor at its measurement location back to the FDM units which are housed in midbody bay 8, roughly bottom center in the fuselage, underneath the payload bay. These sensors do not share any power feeds with other sensors since they do not use a DC bias.

Proximity Switches

Proximity switches are described in drawing no. MC452-0124 and consist of three parts: a target piece, the sensor, and an electronics unit. The target is a thin piece of high permeability alloy, usually Hi-Mu 80, Moly Permalloy, or equivalent, typically about 1.0" × 0.5" × 0.05" in size, and mounted on the moving part of the mechanism whose position is to be sensed. The sensor is a small metal box with mounting lugs that contains two legs of a half bridge. The mating half bridge is contained inside the electronics unit and forms a reluctance bridge whose balance point is perturbed by the position of the target relative to the sensor. The electronics unit contains the mating half bridge, a differential amplifier which serves as a detector, a trigger and output driver circuit, a power supply and oscillator to excite the bridge, and several built-in test equipment (BITE) circuits to verify the operation of the system. The output is a discrete logic voltage, ON = +5.0±1.0 VDC and OFF = 0.0±0.5 VDC, with less than 20 μs rise and fall times. The electronics unit is powered by 115 VAC, single phase. The discrete output goes ON when the target enters the actuation envelope of the sensor, and the discrete output then goes OFF when the target leaves the deactuation envelope of the sensor. The deactuation envelope surrounds the actuation envelope to produce hysteresis in the operation of the proximity switch. The two legs of the bridge inside the sensor, Z_x and Z_a, are both inductors, whose mutual inductance is altered by the position of the target. The operation of this bridge circuit is similar to a linear variable differential transducer (LVDT).

Wiring

Wires

General purpose insulated electrical wire is described in drawing no. MP571-0086. Ten different dash numbers are listed which correspond to even wire gauges, -0001 being #26, and -0010 being #8. The greater majority of the wire used in the sensor instrumentation is -0002, #24 gauge, and is a stranded wire comprised of 19 strands of #36 gauge nickel plated copper wire. It is listed as having 30.10 Ω per 1000 ft. and a weight of 2.0 lbs. per 1000 ft. Each wire is wrapped with two oppositely spun layers of polyimide tape, each 1 mil thick with 0.1 mil coatings of FEP Teflon resin on both sides for lubrication during flexure. The outer insulation coating is 1 mil thick pigmented polyimide resin. For the -0002 #24 gauge wires, the insulation pigment is blue.

Each orbiter contains over 852,000 feet of wire with a weight of over 5,369 lbs. The OV-102 instrumentation load was heavier still, due to the extensive OEX sensor suite that was installed. Kapton insulation was used primarily because of its light weight (25% savings over conventional PVC insulation), size (50% smaller with no thick plastic jacket present), good chemical resistance, and thermal tolerance. However, Kapton has the disadvantage of being susceptible to splitting, cracking, and fraying when handled roughly or abraded. Most of the wiring damage recorded on the orbiter repair logs has been due to the wiring insulation getting mashed, cracked or split, or torn to cause a fault with the internal wires.

Cables

General purpose shielded and jacketed electrical cables are described in drawing nos. MP572-0310 through MP572-0316, for 1 to 7 conductors, respectively. Dash numbers

-0001 through -0006 correspond to wire gauges of #26 through #16, respectively, and match to the same dash numbers of the wire used for creating the cable. Each bundle of wires is wrapped in a braided shield composed of #38 gauge nickel plated copper strands providing at least 85% coverage of the wires contained inside. The shield is then jacketed with two wraps of oppositely spun polyimide tape, 1 mil thick with 0.1 mil of FEP Teflon resin on each side to provide flexure lubrication. Thermocouple extension cables are created using the same construction practice, except that the conductor metal is chosen to match that of the thermocouple being extended. For example, a MP572-0329-0001 thermocouple extension cable is the same as a MP572-0311-0002 wiring cable (2 conductor, #24 gauge), except that one of the wires is copper (MP571-0088-0001) and the other is copper alloy (MP571-0089-0001).

Cables of this type comprise the greater majority of the orbiter wiring. The long length runs from the sensors far out in the orbiter extremities to their signal conditioners in the central fuselage avionics bays add greatly to this sum. The RTD temperature sensors each used a shielded three-wire cable, MP572-0312, while the pressure sensors, strain gauges, and cables from the remotely placed thermocouple reference junctions (TRJs) each used a shielded four-wire cable, MP572-0313.

Splices

All splices are achieved using crimp type sleeves of four basic types: parallel splices (ME416-0030), butt splices (ME416-0031), solder sleeves (ME416-0032), and shielded cable splices (ME416-0034). Two dash numbers are used: -100X for the crew compartment and equipment bays, which are blue Kynar, and -200X for general use everywhere else, which are white Teflon. The shielded cable splices are used primarily for data buses and firing wires on pyrotechnic actuators. Installation practices are described in ML0303-0031 for splice and lug crimping, and in MA0113-304 for wire stripping.

The crimp sleeves appear to be constructed of a nickel alloy, and each is insulated with what appears to be a heat shrinkable polyolefin tubing. Splices are usually left free floating from the wiring harness with no tie wraps or other mechanical hold downs. Apparently, no solder is used anywhere within the wiring systems. The melting points of any solder joints are thus not a concern for the sensor instrumentation.

Connectors, Terminal Boards and Interface Panels

The large number of sensor cables are interconnected via high density multi-pin connectors, usually grouped together on specific interface panels which separate structural sections of the orbiter. The most commonly used are NLS connectors and are used for high density interconnections of 6, 13, 22, 37, 55, 66, 79, 100, or 128 contacts. These are described in NASA MSFC specification 40M38277. These are rated for use over the temperature range of –150°C to +200°C, although the hermetically sealed versions are derated to –100°C to +150°C. These connectors are circular, bayonet coupled, and designed for low outgassing. All of the contacts are size 22D. Smaller numbers of connections, from 3 to 61, with contacts of sizes 12 to 20, are handled by the NB connectors, described in 40M39569. A special version of these, the NBS connectors, have 2, 3, or 4 contacts, are used for pyrotechnic firing circuits, and are described in 40M38298. Another special version, the NC connectors, described in 40M38294, are used on cryogenic systems. All of these connectors have the same temperature ratings as the NLS connectors. Bayonet couplings are typically used for signals, while threaded couplings are used for power. Typical power connectors are described in drawing nos. ME414-0234 (receptacles) and ME414-0235 (plugs).

Grounding straps are used to interconnect frame components together into a low impedance ground network at most junctions between panels. This is achieved with uninsulated braid between crimped frame lugs. The Koropon paint is scraped away below each ground lug and a self-tapping screw is used to bite into the aluminum frame components. Each grounding lug is then coated with RTV-560 to exclude corrosion agents. Central point grounding is achieved though a network of terminal boards where ground leads and cable shields are collected. The terminal boards are described in drawing nos. ME417-0010, -0013, -0014, and -0015.

Multiple bulkhead mounted connectors are collected into interface panels between structural sections of the orbiter. The two most relevant ones are the LH wing interface panel #65, and the LH wheel well interface panel #67. Inside the LH wing box, panel #65 has 14 connectors feeding 5 cable harnesses, four running aft and one running forward. The harnesses are composed primarily of sensor instrumentation on the following connectors: run#1 aft: 65P107, 65P101, 65P113, and 65P115; run#2 aft: 65P123 and 65P121 (a dummy); run#3 aft: 65P109, 65P115, 65P119, 65P117, and 65P143; run#4 aft: 65P107, 65P141, 65P105, 65P103, and 65P111; and run#1 forward; 65P105 and 65P111. Inside the LH wheel well, panel #67 has 18 connectors feeding a large number of short harnesses that service the LH wheel hydraulic system. Panel #67 connectors include: P1, P3, P5, P7, P9, P11, P13, P15, P17, P19, P57, P63, P65, P79, P85, P87, and P89.

The insulating resin materials used in most mil-spec connectors, usually phenolics, provide good stability up to temperatures of 450-500°F, and sometimes higher. The insulating material and the connector pins are both protected by metal shells, making the electrical integrity of the connector typically much higher than that of its cable. Indeed, many electrical connectors were found in the orbiter ground debris, and most were still functional with the internal connectors intact.

Harnesses, Installation and Routing

Wires and cables are grouped together in a parallel lay fashion (without twisting or braiding) and bundled together into harnesses with spot ties. This is described in specifications MLO303-0013 and MLO303-0014. The spot ties are a waxed, woven lacing material that is hand tied around the harness bundle at each point and the ends clipped off short.

The harnesses are secured to the vehicle frame by PTFE Teflon tape, PTFE Teflon adhesive sheet, or TFE Teflon tape. Convoluted tubing and rubber extrusions are used to provide protection of the harnesses around sharp edges and turns. Harnesses involving only a few wires or cables are typically held in place with Teflon tape which is sometimes strengthened with a layer of red RTV-560. The heavy harnesses on OV-102 that contained hundreds of sensor wires were supported by metal cable clamps with rubber linings of up to a few inches in diameter. Close-out photographs of the wing box interior show this construction clearly.

Probable high temperature failure modes for the harness materials are release of the adhesive tapes, allowing the harness itself to wander, or burn-through of the spot ties, allowing individual wires or cables to move about. The metal cable clamps used on the more extensive sensor wiring of OV-102 should have in principle provided better high temperature survivability than the tape and string approach used in the later model orbiters.

Cable Burn Through Patterns

Analysis by the NASA *Columbia* Task Force (CTF) identified the failure mechanisms of many sensors as being a "propagating soft short," that is essentially a zone of insulation breakdown between two conductors of the cable that expands in both directions along its length, traveling away from the heat source along the temperature gradient caused by the thermal conductivity of the wires. Blow torch and oven testing of sample cable bundles showed that the conductor-to-conductor insulation resistance began to fall when the cable temperature rose to 1000°F, and then fell precipitously when the cable temperature rose to 1200°F. This testing also showed that shorting between conductors as a result of oven or torch heating was much more prevalent than the creation of open circuits. This is no great surprise since the melting point for the copper conductors is 1980°F, almost 1000°F higher, as would be required to simply melt away a conductor to create an open circuit. Most organic insulation materials degrade at elevated temperatures by reaction with available oxygen, and ultimately this leads to a black, carbonized composition which can become somewhat conductive and lead to gradual shorting of adjacent conductors. Simple heating, taken by itself, is generally far less of a degradation mechanism than the chemical reactions which can be brought into play by the available reactive compounds in the presence of that same heat.

It should be noted that the initial CTF cable testing was performed with a blow torch in air at atmospheric pressure (nominally 14.7 psia at sea level), and at the time for which the wiring in the orbiter appeared to be damaged, the atmospheric pressure surrounding the orbiter was just rising to less than 0.5 psia. With much less available oxygen, the degradation mechanism of the cables was undoubtedly different from what these sea-level blow torch tests attempted to reproduce. A reduced oxygen environment would tend to restrict the rate of the chemical process and extend the degradation time of a given cable. Some sensors exhibited decay times to off-scale low (OSL) that were over 200 seconds long, and this rather long time could possibly be caused by a restricted oxygen concentration. On the other hand, the momentum transfer of the impacting hot gas stream within the wing box could have acted to accelerate the breakdown of the insulation by direct mechanical erosion, somewhat counteracting the rate limiting by available oxygen. While the blow torch tests do produce some gas velocity, this is only a meager subsonic flow caused by the combustion pressure, and no where near the Mach 15-20 speeds of the air molecules impacting against the leading surfaces of the orbiter. The subsequent arc-jet testing of the cable harnesses much more closely approximated the conditions on the orbiter, although the arc-jet testing was still performed at atmospheric pressure.

Many of the sensor data, particularly those from the OEX/MADS recorder, also showed significant chatter and erratic readings, in many cases transitioning between off-scale high (OSH) and off-scale low (OSL) over an extended period. It was suggested that this might be caused by the hot gases entering the wing box having some degree of ionization, and the impact of these charged ions against the bare or partially insulated cables might create a significant electric current which would saturate the sensitive input amplifiers of the signal conditioners. However, Fig. 4.12 on p. 114 of W. L. Hankley, Re-Entry Aerodynamics, AIAA Education Series, 1988, shows that at an altitude of 200,000 ft and a velocity of 15,000 ft/sec, oxygen is well over 90% dissociated, nitrogen is slightly less than 10% dissociated, and the overall degree of ionization is less than a few percent at most. Hence, ionization related effects such as conductor charging are not likely to be very substantive under these conditions.

What is of perhaps greater importance, is the noted high fraction of dissociated oxygen. Free monoatomic oxygen (O) is an extremely reactive species, far more combustive and reactive than molecular oxygen (O_2). It is very probable that the monoatomic oxygen would cause a much faster degradation of the Kapton insulation for a given temperature, or equivalently, would produce the same damage at much lower temperature. The drastically increased erosion rates of Kapton insulation by monoatomic oxygen are well documented, and were first studied in detail following shuttle mission STS-03 (L. J. Leger, AIAA paper no. AIAA-83-0073, 1983). Typical erosion rates for a low Earth orbit (LEO) environment are $0.01\text{-}0.09 \times 10^{-24}$ cm^3 per incident oxygen atom for aluminum coated Kapton. The best data on monoatomic oxygen exposure is probably that taken from the NASA long duration exposure facility (LDEF) which spent 5.8 years in LEO and which was retrieved in 1990.

Thus, there is great deal of uncertainty about the specific conditions within the wing box that surrounded the burn through of the sensor cabling. In particular, one important question is the degree to which the incoming hot gas was focused into a directional jet, broadly dispersed, or somewhere in between. Some conditions could be pointed to as ones which would increase the burn through time, while there are others that would just as easily have shortened it. The particulars of where a specific cable resided within the harness would also have a significant effect on its burn through speed, with those directly exposed on the periphery going quickly and those concealed within the center holding out for lon-

ger. While the sensor instrumentation system of the orbiter provides an extremely precise time referenced recording of the electrical anomalies, there still exists quite a bit of time uncertainty associated with the physical events which may have prompted the electrical ones when a cabling fault is at cause. A sensor reading may show a wire burn through signature that abruptly transitions to an off-scale limit at a clearly delineated moment in time, but the burn through process of that particular pair of wires could have begun anywhere from 2 to 200 seconds prior, to cite the extremes.

Nonetheless, with the degradation temperature of Kapton insulation in the range of 1000 to 1200°F and the melting point of copper at 1980°F, the failure mode of a cable will involve first a loss of insulation resistance and then a loss of conductor integrity. Simply put, a cable that is subjected to heating or combustion should first develop short circuits between the conductors at roughly 1000°F, and then open circuits only after the individual conductors melt away at roughly 2000°F. This ordering of "shorts before opens" is also true for a bundle of wires that is mechanically mashed, torn, or sheared, and one of the largely unwritten rules of electrical engineering. Temperatures of only 1000-1200°F are all that is required to produce shorting cable faults, and these would be largely indistinguishable from purely mechanical insults which would produce the same electrical effects. So why is there the nearly universal presumption that all of the sensor cables burned through, rather than being mechanically torn apart? For many the justification is quite clear, since there was a temperature sensor in the immediate vicinity which recorded rapidly increasing temperatures. This was clearly the case for the four key sensors behind the damaged leading edge area of the left wing.

Wiring Faults and Failure Modes for Bridge Type Transducers

One of the most distinctive features of the instrumentation vintage used on the space shuttle orbiters is the prevalent use of Wheatstone bridge transducer circuits. A four-resistor Wheatstone bridge is used with each pressure sensor, with each strain gauge, with each thermocouple reference junction, and with each RTD temperature sensor. In the case of the pressure sensors and strain gauges, all four legs of the bridge are within the sensor itself. The thermocouple reference junction contains all four legs of the bridge to which the thermocouple Seebeck voltage is added. The RTD temperature sensors are one leg of a bridge and the remaining three legs are contained in the bridge completion circuit which is part of the central data acquisition system.

The four resistor legs of a Wheatstone bridge form a square, and the bridge is excited by a DC voltage that is applied across two opposite corners of the square, labeled EXC+ and EXC–. The signal output from the bridge is taken from the other two opposite corners of the square and labeled SIG+ and SIG–. Any bundle of N independent wires will produce N possible open circuit and (N – 1)! possible short circuit single wiring faults. Discounting the shield, the four wire cables used for most of the bridge type transducers create 4 open circuit and 6 short circuit single wiring faults. Multiple wiring faults, those involving multiple combinations of shorts and opens, are increasingly complicated to diagnose, but by in large, most cable faults begin with a single wiring fault and then progress from there.

When the resistance ratios on both sides of the bridge are equal, the SIG+ and SIG– nodes will be at the same potential, and the difference between these two nodes, which is what is measured by each of the various signal conditioners, is zero. The physical quantity that each sensor measures causes a deviation away from this balanced condition of the bridge and a difference in potential is produced between the SIG+ and SIG– nodes, which is amplified by the signal conditioners and passed on for digital processing, recording, and transmission by the remainder of the instrumentation avionics.

Various wiring faults can create specific trends in the recorded data, depending upon how the specific signal conditioner reacts to them. For example, if the EXC+ wire happens to short to the SIG+ wire, the SIG+ node is immediately pulled up to the positive DC power supply voltage and the large positive difference between the SIG+ and SIG– nodes creates an off-scale high (OSH) output, essentially saturating at the highest possible value within the input range of the signal conditioner. Similarly, shorting the EXC– wire to the SIG– wire would pull the SIG– node down to the negative power supply voltage and produce the same effect of an OSH. The opposite pairings of a short between EXC+ and SIG– and between EXC– and SIG+ would both produce the opposite off-scale low (OSL) reading from the signal conditioner. These four shorts between adjacent wires of the Wheatstone bridge produce the same patterns of OSH and OSL for all of the different signal conditioners, since the voltages remain well-defined on all four nodes of the bridge.

A symmetrical short between the SIG+ and SIG– nodes clearly produces zero potential difference between the nodes, but this does not necessarily produce a zero reading for the sensor. If the 4-wire cable went to a strain gauge signal conditioner (SGSC), then the input differential amplifier of this unit would have an input of zero and the output would be taken to the level set by the adjusted offset level of the differential amplifier. Each SGSC has a potentiometer screw adjustment to zero out its own offset against that of its sensor, but when the input is shorted, only the adjusted offset of the differential amplifier remains. The recorded output of the shorted sensor is then just the offset level of the differential amplifier, which can be quite some distance away from zero. However, for other signal conditioners, most notably those in the MADS PCM units, to be described shortly, there is no offset adjustment on the differential amplifier and for them, a shorted input creates a off-scale low (OSL) condition, due to the required bias currents of the differential amplifier being no longer supplied by the sensor.

The situation for open circuit wiring faults is more complex still and highly dependent upon the particular characteristics of the differential amplifier of the signal conditioner. When an open circuit occurs, that particular node then floats and the potential that it comes to rest at depends upon the resulting voltage division between whatever internal components are left on the high impedance nodes of the differential amplifier. Without detailed knowledge about the input dif-

ferential amplifier of each signal conditioner, it is nearly impossible to determine with certainty what will happen to the resulting sensor reading. The NASA CTF performed a matrix of tests on each of the sensor types and their possible configurations to determine what would happen for each of the possible single wiring faults. The results ended up being quite different for the different types of signal conditioners and sensor configurations.

Interestingly, the rather important case of a short between EXC+ and EXC– was omitted for all but the thermocouple reference junction (TRJ). For the TRJ, a short between EXC+ and EXC– resulted in simply an offset output, since for the thermocouple, turning off the TRJ simply feeds the un-referenced Seebeck voltage directly to the differential amplifier input. The importance of the case of a EXC+ to EXC– short is that it is central to the common coupling that can exist between several sensors that are each fed by a single DC power supply, as will be discussed later. The design of the instrumentation suggests that the response to a short between EXC+ and EXC– will also vary with the type of signal conditioner and sensor configuration. The lack of complete testing of this wiring fault makes the arguments regarding power supply coupling between simultaneously failing sensors somewhat less conclusive, but certainly not invalid.

One important conclusion from the analysis of the wiring faults for these bridge circuit transducers is that a short circuit can produce any of the three most often seen failure signatures, a jump to OSH, a jump to OSL, or a simple jump up or down to the offset level adjustment of the differential amplifier of the signal conditioner, depending upon which specific pair of wires the short circuit connects. The converse of this is also true, if a sensor reading shows none of the above failure tends, then none of the possible 4 opens or 6 shorts could have occurred. All wiring faults create an abrupt and clearly defined jump in the associated sensor reading.

Data Acquisition

Block Diagram Overview of Instrumentation Avionics

The orbiter flight instrumentation (OFI) is designed to monitor those sensors and systems which are involved with the real-time operational command of the vehicle and its mission. The OFI system collects the analog signals from a variety of physical sensors as well as digital logic signals which give the status of various vehicle functions. This diversity of input signals is put into a common format by the dedicated signal conditioners (DSCs) which are distributed throughout the vehicle's fuselage. Some sensors require more specialized signal conditioning, such as the strain gauges, and strain gauge signal conditioners (SGSCs) are also distributed within the vehicle avionics bays to accomplish this. The conditioned signals from the DSC and SGSC units are collected by seven multiplexer-demultiplexers (MDMs) which perform analog-to-digital conversion, buffer the converted data, and respond to transactions on the orbiter instrumentation (OI) data bus. The MDMs can also route commands from the OI bus to various subsystems in the vehicle. All of the OFI data is centrally handled by the pulse-code-modulation master unit (PCMMU), which converts the raw binary data into a digital pulse code modulated (PCM) format, and combines and organizes the digital data from all of the sensors into a one-second long major data frame, using time division multiplexing (TDM). Time stamps generated by the master timing unit (MTU) are also added to each data frame by the PCMMU. The network signal processor (NSP) routes the data frame to either the S-band or Ku-band communications transceivers for transmission back to the mission control center (MCC) back on the ground, or to a reel-to-reel tape recorder for permanent storage. The communications transceivers also receive commands from the MCC on the ground and pass them to the general purpose computers (GPCs) on the orbiter for processing and execution. A simplified block diagram of the OFI system is shown in Figure 1.

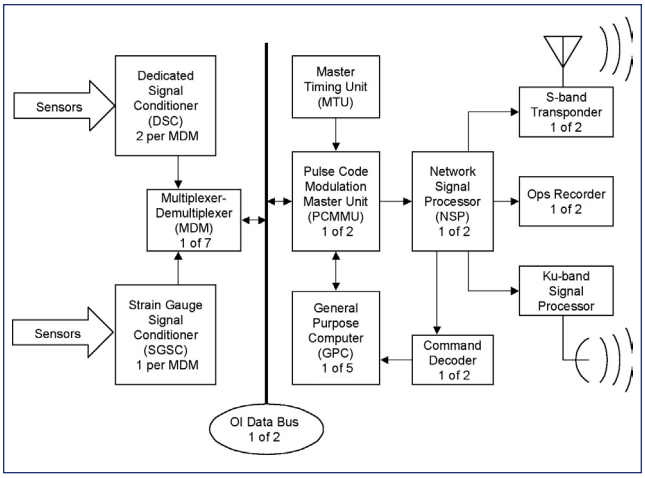

Figure 1. Operational Flight Instrumentation (OFI).

The modular auxiliary data system (MADS) is a supplemental instrumentation system that gathers vehicle flight data for processing after the mission is completed. Sensor inputs to the MADS system are almost exclusively physical sensor readings of temperature, pressure, mechanical strain, acceleration, or vibration. Sensors whose outputs vary comparatively slowly with time, such as temperature, pressure, and strain, are first signal conditioned by either thermocouple reference junctions (TRJs), strain gauge signal conditioners (SGSCs), or by the input circuits of one of the three pulse-code modulation (PCM) units. The PCM units perform analogous functions to what the MDMs and PCMMU do for the OFI system, performing analog-to-digital conversion of each sensor input, converting the raw binary data to pulse code modulation format, and combining all of the sensor readings into a time-stamped time-division-multiplexed frame of data. Sensors whose outputs vary rapidly with time, such as acceleration and vibration, are signal conditioned by wide band signal conditioners (WBSGs), and their data is collected by one of two frequency division multiplexers (FDMs). The FDMs modulate each input channel at different frequencies to combine the data into a single high-bandwidth track. Finally, the outputs from the three PCMs and two FDMs are routed to the appropriate tracks on a reel-to-reel tape recorder for playback once the vehicle is back on the ground. The MADS system is itself controlled by commands sent to it through the OFI system.

The orbiter experiment instrumentation (OEX) is an expanded suite of sensors for the MADS that was installed on the *Columbia* expressly for the purpose of engineering development. Since the *Columbia* was the first space shuttle orbiter to be launched, the engineering teams needed a means to gather more detailed flight data to validate their calculations of the conditions that the vehicle would experience during the critical flight phases of the mission. The voluminous data generated by the OEX suite required the installation of a particularly high capacity reel-to-reel tape recorder, known as the OEX recorder. The three flight phases of ascent, de-orbit, and re-entry are each recorded on chosen tracks of the OEX recorder. A simplified block diagram of the MADS/OEX system is shown in Figure 2.

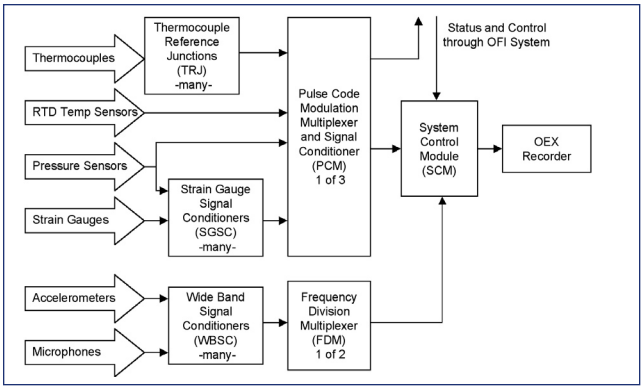

Figure 2. Modular Auxiliary Data System (MADS) and Orbiter Experimental Instrumentation (OEX).

Dedicated Signal Conditioners (DSC)

Fourteen DSC units were on *Columbia*, two for each of the seven multiplexer-demultiplexer (MDM) units, and all located within the fuselage. These were designated as follows: OF1, OF2, and OF3 were located in forward bays 1, 2, and 3, respectively. OF4 was a half-box located forward to support the Reaction Control System (RCS). OM1, OM2, and OM3 were located mid-body. OA1, OA2, and OA3 were located in aft bays 4, 5, and 6. OL1 and OL2 were both half boxes supporting the left Orbital Maneuvering System (OMS), and OR1 and OR2 were similarly half boxes supporting the right OMS. The DSC units could be configured with a variety of plug-in boards to support the measurements that they handled. The DSC units provided the majority of the front-end sensor signal conditioning for the OFI systems, serving much the same role as what the PCM units played for the OEX/MADS systems.

Each DSC consists of a chassis-mother interconnect board (CMIB) or backplane, which is described in drawing no. MC476-0147, a power supply module, a built-in test equipment (BITE) module, and up to 10, 15, or 30 plug-in cards that handle 3 or 4 measurement channels, each with a common power supply for the amplifiers and transducer excitation. The various types of plug-in cards include: a 3-channel pulse to DC converter for variable pulse rate transducers, a 4-channel resistance to DC converter for temperature transducers, a 4-channel AC to DC converter for AC signal transducers, a 4-channel discrete AC voltage converter for AC event voltages, a 4-channel 5 VDC discrete buffer for DC event voltages, a 4-channel DC amplifier-buffer-attenuator for internal DC signal transducers (such as potentiometers), and a 4-channel DC amplifier-buffer-attenuator for external DC signal transducers. The overall organization of the DSC units is best described in the Space Shuttle Systems Handbook, Section 17 (Instrumentation), drawing no. 17.1. The "channelization" of a particular measurement refers to which channel of a particular plug-in card, which card of the DSC, and which DSC through which a certain measurement is routed.

Strain Gauge Signal Conditioners (SGSC)

The Strain Gauge Signal Conditioners (SGSC) are described in drawing no. MC476-0134, and were manufactured by Rockwell International Space Division. The SGSCs are used in both the OFI and MADS/OEX instrumentation systems. There are 47 different dash numbers corresponding to different nominal bridge resistances (350 Ω or 1000 Ω), bridge types (full or half), excitation voltage (+10 VDC or +20 VDC), and gain range. Gain ranges vary from 10-50 up to 150-625. Each unit operates on +28 VDC power, and returns a conditioned signal in the range of 0 to +5 Volts. Typically, four strain gauge channels are combined into a single unit with a common power supply feed and overall dimensions of 3.000" wide × 3.500" long × 1.620" high. Each channel has potentiometer adjustments for gain, coarse offset, and fine offset. For half-bridge strain gauges, the remaining two resistors (R3 and R4) are contained within the SGSC along with a differential amplifier. For full-bridge strain gauges, the SGSC contains only the differential amplifier. A quarter-bridge system was also added in which the SGSC contains the three resistors (R1, R2, & R3) for the Bridge Completion Network (BCN) and the differential amplifier. Quarter-bridge strain gauges are set up with three leads (signal high, signal low, and power low) to balance the voltage drop of the excitation return current. The frequency response of the differential amplifier is flat from DC to 7 kHz and rolls off at –40 dB/decade, although only a 50-200 Hz –3 dB bandwidth is required for the application. Typical input signals range from 8 to 500 mV. Input impedance to the differential amplifier is specified to be greater than 9000 Ω, with an output impedance of less than 500 Ω. The Common-Mode Rejection Ratio (CMRR) is specified to be at least 70 dB at a voltage gain of 20 and at least 90 dB at a voltage gain of 200. Electrical isolation is specified to be at least 50 MΩ for power to signal and for circuit to case. Overall linearity, repeatability, and hysteresis is specified to be better than 0.1% from the best straight line. The specified minimum operating life of the SGSC is 5000 hours.

Inside each SGSC is a regulated power supply on a printed circuit board (#600356) that takes the +28 VDC input, passes it through an EMI filter, then a preregulator module, and then a DC-to-DC (buck) converter to provide a raw stepped-down DC voltage for two different linear regulators. One of these linear regulators provides the DC power supply for each of the four-channel differential amplifiers, and the other provides the DC excitation voltage for the strain gauge bridges. The preregulator module is actually a

separate printed circuit board (#600383). Each channel of the four-channel differential amplifier modules (#600355) takes the strain gauge input signal, completes the bridge if necessary with additional bridge resistors, and then amplifies the signal through a differential amplifier, rejecting the common-mode signal. The output is passed through an active filter and then a clipper to limit its amplitude. Most commonly, a given strain gauge is excited and amplified by the same SGSC unit, so that the excitation power supply and the differential amplifier module remain paired. There are a few exceptions where the excitation power supply is used to power the strain gauge bridge inside a pressure sensor.

Thermocouple Reference Junctions (TRJ)

The Thermocouple Reference Junctions (TRJ) are described in drawing no. MC476-0133 and were manufactured by Rockwell International Space Division. The thermocouple extension wires which are used to connect the thermocouple leads to the TRJs are described in drawing nos. MP572-0278 for Type K and MP572-0329 for Type SX. As a side note, Type SX is copper and a copper alloy known as Constantan (55% Cu, 45% Ni) which provides the same thermoelectric properties as a Type R Pt/Pt:Rh thermocouple, but with greater flexibility for wire routing and less high temperature capability. The thermocouple reference junctions are either a Type-I single channel or a Type-II 10-channel, and are small rectangular metal packages with mounting lugs which are fastened to the inner structural surface of the wing or fuselage, usually within a few feet of the thermocouple sensing junction. The TRJ utilize a Wheatstone bridge arrangement in which the thermocouple is balanced against an adjustable leg to establish the reference temperature for the measurement. There are six classes of the TRJs: class-1 is a chromel/alumel reference junction at 0°F; class-2 is a chromel/alumel reference junction at 500°F; class-3 is a Pt/Pt:Rh reference junction at 0°F; class-4 is a W:Re/W reference junction at –100°F; class-5 is a Pt/Pt:Rh reference junction at 500°F; and class-6 contains both a class-2 and class-3 reference junction in the same package. Different combinations of type and class produce 11 different dash numbers. The bridge is powered by +5.0 VDC power and ground wires that are routed from the data acquisition system (DAQ). Two wires connect the thermocouple to the TRJ, and then four wires connect the TRJ back to the DAQ. While thermocouple junctions generate their own thermoelectric voltage, the TRJ in this instance runs off of +5.0 VDC power. A drop in the power to the TRJ will have the effect of setting the output signal voltage to zero, resulting in a recorded temperature at the off-scale low (OSL) level. Because of the presence of the +5.0 VDC voltage in the same cable, a short between the +5.0 VDC wire and one signal return wire will create an OSL, while a short between the +5.0 VDC wire and the other signal return wire will create an off-scale high (OSH) reading. This latter situation is less probable, since it can occur in only the manner described, whereas an OSL reading can be created by roughly 15 other types of wiring faults. The response time for the TRJs is specified to be no more than 10 milliseconds. Each TRJ is factory calibrated; there are no adjustments on the units themselves. The TRJs are interconnected to the thermocouple extension wires and the general purpose instrumentation harness wiring with crimp splices.

Wide-Band Signal Conditioners (WBSC)

The Wide-Band Signal Conditioners (WBSC) are described in drawing no. MC476-0132 and were manufactured by Rockwell International Space Division. There are 57 different dash numbers of 6 types, corresponding to different frequency ranges, input vibration levels, transducer sensitivities, and amplifier gain ranges. Each are designed to work with piezoelectric transducers and consist of charge amplifiers with overall gains in the ranges of 0.4-2.4 to 50-150 mV/pC (millivolts per picocoulomb). Transducer sensitivities are typically 2.8, 8.0, 11.5, and 12.0 pC/G. Input vibration levels range from ±2 G to ±100 G, and frequency response varies from 2-50 Hz up to 20-8000 Hz. Each is powered by +28 VDC. The inputs from several WBSCs are combined in a Frequency Division Multiplexer (FDM) unit. The WBSCs consist of a small rectangular metal box with mounting lugs, 2.300" wide × 2.250" long × 1.250" high. Coax is used to connect the transducer to the WBSC.

OFI Multiplexer-Demultiplexer (MDM) Units and Instrumentation Data Buses

The Multiplexer-Demultiplexer (MDM) units collect the conditioned analog sensor signals from the Dedicated Signal Conditioners (DSCs), perform an analog-to-digital conversion, and create a Pulse Code Modulated (PCM) digital output that can be sent to the Pulse Code Modulation Master Unit (PCMMU) by way of the Operational Instrumentation (OI) data bus. Analog inputs to the analog-to-digital converters (ADCs) are always signal conditioned to lie within the range of –5.12 V to +5.11 V. A 10-bit conversion is performed so that the digital output is always 10 mV per count. A 10-bit twos complement digital output is produced for each measurement. This assigns a digital output of 0000000000 to a 0.00 V input, 0111111111 to a +5.11 V input, 1000000000 to a –5.12 V input, and 1111111111 to a –0.01 V input. The leading bit is thus interpreted as a sign bit, and the nine following bits give the magnitude in PCM counts, starting from 0.00 V for positive values and –5.12 V for negative values. Six zero bits are padded to the end to create a 16-bit word that is sent out onto the OI data bus.

Each MDM is fed by two Dedicated Signal Conditioners (DSC) and, optionally, a Strain Gauge Signal Conditioner (SGSC) and/or Wide-Band Signal Conditioner (WBSC). A total of 7 MDMs are installed, 4 front and 3 aft in the fuselage. In addition to conditioned analog signal inputs, each MDM can also process three different types of discrete digital inputs: a 28 V DC bi-level, a switch-closure isolated bi-level, and a 5 V DC bi-level. Like the DSCs, the MDMs are organized around a number of plug-in cards, and each measurement is "channelized" by specifying its MDM unit, the card number within the MDM unit, and the channel number within that card.

Two redundant Operational Instrumentation (OI) data buses interconnect each of the MDM units with the two redundant PCMMUs. Each of the OI data buses are 16 bits wide, bi-directional, and support data flow from each MDM to each PCMMU as well as command flow from each PCMMU to each MDM. Only one of the OI data buses is active at a time,

with the secondary being recruited from reserve only in the case of a recognized failure on the primary.

OFI Pulse Code Modulation Master Units (PCMMUs)

The Pulse Code Modulation Master Units (PCMMUs) are the backbone data processor for the Operational Flight Instrumentation (OFI) system. The PCMMUs are directly controlled by the network of five General Purpose Computers (GPCs), and act much like appendage special purpose hardware co-processors that free the GPCs from the chores of repetitive sensor data processing and formatting. The GPCs are the primary on-board computers for the orbiter. Four of the GPCs contain identical software and operate in a voting mode to insure data validity. The fifth GPC is set up in a bare-bones mode with a different and more basic software for emergency use. The flight crew can look at a conspicuous indicator panel in the cockpit to see which GPCs are in agreement at any moment. Well-defined protocols exist for when to switch over to the fifth GPC during emergencies, since once done, the switch back to the four main GPCs is neither easy nor quick. The PCMMUs run more or less unattended by the GPCs, but the GPCs do issue commands to the PCMMUs to program them to select the right sensor data and to organize it properly into the chosen telemetry data format.

Formatted telemetry data is sent from the PCMMUs to the Network Signal Processors (NSPs) which provide a final level of signal aggregation before sending the data to either the S-band transponder, the Ku-band signal processor, or the Operations (Ops) reel-to-reel data recorders. The NSPs combine voice communications channels with the telemetry data for the downlinks in either a High Data Rate (HDR) or Low Data Rate (LDR) mode. In the HDR mode, which is most frequently used, the 128 kbps telemetry data frames are combined with two 32 kbps air-to-ground voice channels for a total of 196 kbps. In the LDR mode, the 64 kbps telemetry data frames are combined with one 32 kbps air-to-ground voice channel for a total of 96 kbps. The NSPs also perform the reverse function of separating the ground-to-air voice channels from the received ground command data.

There are two PCMMUs, two NSPs, and two Ops recorders, but only one of each is used at any given time. Interconnections exist between both OI data buses and both PCMMUs, between both PCMMUs and both NSPs, and between both NSPs and both Ops recorders. This provides complete two-fold redundancy, if needed, so that a failure of either OI data bus, PCMMU, NSP, and Ops recorder can occur and a functional OFI system will still remain. When communications outages cause gaps in the telemetry data, one of the Ops data recorders can be used to downlink the missing data while the other continues to record the real-time data. Payload data is sent to a separate payload data recorder. All three recorders, Ops1, Ops2, and Payload, can send their data to only the Ku-band signal processor, since the S-band transponder does not have sufficient data capacity to handle this type of download. In addition, the *Columbia* (OV-102) utilized an OEX recorder, which does not have any means to transmit its data through a telemetry channel. When the orbiter is on the ground and connected to the Ground Support Equipment (GSE) through its T-0 umbilical, data from either PCMMU, either Ops recorder, the payload recorder, or the OEX recorder can be read out at the normal transfer rate of either 64 or 128 kbps.

All data acquisition and command operations are synchronized by a Master Timing Unit (MTU) which is a double oven-stabilized 4.608 MHz oscillator that provides a uniform frequency reference for all of the electronic systems within the vehicle. The oscillator is divided down to provide clock signals and referenced to a timing mark to provide Greenwich Mean Time (GMT) and Mission Elapsed Time (MET) stamps that are stored in both the Orbiter Timing Buffer (OTB) and Payload Timing Buffer (PTB). The 4.608 MHz oscillator reference is distributed directly to both of the PCMMUs. The PCMMUs in turn each provide 1.152 MHz and 100 Hz clock signals to both of the NSPs.

After each analog-to-digital conversion is completed by any of the MDMs, the 16-bit data is sent through the OI data bus to the PCMMU and stored in its Random Access Memory (RAM). The primary function of the PCMMU is to read out the contents of its RAM at the right times and compose overall, one second long formatted frames of data for telemetry or recording. The process of sequentially stringing together different serial data segments from different sources is termed commutation, and is essentially a word-by-word version of time division multiplexing. The specific set of sensors and other data to be included in the data frame, and their proper sequence and formatting, is specified by the Telemetry Format Load (TFL) instructions. The TFL is supplied to the PCMMU by the GPCs and covers several classes of analog sensor and digital system status data, including: Guidance, Navigation and Control (GNC) data, Systems Management (SM) data, Backup Flight System (BFS) data, Operational Instrumentation (OI) data, and data from the Payload Data Interleaver (PDI). The GNC, SM, and BFS data are collectively termed the GPC downlist data. The TFL is obtained from the Shuttle Data Tape (SDT) which is loaded into the orbiter's Mass Memory Unit (MMU) prior to launch. The SDT is created in two versions at the Johnson Space Center: an engineering version and a flight version. When instructed by commands from the GPCs, the TFL is read out from the MMU and transferred over to the PCMMU, where it then provides the instructions for formatting the next segment of telemetry data.

For each analog sensor measurement, the PCMMU only outputs a single 8-bit data word that is truncated from the original 10-bit analog-to-digital converter data. For bipolar measurements, only the sign bit and the first 7 most significant bits are retained, giving a PCM count in the range of –128 to +127. For unipolar measurements, the sign bit is dropped and the 8 most significant magnitude bits are retained, giving a PCM count in the range of 0 to +255. Each OI sensor measurement is thus only a simple 8-bit word, and these are concatenated to create the overall frame of data that represents a sampling of each of the sensors either once every second, or in some cases ten times per second.

MADS/OEX Pulse Code Modulator (PCM) Units

The Modular Auxiliary Data System (MADS) exists on all

of the orbiter vehicles, but the configuration on *Columbia* (OV-102) was different to support the larger number of sensors in the OEX system. For OV-102, the MADS consisted of 3 Pulse Code Modulator (PCM) units, 2 Frequency Division Multiplex (FDM) units, various Strain Gauge Signal Conditioners (SGSC) and WideBand Signal Conditioners (WBSC), a Remote Manipulator Digitizer Unit (RMDU), and a System Control Module (SCM). All of these avionics boxes were located on shelves 7 and 8 of mid-body bay 8. Sensor inputs were fed into the PCM units either directly or through a SGSC, into the FDM units through the WBSCs, and into the RMDU. The outputs of the PCM, FDM, and RMD units are each fed into the SCM which fed the overall data into the OEX recorder. Timing information from the Orbiter Timing Buffer (OTB) is fed into the PCM and FDM units. Control and monitoring of the MADS is achieved through the standard OFI instrumentation suite. Health and status information of the MADS system is generated by the PCM units and fed via a MDM into a PCMMU of the OFI system. Commands to the MADS system are directed from a MDM unit to the SCM of the MADS. The MADS and its subsystem components are described in detail in Section 35 of the Shuttle Operations document.

Three PCM units are installed in midbody bay 8, shelves 7 and 8, to support the MADS/OEX instrumentation. Each PCM unit contains a power supply, a selection of signal conditioners, an analog signal multiplexer, a sample-and-hold, an analog-to-digital converter (ADC), a reference voltage generator, a timing receiver and decoder, a format PROM, and finally a word generator. The PCM units which are part of the MADS are different from the PCMMUs which are part of the OFI subsystem. The PCM units were originally manufactured by Rockwell International Space Division and are described in drawing no. MC476-0251. Goodrich Data Systems is the present vendor for the PCM units. PCM-1 is operated as a master unit, controlled by command signals from the OFI system, and PCM-2 and PCM-3 are daisy-chained to operate as slave units from PCM-1.

Specification drawing MC476-0251 describes each PCM unit as containing 128 high level analog (HLA) inputs of 0-5.1 V range (#s 1-46 and 77-94 on J8, #s 47-76 and 94-128 on J10), a total of 188 low level analog differential (LLAD) inputs of 0-10 mV (#s 125-159, 35 ea., J7), 0-20 mV (#s 1-40, 40 ea., J6), 0-30 mV (#s 160-188, 29 ea., J7), 0-40 mV (#s 41-56, 16 ea., J6), 0-60 mV (#s 57-60, 4 ea., J6), and 0-15 mV (48 with PPS, #s 77-100 on J13, #s 101-124 on J15, and 16 without PPS, #s 61-76 on J13), 16 bipolar analog (BPA) inputs of ±5.1 V range (J5), 168 bridge completion (BC) inputs (#s 1-42 of −75° to +300°F range on J9, #s 43-84 of various temperature ranges on J11, #s 85-126 of various temperature ranges on J12, #s 127-168 of −200° to +450°F range on J14), 14 low level discrete (LLD) 5 V logic inputs (J4), 16 high level discrete (HLD) 28 V logic inputs (J4), and 112 precision power supply (PPS) outputs of 5.000±0.007 VDC (#s 1-24 on J5, #s 25-48 on J13, #s 49-72 on J15, and #s 73-112 on J3). Connectors J1-J15 on the box provide the interconnections of the inputs and outputs to the vehicle cable harnesses. Input 28 V and 5 V power are supplied to J1 and control and IRIG-B signals to J2.

The PCM units contain differential amplifiers which accept low level analog signals ranging from 0-10 mV to 0-60 mV from various transducer bridges. These have input protection and will indefinitely handle input voltages in the range of ±15 VDC without any damage. Other inputs are designed to handle over-voltages in the range of ±40 VDC. Each of the measurement channels are isolated, so that failure of one will not impact any of the other channels. Each channel is also protected against shorted input lines.

Each of the three PCM units on OV-102 internally contains 36 independent Precision Power Supplies (PPS). These, along with the power supplies in the SGSCs, are used to excite the pressure sensors, strain gauges, and temperature sensor bridges. Each PPS output is specified to produce +5.000±0.007 VDC to a 350 Ω load, recover from a short circuit within 100 ms, and be internally protected to voltages in the range of −1.0 to +10.0 VDC. The 36 outputs are internally connected to 112 PPS output terminals as 20 groups of four terminals and 16 groups of two terminals on J5, J13, and J15. The precision power supplies on each PCM unit are fully independent of the precision power supplies on the other two PCM units. All of the input pins of the PCM unit are designed to tolerate an indefinitely long short to any power supply line or chassis ground. Low-level analog inputs of 60 mV or less are rated to withstand overvoltages in the range of ±15 VDC, and all of the rest are rated to withstand overvoltages of ±40 VDC. All of the PCM unit outputs, including the PPS outputs, are designed to withstand short circuit conditions indefinitely. The outputs are specified to recover after the short circuit condition is removed, implying that no fuses or circuit breakers are used to provide this withstand capability.

Since several sensors are each supplied by a common PPS output group, a disturbance in the power supply excitation to these sensors will propagate through all of the sensors and show up as either a common failure or as an artifact in each of their outputs, such as an abrupt offset. PPS commonality can be either internal to the PCM unit, since a given precision power supply feeds two or four output terminals on the connector, or external, with the power feed going to a terminal board or splice where it branches to feed several sensors at different locations. PPS commonality is an important consideration in reviewing all of the sensor data, because a disturbance in the power feed to one sensor, for example a short between power and ground, can then cause other sensors on the same power feed to react to this disturbance, even though the sensors themselves may not be physically or geometrically related. However, if the short is removed, the design of the PCM PPS circuits should quickly recover (within 100 ms), and the unharmed sensors should also return to their normal, operational state. An important case of this on STS-107 is the abrupt jump that was recorded in the outputs of fuselage lower surface temperatures V07T9480A, V07T9489A, V07T9492A, V07T9522A, and V07T9636A at a time of GMT 13:52:22 (EI + 493 sec). All five of these thermocouple temperature sensors were fed from the same terminal board that was supplied +5.0 VDC from PCM-1 PPS 89. Another temperature sensor, V07T9666A, was also fed power from the same PCM-1 PPS, but not through the terminal board. NASA attributed the common fault point to the terminal board, as all five thermocouple temperature

sensors produced invalid data past the time of this fault. As will be discussed later, this sensor V07T9666A was one of the first to fail at GMT 13:52:24 (EI + 495 sec), and this failure could have also been responsible for these other five lower fuselage surface temperatures to have an abrupt jump in their readings at a few seconds prior.

The status and health of the PCM units themselves are recorded by means of several internal diagnostic voltages which are given MSIDs of V78V96xxD (17 ea.), V78V98xxD (17 ea.), and V78V99xxD (17 ea.) for PCM-1, PCM-2, and PCM-3, respectively. These measure low limit and high limit analog signal levels for the ADCs, typically at the 20% and 80% levels. In addition, V78V9638A and V78V9639A are internal diagnostics in which a +5.0 VDC output from PCM-1 and PCM-2 is wrapped around to a bipolar signal input to monitor the output excitation voltage. In addition, each PCM has 2 ea. internal diagnostic status flags which are given MSIDs of V78X9655D, V78X9656D, V78X9855D, V78X9856D, V78X9955D, V78X9956D for PCM-1, PCM-2, and PCM-3, respectively. These indicate the calibration settings for high and low level thresholds of the LLDs. These are each recorded on the OEX recorder tape.

PCM-1 internal diagnostic voltage V78V9638A fell from +5.0 VDC (254 counts) at GMT 13:53:09 (EI + 540 sec) to 0.0 VDC (129 counts) at GMT 13:53:18 (EI + 549 sec). This voltage is the output of PCM-1 PPS 83, and it wraps around to a bipolar signal input (BPA1) by means of a jumper wire located on the PCM1 connector. PPS 11, 12, 83, and 84 are tied together and supply +5.0 VDC to sensors V07T9713A, V07P8114A, V07P8162A on PCM-1. V07T9713A is a left wing lower surface elevon temperature sensor that went to OSL at EI + 540 sec. However, V07P8114A and V07P8162A remained functional up through EI + 940 sec.

In another instance, PCM-1 PPS 27 and 28 are tied together to supply +5.0 VDC to pressure sensors V07P8004A and V07P8005A (left wing upper surface pressures) and V07P8158A and V07P8176A (right wing lower surface pressures). The four pressure sensors on PCM-1 all go abruptly OSL at GMT 13:52:52 (EI + 523 sec). Due to the simultaneous timing, one or the other (or both) of the left wing sensors must have failed when the associated cable harness on the outside top of the left wheel well burnt through. The simultaneous failure of the other left wing sensor and both right wing sensors can be attributed to a loss of the common power supply lines that feed them from PCM-1. The wiring burn-through cause and effect appears very clear cut for this set of four sensors.

Besides the diagnostics which were recorded on tape, there were several diagnostic MSIDs which were downlinked through the OFI telemetry. Each PCM unit contains built-in test equipment (BITE), and the BITE status for the MUX components of PCM-1, PCM-2, and PCM-3 is downlinked as MSID V78X9611E, V78X9614E, and V78X9615E, respectively. The telemetry data showed that the master BITE was a logical 1, indicating good, for all three PCM units from Entry Interface (EI) up until the Loss Of Signal (LOS).

The internal diagnostics indicated that all three PCM units were for the most part functional throughout the re-entry flight, aside from disturbances resulting from the propagating left wing damage. PCM-1 and PCM-2 were fully functional through to the end of the OEX data at GMT 14:00:19 (EI + 970 sec), except that PCM-1 lost output signal amplitude during GMT 13:51:37 to 13:51:39 (EI + 448 to 450 sec), and PCM-2 lost output signal amplitude during GMT 13:54:52 to 13:54:55 (EI + 643 to 646 sec). PCM-3 also began snapshot acquisition of its data at GMT 13:39:30 (pre-EI). Several +5.0 VDC PPS outputs were lost at approximately GMT 13:53:00 (EI + 531 sec), and this would be most likely associated with the shorting of power supply feeds to sensors whose wiring was burnt through at around this time.

There also exist three temperature sensors which monitor the conditions surrounding the OEX and OFI avionics boxes in mid-body bay 8. All three of these are surface mounted RTDs which monitor temperatures over a range of –75°F to +175°F, and are sampled once per second. V78T9606A is located next to PCM-1 on the upper part of shelf 8; V78T9607A is located next to the FDM on the lower part of shelf 8; and V78T9608A is located near the FASCOS heat sink on the top of shelf 7. Since the FASCOS unit was not present on STS-107, only the two temperature measurements V78T9606A and V78T9607A on the upper and lower side of shelf 8 were recorded in the telemetry data. Sensor V78T9606A recorded a temperature of 50.2°F at the Entry Interface (EI) of GMT 13:44:09, which rose smoothly upward by 4 bits to a final value of 54.2°F at GMT 13:59:32 (EI + 923 sec) where the telemetry signal was lost. Similarly, sensor V78T9607A recorded a temperature of 49.2°F at EI which rose smoothly upward by 3 bits to a final value of 52.2°F at the point where the telemetry signal was lost. Both of these temperature sensor readings are completely consistent with the behavior of prior flights and indicate that there was no abnormal heating within these avionics bays which might have contributed to faulty telemetry data.

NASA staff indicated that on prior flights of OV-102, several sensors (V07T9253A, V07T9270A, V07T9468A, V07T9470A, and V07T9478A, all fuselage surface temperatures) showed "step function" behavior, similar to what was recorded for STS-107. These prior flights were STS-73, STS-75, and STS-78. This prompted PCM-1 (S/N 304) to be shipped back to the vendor, Goodrich Data Systems, for thermal testing and evaluation. No failures were found during these tests and the unit was shipped back and reinstalled in OV-102. Similar "step function" failures were then observed on STS-80, STS-94, and STS-87. It was felt that the problem was not within PCM-1, but the ultimate source of the problem was never identified.

MADS/OEX Frequency Division Multiplex (FDM) Units

Two FDM units are installed in midbody bay 8, shelves 7 and 8, to support the OEX instrumentation. Each FDM unit takes wideband signal data from accelerometers, vibrometers, and microphones, heterodynes each signal up to a higher center frequency, and combines up to fifteen of the signals into each of four separate channels that are routed to specific

tracks on the OEX recorder. A 16th constant frequency 240 kHz signal is combined into each channel to provide a reference signal for compensation of tape speed variations (wow and flutter). FDM unit 1 creates output channels designated M1A, M1B, M1C, and M1D; while FDM unit 2 similarly creates the M2A, M2B, M2C, and M2D channels. Each input signal is input to a voltage-controlled oscillator (VCO) to produce frequency modulation (FM). For each FDM unit, the first 7 VCO channels have center frequencies of 12, 16, 20, 24, 28, 32, and 36 kHz, and each of these channels has a response bandwidth of 500 Hz. The next 7 VCO channels have center frequencies of 48, 64, 80, 96, 112, 128, and 144 kHz, and each of these channels has a response bandwidth of 2.0 kHz. The 15th VCO channel has a center frequency of 184 kHz and supports a response bandwidth of 8.0 kHz. Specific OEX recorder tracks are assigned to each of the four channels from each FDM unit for the three mission phases of ascent, de-orbit, and re-entry. The lowest VCO frequency (12 kHz) of the first channel of each FDM unit (M1A and M2A) is used for recording the FDM time reference. These timing references are also given MSIDs: V75W9006D for M1A, and V75W9016D for M2A. The remaining sensor inputs can be arbitrarily assigned to various channels, frequencies, and units to accommodate the needed bandwidth of the measurements. These measurements can be any combination of vehicle strains, engine strains, vehicle accelerations, vehicle vibrations, engine vibrations, and vehicle acoustics. Because of the more complex method of combining, FDM data requires more time and effort to extract from the OEX recorder tape. This data extraction is normally performed by the Boeing Company, Huntington Beach, under contract to NASA. Under normal circumstances, both time and frequency representations of the data are created. Power Spectral Density (PSD) plots are also created to provide a mixed time-frequency representation of the data.

Like the PCM units, the FDM units also contain built-in test equipment (BITE) and the BITE status of the four MUX units is downlinked as MSIDs V78X9380E – V78X9383E for FDM-1 and as V78X9390E – V78X9393E for FDM-2. The telemetry data showed all four of these bits for both FDM-1 and FDM-2 remained in the logical "1" state from EI to LOS, indicating that all four MUX channels of both FDM units were operating properly. The data mode for FDM-1 and FDM-2 is also downlinked as MSID V78X9309E and V78X9310E, respectively, indicating if these units were operating in their wideband mode or not. The telemetry data showed that both FDM-1 and FDM-2 were indeed operating in their wideband modes.

Data Formatting

OFI data is exchanged in a common format to allow it to be either transmitted or recorded. The format consists of a major frame which is produced each second, and each major frame is composed of 100 minor frames, produced every 10 ms. There are two data rates: a high data rate at 128 kbps and a low data rate at 64 kbps. At the high data rate, 160 words compose each minor frame, and at the low data rate, 80 words compose a minor frame. Each word is 8 bits long. For both the high and low data rates, the first three words of each minor frame (24 bits) comprise a sync pattern for which 76571440 octal (FAF320 hex) is used for all shuttle telemetry systems. The 4th word in each minor frame gives the minor frame count in binary format with the first minor frame being number "0". Minor frames are error checked and the number of perfectly received minor frames is known as the frame count for each major frame of telemetry data. The 5th word of only the 1st minor frame contains the format ID. The MADS/OEX data is exchanged in an identical format, with the exception that each of the three PCM units outputs data at half of the OFI rate: a high data rate of 64 kbps and a low data rate of 32 kbps, with each major frame containing only 50 minor frames. Two MADS/OEX PCM units could thus be interleaved to produce the equivalent data throughput of one of the OFI PCMMUs.

Following after the sync pattern and the frame number, each minor frame then contains from 2 to 7 subcommutated windows of varying length. Each of these begins with a specific header that announces its beginning and then a sequence of 8-bit data words, one for each sensor reading within that subcommutated window. Each minor frame will contain exactly one OI sensor data window, 0 to 4 Payload Data Interleaver (PDI) data formats, and from 1 to 5 GPC downlist formats which may include GNC, SM, or BFS data. The first three minor frames usually contain the TFL ID, the GMT time stamp, and the MET time stamp in words 5-12.

Both Non-Return to Zero (NRZ) and Bi-Phase (Bi-ϕ), also known as Return to Zero (RZ), digital signaling formats are used within the orbiter data processing, recording, and telemetry hardware. NRZ data assigns a specific level (high or low) to a binary 0 or 1. Bi-ϕ data assigns a transition (up or down) to a binary 0 or 1. Both Level (L), Mark (M), and Space (S) subformats are also used. A binary 0 is represented as a low level in NRZ-L, no change in level in NRZ-M, a change in level for NRZ-S, a midperiod low to high transition in Bi-ϕ-L, no midperiod change in level for Bi-ϕ-M, and a midperiod change in level for Bi-ϕ-S. A binary 1 is represented by the opposite in each case. Bi-ϕ-L is also known as Manchester II coding and is used frequently within the orbiter avionics systems. OFI, OEX, and command data frames each use NRZ-L formatting, while Bi-ϕ-L formatting is used for radio transmission of the same data.

Command data that is sent to the space shuttle orbiter (SSO) is encoded to provide error checking capability. The 48-bit command words at 50 words/sec, 2.4 kbps, are padded with 2 leading zero bits and fed into a BCH(127,50) encoder. This appends 77 check bits to the incoming 50 bits, and finally, another leading zero bit is added to create the 128-bit encoded command word, still at 50 words/sec, but now 6.4 kbps. The BCH(127,50) command encoder is implemented as a 50-stage shift register with appropriate feedback coefficients. Once received by the SSO, the first 50 bits after the zero padding bit are passed through an identical BCH(127,50) encoder circuit to create the 77 check bits. If these generated check bits do not agree with those that were sent, the command is discarded. Encoded commands are also authenticated by being sent in a permuted form by modulo-2 addition with a 128-bit timing word that is created as an IRIG-B format GMT time stamp. Once received by the SSO, the encoded and permuted command word is retrieved

by another modulo-2 addition with the same 128-bit timing word that is generated independently within the SSO. After the command has been authenticated, by successful de-permuting and decoding, it is finally accepted as valid and allowed to perform its function within the SSO systems. Telemetry data that is sent back from the SSO is neither encoded in this manner, nor permuted with a time stamp.

Data Time Stamping

GMT time stamps are formatted according to the International Radio Instrumentation Group (IRIG) -B standard to 10 ms resolution. This formatting standard for time stamps is fully defined in IRIG Standard 200-95. These are produced by the Orbiter Timing Buffer (OTB) that runs from the Master Timing Unit (MTU) 4.608 MHz oscillator. A Payload Timing Buffer (PTB) performs the same function for the payload instrumentation. The most significant bit (MSB) and digits are sent first. Bits 1-10 contain days 1-365 in BCD format with the bit weightings being 200, 100, 80, 40, 20, 10, 8, 4, 2, and 1 days. Bits 11-16 contain hours 0-23 in BCD format with bit weightings of 20, 10, 8, 4, 2, and 1 hours. Bits 17-23 contain minutes 0-55 in BCD format with bit weightings of 40, 20, 10, 8, 4, 2, and 1 minute. Bits 24-30 contain seconds 0-55 in BCD format with bit weightings of 40, 20, 10, 8, 4, 2, and 1 second. Bits 31-38 contain tens of milliseconds 0-99 in binary format with bit weightings of 1280, 640, 320, 160, 80, 40, 20, and 10 milliseconds. MET time stamps are created from a simple, continuously running BCD counter. Both GMT and MET time stamps are usually inserted into words 5-12 of the first three minor frames of each one second long major frame, each occupying four words, or 32 bits.

For telemetry command authentication, the IRIG-B formatted GMT time stamp has its transmission order reversed and the milliseconds field replaced by 4 leading zeros to give a resolution of 1 second. Two more trailing zero bits are padded at the end following the days field to give a 32-bit command authentication timing byte. Uplink commands consist of 4 such 32-bit bytes, the first byte always being the IRIG-B time stamp, and each command is thus a 128-bit timing word that occupies sixteen 8-bit words within a minor frame.

Recording

MADS/OEX Recorder

The data recorder for the OEX sensor suite is a mostly standard Bell and Howell Modular Recording System (MARS) that has been only slightly modified for use on OV-102. It is a 28-track, wideband, reel-to-reel magnetic tape recorder of coaxial design, so that the two reels sit over top of one another and share the same spindle axis. It contains 9000 feet of tape, which at the usual tape speed of 15 ips provides about 2 hours of recording time. It contains both record and playback heads, but only electronics for recording. Playback is accomplished via a separate Driver Amplifier Module (DAM) which can dump the data to the Ground Support Equipment (GSE) through the T-O umbilical after the orbiter has landed. There is no means by which to take data off of the recorder while the orbiter is in flight. The tape transport is capable of speeds of 1-7/8, 3-3/4, 7-1/2, 15, 30, and 60 ips. At the nominal tape speed of 15 ips, analog frequencies in the range of 400 Hz to 250 kHz can be recorded, or digital biphase-L data at rates of 8 to 128 kbps. The recorder weighs 58 lbs and runs from +28 VDC. On OV-102, it was located in section G of the Environmental Control and Life Support System (ECLSS) bay, essentially lowest down in the belly of the fuselage along the midline, approximately midway along the length of the fuselage. MADS shelves 7 and 8 are located adjacent to this, underneath the floor of the payload bay. A detailed description of the MADS and OEX recorder can be found in Section 35 of the Space Shuttle Operations document. The OEX recorder, like the rest of the MADS, is rated to operate over a temperature range of 35°F to 120°F. The tape transport has hardware sensing for beginning of tape (BOT) and end of tape (EOT) that are implemented by optical sensors and a 15 ft. cut out window that exists 15 ft. from both ends of the tape. An analog voltage output is used to indicate the percent of tape remaining and is implemented as a 1850-turn, 1 kΩ potentiometer, of which only 92 turns and 50 Ω are used, with +10 V indicating a full tape at BOT, and 0.0 V indicating an empty tape at EOT. The OEX recorder can record in either tape direction, and typically for a given flight three passes are used to record the three different phases of ascent, de-orbit, and re-entry. Different recording tracks are assigned to different sets of data during each pass.

The OEX recorder operates nearly autonomously of the crew of the orbiter. The only crew controls on the system are for master OEX power on panel C3A5 and OEX power on panel A7L. There was also a switch for the Shuttle Infrared Left Temperature System (SILTS) pod, but this instrumentation was removed in 1991. The switch remains on the panel but is inactive. Interestingly, the SILTS pod, which is located on the forward tip of the vertical stabilizer, previously contained an IR camera that took images of the left wing thermal profile during re-entry. If this camera had been in place on STS-107, a telemetry movie of the thermal profile and break up of the left wing would have been available. The OEX recorder operates primarily through uplinked commands that are passed to it through the System Control Module (SCM). The SCM responds to 66 different ground commands which are detailed in Section 36 of the Shuttle Operations document. The real-time commands (RTC) are a sequence of opcodes which are concatenated to form a command sequence for either the SCM itself, the PCM units, the FDM units, or the OEX recorder. The commands are sent from the ground by the Mission Operations Computer (MOC). Eight-character hexadecimal commands either set or reset the 66 different command functions. Many of the command functions are actually arguments, that is, numerical values which are uplinked for a given opcode to act upon. Since many opcodes may be needed to trigger given functions, macros (MRTC) can be pre-programmed into the PROM for a given mission and then called with a single “continue at label” command. When the SCM receives a command string of opcodes that it recognizes, it then echoes them back on the downlink. If the command string is not recognized, an error code is downlinked instead.

Housekeeping data from the OEX recorder is also downlinked to the ground via OFI telemetry. These are given MSIDs like any other vehicle measurement. The status of

the OEX recorder built-in test equipment (BITE) is given on V78X9511E, which the telemetry data showed to remain in the logical "1" state, indicating a properly functioning system, from EI up until LOS. Recording on and tape motion bits are given on V78X9512E and V78X9513E, and the telemetry data showed both of these to be in the logical "1" state from EI up until LOS. Tape speed is given by three bits on V78X9548E – V78X9550E, which were in the "100" state from EI up until LOS, indicating the normal 15 ips speed. Tape position (analog) and tape direction (digital) are given on V78Q9551A and V78X9552E. The reading from V78Q9551A rose smoothly and continuously from EI up until LOS, and V78X9552E gave a logical "0" from EI up until LOS. The highest track recording is given by 5 bits on V78X9553E – V78X9557E, which gave a logical "11100" state from EI up until LOS. Because all of the built-in telemetry diagnostics indicated a normal and properly functioning OEX recording system, which was verified by the excellent quality of the retrieved data itself, there is no reason to suspect that the OEX recorder was suffering from any of the effects occurring in the left wing area prior to break up of the overall vehicle. The break up of the vehicle should in principle cause all of the avionics systems to halt their functions as the power supply feeds to them become interrupted. The final position of the tape in the OEX recorder also gives a useful timing point for this, indicating that the main fuselage of the vehicle was still largely intact at a time of GMT 14:00: 19 (EI + 970 sec). This is 47 seconds beyond the MCC LOS point at GMT 13:59:32 (EI + 923 sec).

A combination of extremely fortuitous circumstances allowed the data that was recorded on the OEX recorder to be retrieved and added into the engineering analysis of the accident investigation. First, the shuttle broke apart over the continental Southwest United States, allowing the debris to fall into a largely uninhabited and controllable area in which it could be methodically searched and collected. Second, the OEX recorder was located within this debris. Third, the OEX recorder fell through the atmosphere to the ground without even a scratch. Virtually all of the other avionics boxes aboard the *Columbia* were so severely burnt upon re-entry as to be barely recognizable and certainly not functional. Fourth, the OEX recorder managed to land right side up, like a pancake, so that the weight of the motors did not crush the tape spools that were sitting above them. If the OEX recorder had landed upside down, the data on the magnetic tape would almost certainly have been irretrievable. Fifth, the OEX recorder landed in a dry spot, so that its several days out in the weather did not cause any deterioration of its working parts or magnetic tape. The recorder suffered only a slightly broken case and electrical connectors, and the internal silica gel dessicant cartridge spilled open. Other than these effects, the OEX recorder was miraculously in perfect condition.

The Boeing Integrated Part and Component Locator (IPCL) 77BT listing details all of the 993 different sensor MSIDs for the MADS which were ever installed on *Columbia*. The first four characters of the MSID identifies the measurement type and system. The 993 MSIDs include: 24 main engine vibrations E41D, 12 main engine strains E41G, 8 ACIP accelerations V07A, 1 unknown ACIP measurement V07M, 35 left wing upper surface pressures V07P, 46 left wing lower surface pressures V07P, 36 right wing upper surface pressures V07P, 48 right wing lower surface pressures V07P, 22 vertical stabilizer surface pressures V07P, 25 unspecified wing surface pressures V07P, 22 fuselage side surface pressures V07P, (234 aerodynamic pressures V07P total), 3 ACIP axis rate gyros V07R, 9 OMS pod temperatures V07T, 70 fuselage surface temperatures V07T, 19 wing upper surface temperatures V07T, 4 wing lower surface temperatures V07T, 2 left elevon lower surface temperatures V07T, 2 vertical stabilizer surface temperatures V07T (106 temperatures V07T total), 2 ACIP calibration voltages V07U, 6 pressure range switches V07X, 19 vibrations V08D, 2 heat shield strains V08G, 4 payload acoustic pressures V08Y, 22 structural temperatures V09T, 121 left wing strains V12G, 126 right wing strains, 26 right elevon hinge strains V13G, 26 left elevon hinge strains V13G, 38 vertical stabilizer strains V22G, 12 rudder hinge moment strains V23G, 9 mid-fuselage accelerations V34A, 40 mid-fuselage strains V34G, 20 aft fuselage OMS deck strains V35G, 15 payload bay door hinge line strains V37G, 11 RCS thrust chamber pressures V42P, 1 ACIP rudder position V57H, 4 ACIP elevon positions V58H, 12 MADS PCM status measurements V75M, 21 PCM MUX IRIG-B time stamps V75M, 6 OTB IRIG-B time stamps V75W, 3 MADS PCM frame counters V78J, 53 MADS PCM test voltages V78V, and 6 MADS PCM calibration switches V78X.

Only a subset of the 993 MSIDs in the Boeing IPCL-77BT listing were actually active measurements on flight STS-107. This is a result of certain sensors failing over time and simply being disconnected from the data acquisition systems. Of the 128 temperature sensors, only 49 remained as active measurements on flight STS-107, and one of these, a door temperature, was known to be a failed sensor. Out of the 234 original pressure sensors, only 181 were active measurements, and of these, 55 were known to be broken or producing unreliable readings, leaving 126 valid pressure measurements. Out of the 426 strain measurements, 422 were remaining as active measurements. There were a total of 36 main engine sensors and 25 Aerodynamic Coefficient Instrumentation Package (ACIP) sensors that were not relevant for the re-entry phase of the flight. The MADS system also used 101 MSIDs for recording the health status of the instrumentation package (V75M, V75W, V78J, V78V, V78X). All totaled, there were 719 active measurements in the MADS system. One of these, a heat sink temperature on the MADS instrumentation shelf, was sent back as telemetry data, leaving 718 active measurements that were sent to the OEX recorder. This total excludes the 11 RCS pressures, 25 ACIP sensors, and 101 MADS diagnostics. One strain gauge, V12G9653A, recorded ascent data, but failed sometime thereafter, and thus did not provide data for the re-entry flight.

Ops Recorders

The operational flight instrumentation (OFI) data that is sent back from the orbiter's telemetry system is also recorded on a reel-to-reel data recorder, known as the ops recorder. Like most critical components of the OFI instrumentation system, two ops recorders are installed in a redundant fashion. Under normal conditions only one of the two is used, but a failure in one can be dealt with by switching over to the other. Unlike the MADS/OEX recorder, both of the ops recorders can

be played back during flight and their data transmitted back to Earth. When the orbiter is back on the ground, the data from the ops recorders can also be played back and downloaded through the T-0 umbilical. An instance of when this becomes used is during a normal re-entry flight, during the first half of which the telemetry data becomes broken up by various randomly timed communications drop outs, and during the second half when the telemetry data drops out almost entirely. The same data that is sent through the S-band radio telemetry is also recorded on the ops recorders. After the orbiter has safely landed, the entire, unbroken telemetry data stream can be retrieved to fill in the missing segments that the communications drop outs obliterated.

Neither of the ops recorders were recovered from the *Columbia*. Only one of the two would have contained the telemetry data that was being transmitted back from the orbiter during the re-entry flight. Because the telemetry data was fairly complete up until the loss of signal, in spite of the various anomalous, but brief, communications drop outs, the retrieval of the missing ops recorder would not have added that much new data. A payload data recorder also exists, but it does not contain much in the way of re-entry flight information. It was not recovered from the wreckage debris, either.

Telemetry and Radio Communication Links

Signal Formatting

The Space Shuttle Orbiter (SSO) can communicate with the Mission Control Center (MCC) via the ground station at the White Sands Complex (WSC) through several different systems operating at primarily S-band (2.1 GHz) and Ku-band (13.8 GHz). Only the S-band system will be described in detail, since that was the one operating during the time at which the SSO broke up during re-entry. Communication between the SSO and MCC can be either direct to the ground from the SSO to the WSC, or via a geosynchronous Telemetry and Data Relay Satellite (TDRS). Only the TDRS linked communications will be described in detail, again because that was the system in use during the re-entry phase of flight STS-107. The four links of this system are referred to as follows: MCC to TDRS is the up link, TDRS to SSO is the forward link, SSO to TDRS is the return link, and TDRS to MCC is the down link. The TDRS satellites do not perform any data manipulation; they only amplify the received signal power and then retransmit the signal, acting as a simple repeater. The signal format and content is thus unchanged passing through the TDRS satellite. The up and forward links use the same signal format as the return and down links, although the transmission frequency differs to allow full duplex communication (signals can be going both ways at once without interfering). The up and forward links are used to transmit command data from MCC to the SSO, while the return and down links are used to transmit telemetry data from the SSO to MCC. This organization reflects the fact that the SSO is under the control of the MCC and not vice-versa. An extremely large number of operations aboard the SSO are commanded directly from the MCC ground station without any astronaut intervention or direct awareness. The telemetry and communication interface specifications are found in the Space Shuttle Interface Control Document ICD-2-0D004.

Two data rates are used for command data sent on the up and forward link. A low 32 kbps data rate is created with a single 32 kbps voice channel. Alternatively, a high 76 kbps data rate is created by time division multiplex (TDM) of two 32 kbps voice channels, 6.4 kbps permuted and encoded command data, and a 1.6 kbps synchronization signal, all in non-return-to-zero, level (NRZ-L) format. The raw command data at 2.4 kbps is permuted and encoded prior to TDM to create the 6.4 kbps stream. Following the TDM formatting of the command and voice signals, a NSA-grade data encryptor is used prior to transmitting the signal from MCC to the White Sands Complex (WSC) ground station. This is set up to implement the 128-bit Data Encryption Standard (DES) that was established by NSA. The data encryption process does not change the bit rate. Under normal circumstances the high data rate is used; the low data rate is essentially a back up system for when the bit error rate (BER) of the channel becomes too large to support the higher data rate. At the White Sands Complex (WSC) ground station the received encrypted command data is then encoded to improve the BER of the links. A (V = 3, K = 7) convolutional encoder is used to create a 216/96 kbps NRZ-L stream from the incoming 72/32 kbps NRZ-L command data. The NRZ-L data is then converted to Bi-ϕ-L data and fed into a Phase-Shift Keying (PSK) spread spectrum transmitter which uses a 11.232 Mbps pseudo-noise sequence generator. Transmission is then sent out over a 2.041947900 GHz or 2.106406300 GHz carrier frequency. The pseudo-noise sequence generator consists of a 10-stage shift register with feedback coefficients set according to 2201_8 (octal) which produces a code length of 1023 chips. The (V = 3, K = 7) convolutional encoder consists of a 7-stage shift register, 3 modulo-2 adders with weightings 1111001, 1011011, 1100101, and a 3-position commutator that operates with a generator sequence of 7588127_H (hex). Upon reaching the SSO after passing through a TDRS, the up and forward link signal is amplified and detected by a PSK spread spectrum receiver. Bit synchronization is then performed, and a Viterbi decoder is used to extract the effects of the convolutional encoding. The data stream is then decrypted and command authenticated and finally passed through a TDM demultiplexer to separate the voice channels and command data.

The return and down link operates in a very similar manner but at two higher data rates. A low 96 kbps data stream is created from TDM of one 32 kbps voice channel and 64 kbps telemetry data. A high 192 kbps data stream is created from TDM of two 32 kbps voice channels and 128 kbps telemetry data. Both of these are formatted as NRZ-L data streams, and the higher data rate is the normally used one; the lower data rate is again a back-up for when the BER precludes the use of the higher rate of operation. From the TDM multiplexer, the data passes through an encryptor, a (V = 3, K = 7) convolutional encoder, a Bi-ϕ-L converter, and then the PSK spread spectrum transmitter. The (V = 3, K = 7) convolutional encoder works the same as in the reverse link, but converts the 192/96 kbps data into a 576/288 kbps output stream. The spread spectrum transmitter also uses a 10-stage shift register pseudo-noise sequence generator to create encoded words of 1023 chips. These are sent out on a 2.2175 GHz or 2.2875 GHz carrier frequency, passing through a TDRS, and picked up by the White Sands ground

station receiving antenna. The PSK spread spectrum receiver at the White Sands Complex detects the signal and also extracts a Doppler signal that can be used for ranging and tracking purposes. After bit synchronization, an 8-level soft-decision output at 576/288 kbps is fed into a Viterbi decoder to produce the hard-decision output at 192/96 kbps. After decryption, the telemetry data stream is passed through a TDM demultiplexer to separate out the voice channels and telemetry data at 128/64 kbps. The transponder in the SSO operates in a coherent mode which allows the Doppler ranging functions. The return link transmission carrier frequency is obtained by multiplying the received S-band carrier frequency by a factor of 240/221. If the forward link carrier frequency is not available for some reason, the transponder then uses its own free-running oscillator to provide a non-coherent replacement.

S-band (2.1 GHz) Telemetry and Data Relay Satellite (TDRS) Links

Two NASA geosynchronous orbit satellites (33,579 km circular geodetic altitude at 0° inclination) were programmed to be active during the STS-107 re-entry mission phase. TDRS-171, also know as TDRS-West, and stationed roughly over Guam, relayed the majority of the radio communication during re-entry. TDRS-047, also known as TDRS-East, picked up partial data frames toward the last few remaining seconds of the re-entry before STS-107 broke apart. The last three digits of each TDRS identifier give the geostationary longitude in degrees West from the Prime Meridian in Greenwich, England.

The S-band antennas are located on the front of the orbiter, directly above and below the crew cabin. Two antennas are used for frequency modulation (FM) transmission, and both are located on the vehicle centerline, one on the top and one on the bottom. Each of these have a hemispherical radiation pattern and are referred to as "hemis." These provide essentially the same gain as an isotropic radiator, i.e. 0 dB. Eight antennas make up the higher gain, more directional system that uses phase modulation (PM). Pairs of two are located in four locations around the crew cabin: upper left, upper right, lower left, and lower right. Each pair contains a forward pointing antenna and an aft pointing antenna. The eight antennas are thus designated ULF for upper left forward, ULA for upper left aft, and so on for the URF, URA, LLF, LLA, LRF, and LRA. Each of the antennas is constructed as a pair of crossed dipoles which are fed in quadrature to create a right hand circularly (RHC) polarized wave. The circularly polarized pattern makes each antenna insensitive to rotation about its normal axis. Each of these antennas are known as "quads" even though each is pointed into a specific octant of space. The forward quads cover an elevation angle of approximately +10° to +70°, while the aft quads cover elevation angles of approximately –50° to 0°. The azimuth angles of each quad (LL, UL, UR, LR) are approximately 90° wide. Note that elevation and azimuth in this context are with respect to vehicle pointing nose up, as if on the launch pad. Each of the antenna pairs is installed with a slight angle in toward the nose to match the vehicle's exterior contour. This and the presence of the vertical tail structure makes the coverage looking directly forward better than that looking directly aft. This coverage at the 2041.9 MHz receive frequency is generally better optimized than at the transmit frequency of 2217.5 MHz. The peak gain of each of the quads is approximately 6-7 dB above that for an isotropic radiator.

Switching of the S-band quad antennas is accomplished electronically. Switching between each of the four quad antenna pairs (LL, UL, UR, LR) is performed by an S-band antenna switch module which accepts commands either manually from the orbiter cockpit or from the telemetry ground command signals processed through the multiplexer – demultiplexer (MDM) units. The selection of the particular antenna is based upon calculations of the orbiter's position and attitude relative to either the White Sands Complex ground station or the TDRS satellites. Antenna selection is not based upon received signal strength. Transmit signals are fed into the antenna switch module from one of two redundant traveling wave tube (TWT) power amplifiers, each capable of producing 135 Watts of RF power. Received signals are taken from the antenna switch module and fed into one of two redundant preamplifier modules. The transmit and receive functions are isolated by a dual diplexer which handles both the low range (2217.5 MHz transmit, 2041.9 MHz receive) and high range (2287.5 MHz transmit, 2106.4 MHz receive) operating frequencies. After the transmit and receive signals are switched to one of the four selected quads, the forward versus aft antenna is selected by a relay switch on each of the quads that is energized by a switch beam control electronics module. The relay switch controls the phasing of a pair of –3 dB hybrid directional couplers which are in turn fed in quadrature by a third –3 dB hybrid coupler. One of the two antennas is made active by feeding the crossed dipoles in quadrature to create the RHC polarized beam. The other antenna is made inactive by feeding the crossed dipoles in opposite phase, for which the signals interfere destructively and cancel out. The overall insertion loss of the combined system of switches, circulators, diplexers, and transmission cable is estimated to be 4.6 dB.

The performance of the communication link can be monitored by several measures. The automatic gain control (AGC) level of the received forward link signal from TDRS to the SSO is monitored within the shuttle and then transmitted back as a measurement on the return link. When the forward link carrier signal is being received by the shuttle, several different status flag bits record the state of the carrier frequency lock, and these are also sent back as measurements on the return link. On the return link from the orbiter to TDRS, the minor frame count lock is monitored. If less than 95 of the 100 minor frames are not received correctly on at least one of the two integrated receivers, the entire major frame is discarded as invalid data by the MCC. This is what constitutes a formal communications drop out of the type that was observed during the early re-entry flight of STS-107. The signal-to-noise ratio of the integrated receiver for the return link is also monitored, although this is performed in the context of a digital data stream. The actual signal-to-noise ratio (SNR) of the received signal is equal to twice the ratio E_s/N_o, where E_s is the symbol energy and N_o is the noise density. The integrated receiver only samples the digital data stream and thus creates only an estimate

of the ratio E_s/N_o. 1024 samples are used each second for normal 192 kbps data rates. Because the 192 kbps digital data is convolutionally encoded as a 576 ksps symbol rate (three times the data rate), the ratio of energy per data bit to noise density is $E_b/N_o = 3\ E_s/N_o = 1.5$ SNR. The E_b/N_o value is computed every 100 ms from the sampled received data signal, and the reported value of E_b/N_o is constructed as a sliding (boxcar) average of the last 40 of the computed E_b/N_o values. Normal values of E_b/N_o during the re-entry flight are in the range of +13 to +19 dB.

Because the return link carrier signal is obtained by coherently multiplying the received forward link carrier by a factor of 240/221, the shift in the carrier signal frequency received back by TDRS can be used as a Doppler signal that reveals the relative speed between the orbiter and TDRS. Because TDRS is geostationary, there is no additional Doppler shift between it and the ground station. For example, the 2041.9 MHz signal transmitted from TDRS to the shuttle would be down shifted by a factor of $f'/f = (1 - v/c)$, where v is the relative velocity of separation between the TDRS and the shuttle and c is the speed of light, or as in this case radio wave propagation. The carrier frequency received by the shuttle would be down shifted by this factor, and this would be multiplied by the transponder factor of 240/221 to produce the return carrier frequency of nominally 2217.5 MHz. The return link carrier signal would also experience a Doppler shift in propagating back to the TDRS, so the overall round trip shift would be $f''/f = 2(1 - v/c) * (240/221)$. For typical shuttle re-entry velocities in the range of 5000 m/s, this produces Doppler shifts of approximately –70 kHz at S-band. It should be noted that the Doppler shift arises from the relative motion between the shuttle and TDRS, and that this is in general smaller than the re-entry velocity of the shuttle (as measured against a geostationary reference frame) by a factor which is the cosine of the angle between the shuttle's forward trajectory and its line of sight vector to TDRS.

If the forward link from TDRS to the shuttle were to drop, the transponder would shift over to its own internal local oscillator and continue to transmit telemetry back to TDRS on this frequency. This switch over of the carrier frequency oscillator would normally result in a brief 5 ms or less loss of carrier lock and this would cause up to one entire one second frame of telemetry data to be rejected as invalid by the MCC. The forward link AGC signal in the telemetry data would then show the forward link to have been lost during this time. When the forward link is restored, the transponder oscillator then switches back to a frequency lock on the forward link carrier which is multiplied by the 240/221 factor and used as the return link carrier frequency again. This switch over would once more cause a brief loss of carrier lock and the rejection of up to one full frame of telemetry data by MCC. The loss of a forward link carrier would also cause the Doppler frequency shift to show a jump when the original carrier frequency was restored.

If the return link from the shuttle to TDRS were to drop, no information would be received by MCC during this time, and all of the data displays would show an idle condition, with the last valid data remaining on each display. When the return link comes back after a dropout, the telemetry would indicate the state of the forward link lock flags and the forward link AGC level that existed at the one second frame prior to that instant. This is because there is a one second delay between when the communication receiver creates the lock flags and AGC signal level measurements and when these are interleaved into the telemetry data stream for transmission. If the dropout was brief and the forward link lock flags still show a locked forward carrier signal, then in all probability the forward link was not disturbed during this time. Similarly, because the return carrier signal frequency was not disturbed by a loss of forward lock, the Doppler signal would not show any jumps when the link was restored. For most of the communications drop outs that were observed during the early re-entry flight of STS-107, the Doppler signal did not jump and the forward link lock flags indicated a continued state of lock immediately after the link was restored. This indicates that these communications drop outs were associated with the return link, rather than the forward link.

Ku-band (13.8 GHz) Telemetry

A Ku-band dish antenna is located on a steerable mount within the payload bay. When the shuttle is in its normal orbit about the Earth with the payload bay doors open and the cargo hold facing the Earth, the Ku-band antenna can be used for data telemetry back to the Mission Control Center (MCC) using essentially the same formatting as for the S-band links. The Ku-band dish antenna is considerably more directional and must be accurately pointed to the ground station receiver to establish this link. The Ku-band antenna system also provides a much higher data throughput that is typically used for multiple video signals. However, since the orbiter had its belly to the Earth and the payload bay doors closed during the re-entry flight, the Ku-band antenna system was not in operation.

Calibration

Calibration of the sensor systems on the Space Shuttle Orbiter was designed in principle to be "potentiometer-free," so that there would be no manual adjustments to be made anywhere on the vehicle itself. However, each of the signal conditioners contain some combination of gain, span, offset, and balance adjustments. Some of these potentiometers are accessible through a screwdriver hole; others are potted over after being set to the proper adjustment by the vendor, usually Rockwell. Technicians sometimes adjust these potentiometer settings to bring readings on scale. It is unknown if the overall system is recalibrated after such adjustments.

All raw 8-bit PCM data must be manipulated through software computations on a digital computer, either on board or on the ground, to implement the proper calibration curve for each sensor. The calibration takes the general form of a polynomial of up to 5th order, $f(x) = a_o + a_1x^1 + a_2x^2 + a_3x^3 + a_4x^4 + a_5x^5$, where x is the raw digitized voltage signal from any sensor channel (8 bits), and f(x) is the final calibrated measurement. This system can thus be adjusted to correct for systematic offsets, nonlinearities, and unit scaling in any of the individual sensor measurements. Data from both the orbiter flight instrumentation (OFI) and orbiter experiment

instrumentation (OEX) are handled in this manner. The polynomial coefficients can, in principle, be different for each measurement system ID (MSID), and can, in principle, be different for each of the four Space Shuttle Orbiter vehicles. However, the majority of the sensor MSIDs are calibrated using generic data from the vendor, using transfer function values listed in the specification drawings for each sensor type. These produce calibration curve numbers that can be applied uniformly to a family of sensors. For example, calibration curve number N0432 is used to set the polynomial coefficients for strain gauge V12G9921A, and calibration curve number N1305 is used to calibrate temperature sensor V09T9895A. Calibration curve numbers and their specific polynomial coefficients are maintained in the Boeing MSID database, which is part of the "MML (Master Measurements List) Notebook" and is maintained on the Boeing NASA Systems FSSO database server.

While these calibration coefficients are stored as digital data, and thus do not drift over time, the sensors that they correspond to certainly do. It appears that the orbiter vehicle does not get any periodic recalibration of its sensor polynomial coefficients, nor of the adjustments to the signal conditioners. The specifications for each sensor are in general phrased to have the sensor remain within tight performance bounds for a period of 10 years. Many other sensors, such as pressure and strain, are only guaranteed by the manufacturer to have a 10 year shelf life. Many of these same sensors were installed on the vehicle when it was originally built in 1981 and along with the vehicle's airframe are 22 or more years old. The OEX sensor suite was originally installed for development purposes, and was not intended to be a long-life-span system, although it has produced reliable data up through the present.

Anomalous Events and Time Correlations

Orbiter Flight Instrumentation (OFI) – Telemetry Data

Fuselage Nozzle Temperatures

The fuselage nozzle temperatures were some of the earliest sensors to register anomalous readings among the OFI telemetry data. There are two nozzles on the left side of the fuselage, located just aft of the main bulkhead separating the crew cabin from the payload bay, which are used to discharge waste and supply water. A third nozzle located about 18 inches forward of these two is a vacuum vent. Each of the water nozzles consists of an approximately 2-inch diameter stainless steel plug with a single, approximately 1 mm diameter hole for discharging water. The outer surfaces of the nozzles are nominally flush with the finished surface of the vehicle. The vacuum vent nozzle is slightly smaller, about 1 inch in diameter, and also consists of a single small hole in a stainless steel flush mounted plug. Both the waste and supply water dump nozzles have built-in heaters to raise the nozzle temperatures above 32°F for which the water would otherwise be frozen into ice. Each of the nozzles have two redundant temperature sensors, named A and B, to measure the nozzle temperatures and provide feedback control to the nozzle heaters. The temperature sensors on the water dump nozzles and on the vacuum vent are each RTD type sensors with a range of 0 to 450°F. The supply water dump nozzle is located about 6 inches higher on the side of the fuselage than the waste water dump nozzle. While this difference might seem minor, visual inspection of the orbiter (the Discovery at KSC) showed that the lower waste water dump nozzle is actually much more protected by the leading chine of the left wing. As a result, the waste water dump nozzle typically does not heat up as much as the supply water dump nozzle during re-entry.

Like all of the OFI telemetry data, the readings from these sensors are discontinuous because of the communications drop outs that occurred. For these nozzle temperatures in particular, the anomalous part of the readings consists of a noticeable increase in the rate of the temperature rise for the vacuum vent and the supply water dump nozzle, but not for the waste water dump nozzle. Both the beginning and end of these increased rates of temperature rise happen to occur simultaneously with a communications drop out, and thus, the exact timing of their start and end is imprecise. The communications drop out which precedes the increased rate of temperature rise occurred over GMT 13:52:25 to 13:52:26 (EI + 496 to 497 sec), and then again over GMT 13:52:29 to 13:52:31 (EI + 500 to 502 sec). While the communications were restored briefly over GMT 13:52:27 to 13:52:28 (EI + 498 to 499 sec), the data in this period is not considered valid by the MCC, and thus no data is plotted during these two frames. This communications drop thus appears as a blank spot in the data from GMT 13:52:25 to 13:52:31, corresponding to EI + 496 to 502 seconds. Another communications drop out from GMT 13:52:49 to 13:52:55, corresponding to EI + 520 to 526 seconds, produced a blank spot in the data at about the same time at which the temperature returned to its more normal rate of rise.

Sensor V62T0439A is the supply water dump nozzle temperature B and the data from this sensor followed the normal trends of past vehicle flights up until a communications drop out at GMT 13:52:24 (EI + 495 sec). After the communications link was restored at GMT 13:52:32 (EI + 503 sec), the rate of temperature rise was approximately double and continued up to the next communications drop out at GMT 13:52:48 (EI + 519 sec). After the communications link was restored again at GMT 13:52:56 (EI + 527 sec), the rate of temperature rise had returned to its normal value, although the additional higher temperature did not return to its lower values. Sensor V62T0440A is the supply water dump nozzle temperature A, and the data from this sensor is virtually identical in value and trend as that from V62T039A. This indicates that the anomalous temperature rise is most likely not an artifact from some instrumentation system problem, and that both of these sensors were most likely recording the real temperature of the supply water dump nozzle. This seems to clearly indicate that a higher rate of heating occurred on the supply water dump nozzle in between the two communications drop out periods. Past flight data for these sensors show an increasing rate of temperature rise over EI + 150 to 300 seconds, and then this rate becomes fairly constant over EI + 300 to 800 seconds. The family of past flights bounds this temperature rise rate from (400°F

– 150°F)/(800 sec – 300 sec) = 0.500°F/sec for STS-050 to (400°F – 100°F)/(885 sec – 380 sec) = 0.594°F/sec for STS-087. For STS-107, the nominal rate of rise prior to the anomaly was (200°F – 100°F)/(485 sec – 310 sec) = 0.571°F/sec. In between the two communications drop outs, the anomalous rate of rise was (230°F – 210°F)/(519 sec – 503 sec) = 1.250°F/sec, more than double the rate of rise prior to the loss of communications.

Sensors V62T0519A and V62T0520A are the waste water dump nozzle temperatures, B and A, respectively, and the telemetry data from both of these was virtually identical, indicating a properly functioning measurement system, and also completely in keeping with the values and trends of past flights. As noted, the waste water dump nozzle is somewhat more protected by the leading chine of the left wing, and this nozzle does not experience as much heating during re-entry as the supply water dump nozzle. For STS-107 as well as all past flights, these sensors show an increasing temperature and rate of temperature rise over EI + 150 to 300 seconds. From EI + 300 to 900 seconds, the temperature still steadily increases but the rate of rise slows down. For STS-107, the maximum rate of temperature rise was (125°F – 65°F)/(420 sec – 300 sec) = 0.500°F/sec, which then fell back to (315°F – 280°F)/(900 sec – 780 sec) = 0.292°F/sec just prior to the breakup of the vehicle.

Sensor V62T0551A is the vacuum vent temperature. The re-entry heating that this vent experiences is much less than the water dump nozzles, in spite of its location being farther forward. This is probably due to the vent being physically much smaller than the water dump nozzles, and it may have better conductive heat dissipation from the plumbing immediately behind it. Over the re-entry flight period from EI to EI + 900 seconds this sensor typically records a temperature going from only 62°F to 85°F with the same quantization of approximately 1.4°F per bit as the water dump nozzles. Thus, this telemetry data from this sensor appears coarse because of the much smaller changes in its temperature during the re-entry period. Immediately after the communications link was restored at GMT 13:52:32 (EI + 503 sec), this sensor showed a much higher rate of temperature rise than just before the communications drop out. A normal rate of rise during this period of time would be (55°F – 52°F)/(585 sec – 465 sec) = 0.025°F/sec for STS-087, for example. For STS-107, the anomalous rate of temperature rise was (70°F – 67°F)/(538 sec – 503 sec) = 0.086°F/sec, over three times as great. All prior flights show this vacuum vent temperature as steadily rising with an increasing rate up through EI + 1000 seconds and beyond. Toward the end of this period, the rate of rise reaches values as high as (84°F – 70°F)/(1020 sec – 900 sec) = 0.117°F/sec. However, around the time period of EI + 503 to 519 seconds, none of the prior flights showed any rate of temperature rise near to that recorded by STS-107. Since the vacuum vent is essentially along the line of sight between the waste water dump nozzle and the most forward part of the left wing chine, any abnormal aerothermal vortex spinning off of the nose of the vehicle would affect both of these sensors in similar ways. Because of the similarity in their signatures and their identical timing, such a circumstance is most probably the physical situation which led to their anomalous readings. However, the manner in which this ties into the overall failure scenario for the orbiter is still unclear, and somewhat difficult to understand because these sensors were all located well forward of any of the supposed damaged area of the left wing leading edge.

Main Landing Gear (MLG) Proximity Switches

Four proximity switches are located within each of the main landing gear wheel wells to sense the mechanical position of the main landing gear and door latch moving parts. The sensors are mounted within the wheel well at various places to sense the position of the main landing gear door lock linkage, the main landing gear uplock, the main landing gear strut, and if the main landing gear is compressed with the weight of the vehicle. The wires from the sensors run outside of the wheel well to the electronics packages which convert the analog distance signal to a binary logic level indicating whether the magnetic target piece is near or far from the sensor. The electronics package which performs this operation is known as the "prox box." The prox box can be wired for either standard logic, in which a near target causes the digital output to be a logical "1" (nominally +5.0 Volts), or reverse logic, in which a near target causes the digital output to be a logical "0" (nominally 0.0 Volts).

Sensor V51X0116X, "left main gear door uplocked," is located at the front of the left wheel well on the main landing gear door latch linkage. When the door is closed and locked, so that all of the uplock rollers are captured by their hooks, the target which is attached to the most forward uplock hook is rotated to be in front of the sensor. This sensor is the one of the four which is wired for reverse logic, so that the normal door closed state which puts the target near to the sensor creates a logical "0" output. This sensor remained in the "0" state for the entire time that the telemetry signal was available.

Sensor V51X0100X, "left main gear uplocked," is located on the large inconel uplock arm that retains the left main landing gear strut in the up or stowed position. This sensor is wired for standard logic, and when the left main landing gear strut is captured in the uplock position by this assembly, the target is near to the sensor and the output of the prox box is a logical "1." The output of this sensor remained in a logical "1" state for the entire time of the re-entry flight telemetry.

Sensor V51X0130X, "left main gear no weight on wheels," is located on the left main landing gear strut itself and its wiring is routed along the backside of the strut, along with the wiring for several other sensors. When the vehicle is above the ground, the landing gear is not compressed, and the target remains in front of the sensor. This sensor is wired for standard logic, so that the near condition produces a logical "1" which is interpreted to mean "no weight on wheels" or no-WOW. This sensor also remained in the logical "1" state for the entire duration of the re-entry flight telemetry.
Sensor V51X0125E, "left main gear downlocked," is located on the folding linkage that locks the wheels down when they deploy. This sensor is different from the other three in that when the main landing gear is up and stowed position and the door is closed, the targets are near to the other three sensors, whereas for this sensor, the target is normally far

and then becomes near when the gear locks down. When the main landing gear fully deploys, the target then rotates to be in front of the sensor. The V51X0125E sensor is wired for standard logic, so that when the gear is up and target is far from the sensor, the output is a logical "0." The OFI telemetry data shows that at GMT 13:59:06 (EI + 897 sec), the output from this sensor abruptly transitioned from a "0" to a "1" state. This occurred only 26 seconds prior to the loss of signal (LOS) at GMT 13:59:32 (EI + 932 sec). This is physically inconsistent with the outputs from the V51X0116X sensor which indicated that the door was still locked closed and the V51X0100X sensor which indicated that the main landing gear was still locked in the up position. The wreckage debris showed clearly that the left main landing gear had not deployed and the wheel well door had not opened at anytime prior to the break up and loss of signal (LOS). Burn-through testing of the wires to this sensor showed that a burn-induced short in the wiring between the sensor and the prox box could produce the same transition from a logical "0" to a logical "1" state. The anomalous output transition for this sensor is thus interpreted almost conclusively as being caused by a burn through in the wiring which then caused an electrical short. Normally, a burn-induced soft short in the Kapton wiring would produce a slowly increasing insulation conductance which would be seen over several seconds. However, in the case of the proximity switches, the prox box electronics produce a hard binary decision output, and this threshold level masks any gradual changes in the wiring insulation conductance. All four of the corresponding proximity switch sensors for the right main landing gear remained at their normal values through out the re-entry flight up until the point where the telemetry was lost.

Tire Pressures and Wheel Temperatures

Because of the combination of high vehicle weight (233,995 lbs. on re-entry for STS-107), the comparatively hard landing, and the small number of main landing gear wheels to support the overall vehicle weight and landing forces, each of the four main landing gear tires were designed for and operated at high pressures of nominally 360 psia. Because tire pressure becomes such a critical issue in a safe landing of the vehicle, each of the four main landing gear tires had two redundant pressure sensors which provided continuous telemetry data to the ground. Each of these eight main landing gear tire pressure sensors were part number ME449-0177-1011 and were calibrated to measure absolute pressure over a range of 230 to 401 psia. The eight bit telemetry signal thus produced a bit quantization of 171 psia / 256 = 0.668 psia. The wiring for each of these pressure sensors runs down along the backside of each wheel strut to a break-away harness. The break-away harness consists mainly of a smaller diameter wire which connects the pressure sensors on each wheel to the cable on the strut. As soon as the main landing gear wheels touch the pavement, the wheels begin to spin, and the smaller diameter wire of the break-away harness is severed. Thus, tire pressures can only be monitored up until the point of touch-down. New break-away harnesses are replaced for each flight.

Each of the four tire pressure sensors on the left side of the vehicle showed a wiring burn-through signature in its telemetry data that began around GMT 13:58:27 to 13:58:41 (EI + 858 to 872 sec). An important feature is that the starting and ending times of these burn-through signatures differ, not between individual wheels, but between individual measurement channels. Sensor V51P0571A, the left-hand in-board tire channel 1, showed the first observable abnormality at GMT 13:58:27 (EI + 858 sec), which was a characteristic initially slow and then rapid decrease in signal that reached the off-scale low (OSL) value of 232 psia at GMT 13:58:39 (EI + 870 sec). This signature is characteristic of a wire burn-through in which the Kapton insulation resistance slowly degrades until it produces a "soft short" across the sensor wires, usually over the span of 10-15 seconds. Over nearly the same exact time span, sensor V51P0570A, the left-hand out-board tire channel 1, showed a similar soft short wire burn through pattern, beginning at GMT 13:58:29 (EI + 860 sec) and ending at an OSL value of 232 psia at GMT 13:58:39 (EI + 870 sec). The channel 2 sensors showed a similar trend but were delayed by approximately 10 seconds. Sensor V51P0572A, the left-hand out-board tire channel 2, began its decrease at GMT 13:58:39 (EI + 870 sec) and reached the OSL value of 232 psia at GMT 13:58:51 (EI + 882 sec). Sensor V51P0573A, the left-hand in-board tire channel 2, began its decrease at GMT 13:58:41 (EI + 872 sec), but fell abruptly to an OSL value of 232 psia at the next data point. All four of these tire pressure measurements read a normal value of 354-355 psia prior to the start of the failure signature.

Because of the high tire pressure and large volume of the tires as well, there was initial speculation that a rupture of one of the tires in the left wheel well could have been either a root or contributory cause of the demise of the vehicle. The tire pressure sensor data clearly rules this out, however. If a tire were to have ruptured, either spontaneously or as a result of some other event in the break-up, both pressure sensors on that one tire, i.e. channel 1 and channel 2, would have simultaneously recorded at least the first instant of such an event. However, the channel 1 and channel 2 sensors on the same tire, both for the in-board and out-board tires, show an approximately 10 second delay between their failure signatures. Furthermore, the channel 1 failure signatures on both tires (left in-board and left out-board) are nearly simultaneous and approximately 10 seconds earlier than the channel 2 failure signatures for the same two tires. Thus, it is fairly certain that the recorded failure signatures are those of a soft-short wiring burn through that affected channel 1 slightly before channel 2. There is no evidence in the sensor data that either tire experienced a rupture or even a slight depressurization prior to the failure modes of these tire pressure sensors.

Further confirmation of this conclusion exists in the tire pressure sensor data for the right main landing gear. While each of these four tire pressure sensors recorded an essentially nominal pressure up until the loss of the telemetry signal, upon close examination, all four of these pressure sensors show an unusual momentary 3-bit drop over the same time span of GMT 13:58:34 to 13:58:49 (EI + 865 to 880 sec). Prior flights show some single bit toggling as a normal occurrence for all of the tire pressure sensors, but the three bit drop is not seen in any of these prior flights. Sensor V51P0471A, right-hand in-board tire channel 1, and sensor V51P0470A,

right-hand out-board tire channel 1, both showed a continuous and nominal pressure of 356 psia prior to the three bit drop which began at GMT 13:58:37 (EI + 868 sec), and then returned to this nominal value afterwards. Similarly, sensor V51P0472A, right-hand out-board tire channel 2, and sensor V51P0473A, right-hand in-board tire channel 2, both showed a continuous and nominal pressure of 360-361 psia before and after the three bit drop that started at GMT 13:58:41 (EI + 872 sec). While each of the four three bit drops involves a slightly different shape, the channel 1 drops occur several seconds earlier than the channel 2 drops, again indicating that the anomaly is associated with the common instrumentation wiring of channel 1 versus channel 2, rather than with a particular tire. Because none of the other sensors within the right-hand wheel well give any indication of anomalous events, the simultaneous timing of these three bit drops with the wire burn-through signatures of the left-hand tire pressure sensors indicate that the common instrumentation aspects of the channel 1 versus channel 2 sensors are responsible for the anomalies seen in the right-hand tire pressures.

The temperatures of each wheel of the main landing gear are also measured, primarily to monitor the health of the braking system upon landing. Each sensor is an RTD temperature sensor of part number ME449-0160-0008, and is calibrated to measure temperatures over a range of −75°F to +175°F. The eight bit telemetry signal thus produces a single bit quantization of 250°F / 256 = 0.9766°F. The telemetry data from these four sensors yields a very similar story. Sensor V51T0574A, the left-hand out-board wheel temperature, showed a normal 34°F from EI up to GMT 13:58:27 (EI + 858 sec), after which it showed a characteristic soft short burn through pattern that reach an OSL value of −75°F at GMT 13:58:39 (EI + 870 sec). Sensor V51T0575A, the left-hand in-board wheel temperature, also showed a nominal 34°F from EI up to GMT 13:58:34 (EI + 865 sec), then a soft short burn through signature that reached an OSL of −75°F at GMT 13:58:49 (EI + 880 sec). The pattern between the two temperature measurements was virtually identical, but with the out-board wheel sensor failure occurring several seconds earlier. Sensor V51T0474A, the right-hand out-board wheel temperature, recorded a nominal 42-43°F from EI up until LOS, and sensor V51T0475A, the right-hand in-board wheel temperature, recorded a nominal 39°F from EI up until LOS, also. There were no observable anomalies in the right-hand wheel temperatures.

All of the left-hand tire pressure and wheel temperature failure signatures, as well as the three-bit momentary drops in the right-hand tire pressures, physically fit the circumstances of a Kapton wiring burn-through that produced a soft short in the sensor cabling. This burn-through process was most likely caused by the wiring to one tire or wheel sensor, but the commonality of the wiring and instrumentation channels caused the other measurements in the left-hand wheel well to fail, along with causing a minor perturbation of a few of the sensors in the right-hand wheel well which were also connected to that instrumentation channel. None of the instrumentation telemetry data indicates any rupture of the main landing gear tires, nor of any associated types of events, such as an induced leak which would cause a slower depressurization.

Main Landing Gear (MLG) Hydraulic System Temperatures

Within the left main landing gear wheel well there are also eight hydraulic system temperature sensors that recorded anomalous readings during the re-entry flight. All eight of these are RTD temperature sensors measuring hydraulic line temperatures over the range of −75°F to +300°F. In each case, the RTD sensor was adhesively attached to the stainless steel brake line tubing and covered with a combination of aluminum foil and red RTV-560. Sensors V58T1700A, V58T1701A, V58T1702A, and V58T1703A are sequentially placed along the left main landing gear brake line, designated A, B, C, and D, respectively. A and B are located on the main landing gear strut itself, while C and D are located toward the rear of the inboard wall of the wheel well within a cluster of hydraulic plumbing. Sensors V58T0841A and V58T0842A measure the aft and forward brake switch valve return line temperatures, respectively, and are also located within the inboard rear cluster of hydraulic plumbing. Sensor V58T0405A is located on and measures the temperature of the left main landing gear strut actuator, the large hydraulic cylinder located toward the inboard rear of the wheel well, which is used to hydraulically damp the deployment of the main landing gear, and also to hoist the gear back up into the stowed position. Sensor V58T0125A is located on the main landing gear uplock actuator and measures the hydraulic line temperature to this actuator which holds the main landing gear in the up and stowed position. All eight of these sensors exhibited an off nominal temperature rise at various times during the re-entry flight. Only one appears to have failed outright due to a wire burn through before the loss of signal (LOS) at GMT 13:59:32.

The four brake line temperature sensors exhibited the off normal trends first. Sensor V58T1703A measuring the left brake line temperature D was the first sensor of this group to record an off nominal temperature rise at GMT 13:52:17 (EI + 488 sec). It recorded a nominal 84°F temperature up to this time, after which the temperature rose abnormally to 100°F at the time of the LOS. Similarly, but slightly delayed, sensor V58T1702A measuring the left brake line temperature C recorded an off nominal temperature rise at GMT 13:52:41 (EI + 512 sec), beginning at a value of 70°F and rising ultimately up to 104°F at LOS. At the same moment, sensor V58T1700A measuring the left brake line temperature A recorded an off nominal temperature rise from a nominal value of 125°F that ultimately climbed to 172°F at LOS. Likewise, sensor V58T1701A measuring the left brake line temperature B recorded an off nominal temperature rise at GMT 13:54:10 (EI + 610 sec) that began at a nominal value of 110°F and rose to 154°F at LOS. Each of the corresponding sensors for the right main landing gear brake line temperatures A, B, C, and D, that is, V58T1750A, V58T1751A, V58T1752A, and V58T1753A, respectively, showed essentially a constant and normal temperature over the entire time span of the telemetry data.

The remaining hydraulic system temperature sensors then sequentially recorded similar off normal temperature rises. Sensor V58T0405A measuring the temperature of the left main gear strut actuator body showed an off nominal tem-

perature rise at GMT 13:54:24 (EI + 615 sec) that began at 37°F and ultimately rose to a value of 76°F at LOS. Sensor V58T0842A that measured the temperature of the forward brake switch valve return line showed an off nominal temperature rise at GMT 13:55:12 (EI + 663 sec) that began at 40°F and rose to 67°F at LOS. Sensor V58T0125A measuring the temperature of the left main gear uplock actuator hydraulic line showed an off nominal temperature rise at GMT 13:56:16 (EI + 727 sec) that began at 30°F and rose to 53°F at LOS. Sensor V58T0841A that measured the temperature of the aft brake switch valve return line showed an off nominal temperature rise at GMT 13:57:54 (EI + 825 sec) that began at 45°F and rose to 66°F at LOS. Each of the corresponding temperature sensors for the right main landing gear, V58T0406A, V58T0846A, V58T0128A, and V58T0845A, showed completely normal behavior over the period from EI to LOS.

Only one of these eight sensors showed any evidence of a complete failure mode. Sensor V58T0841A measuring the temperature of the aft brake switch valve return line showed the beginnings of a soft short wire burn through failure mode at GMT 13:59:22 (EI + 913 sec), just 10 seconds prior to LOS. This amounted to only a few bit changes in a downward trend at this point. NASA categorized this as a wire damage trend, but the few bit changes are not fully conclusive of this, since an OSL or OSH condition was never reached.

The primary conclusion to be drawn from this set of eight sensors is that there was a clear source of abnormal heating within the left wheel well as early as GMT 13:52:17 (EI + 488 sec) when the first of these, V58T1703A, started showing a rapid rise in temperature in the brake line. The heating appears to have been distributed throughout the back and inboard side of the wheel well, because of the varied locations of the temperature sensors and the difference in timing in their abnormal rise rates. Because of the heat dissipation capacity of the large metal masses in the wheel well, none of these abnormal temperature rises exceeded 50°F, but all of the temperature sensors showed a significant rise of at least 15°F.

Sensor V58T1700A measuring the left brake line temperature A, in addition to its more drastic abnormal behavior at GMT 13:52:41 (EI + 512 sec), showed a 3-bit (4.5°F), short duration rise at a very early time of GMT 13:47:56 (EI + 227 sec). This short rise, while clearly discernable, was thought to be an even earlier indication of some heating process taking place within the left wheel well. However, past flight data shows that similar short duration rises have occurred over the course of the re-entry flights. Thus, this 3-bit early rise in V58T1700A cannot be conclusively associated with an early breach of the left wheel well area. The sensor V58T1753A measuring the right main gear brake line temperature D also exhibited a few unexplained short duration, small amplitude rises during the re-entry flight. It rose and fell by 4 bits (6°F) over GMT 13:47:54 to 13:48:39 (EI + 225 to 270 sec), and then it rose and fell by 3 bits (4.5°F) over GMT 13:56:14 to 13:57:04 (EI + 725 to 775 sec). The other three right main gear brake line temperature sensors were completely quiet during the same time periods.
NASA has provided some explanation for these small-amplitude, small-duration temperature pulses as originating from a transfer of the hydraulic fluid from a reservoir at one temperature to the line which was at a different temperature, as the temperature pulse then represents the heat transfer associated with the fluid and the line reaching an equilibrium. While no parts of the main landing gear hydraulic system were being actuated during this phase of the re-entry flight, the circulation of neutral pressure hydraulic fluid does provide a reasonable explanation for these temperature variations. The only unexplainable feature of the behavior of these sensors is that they did not appear to completely fail with a wire burn through signature. The wiring for V58T1700A and V58T1701A was routed along the back of the left main landing gear strut, the same as for the tire pressures and wheel temperatures discussed previously. However, all of the tire pressures and wheel temperature sensors did show a wire burn through failure signature, while none of the hydraulic line temperature sensors did so. It is not clear why the soft short burn through process would favor the wires of one type of system over another.

Elevon Hydraulic System Temperatures

The four control surfaces on the shuttle wings, termed "elevons" as a dual purpose combination of elevator and aileron, are hydraulically actuated, and the hydraulic fluid return line temperatures are measured for each, along with the body temperature of the actuator cylinder. Each actuator can be driven by any one of three redundant hydraulic systems, numbered 1, 2, and 3. Each of the three hydraulic system return line temperatures and actuator body temperature for each of the four elevons is measured using an RTD temperature sensor, part number ME449-0160-0001, which are calibrated to measure temperatures over the range of –75°F to +300°F. The 8-bit telemetry data thus gives a quantization of 1.46°F per bit.

The elevon hydraulic system temperatures reveal a wiring burn through pattern within the left wing quite distinctly, because half of the sensors had their wiring routed forward along the wheel well while the other half of the sensors had their wiring routed inboard into the fuselage through an aft interconnect panel. Those with their wiring routed forward along the left wheel well showed a clear burn through failure mode, while those with their wiring routed inboard and aft stayed on-line and responded normally all the way up to the loss of signal (LOS) at GMT 13:59:32.

At GMT 13:53:02 (EI + 533 sec), sensor V58T0394A, the left outboard elevon hydraulic system 3 return line temperature, showed the beginning of a burn-through failure mode which took the measurement to OSL at GMT 13:53:10 (EI + 541 sec). Prior to this, the sensor had been responding normally, following a gentle rise up from 95°F at EI to 125°F when the failure mode began. Simultaneously, sensor V58T0157A, the left inboard elevon hydraulic system 1 return line temperature, which started out at 67°F at EI, showed a burn through failure mode that began at 100°F at GMT 13:53:02 (EI + 533 sec) and which went to OSL at GMT 13:53:11 (EI + 542 sec). Shortly thereafter at GMT 13:53:34 (EI + 565 sec), sensor V58T0257A, the left inboard elevon hydraulic system 2 return line temperature, began a burn

through failure mode which went to OSL at GMT 13:53:36 (EI + 567 sec). This sensor had been following a gentle rise from 135°F at EI up to 160°F when the failure mode began. Simultaneously, sensor V58T0193A, the left outboard elevon hydraulic system 1 return line temperature, which had been constant at 42°F since EI, showed an abrupt drop to OSL at GMT 13:53:34 (EI + 565 sec). All four of these sensors had their cables routed first inboard along the cross spar and then forward, following the service access ports in the cross spars until the harness ran along the upper outside wall of the left wheel well, finally crossing inboard along the 1040 spar to the interconnect panel P65 on the fuselage. This routing took all four of these sensor wires directly in front of the supposed breach area of the leading edge spar behind RCC panel # 9, along side many other sensor cables which also appear to have failed during this same general time period.

In contrast, sensor V58T0883A, the left outboard elevon hydraulic system 2 return line temperature, remained nearly constant from 72°F at EI to 74°F at LOS. Sensor V58T0833A, the left inboard elevon hydraulic system 3 return line temperature, followed a smooth and normal rise from 50°F at EI up to 100°F at LOS. Sensor V58T0880A, the left outboard elevon actuator body temperature, showed a smooth and normal rise from 63°F at EI up to 108°F at LOS. And similarly, sensor V58T0830A, the left inboard elevon actuator body temperature, showed a smooth and normal rise from 86°F up to 141°F at LOS. Even though these four sensors were physically located in essentially the same places as the preceding four, none of these showed any burn through failure modes, all remained on-line all the way up until the LOS, and all of their readings were normal as compared to prior flights of the vehicle. The difference is that their wiring cables were routed all the way inboard, aft of the left wheel well, and entered the fuselage at an aft interconnect panel. These sensor's cables thus did not pass anywhere near to the supposed breach area farther forward on the left wing leading edge.

All eight of the corresponding temperature sensors on the right wing showed perfectly normal responses over the entire time from EI up until the LOS. These included: V58T0359A, the right inboard elevon hydraulic system 3 temperature which went from 125°F to 156°F; V58T0159A, the right inboard elevon hydraulic system 1 temperature which went from 62°F to 82°F; V58T0933A, the right inboard elevon hydraulic system 2 temperature which went from 80°F to 84°F; V58T0930A, the right inboard elevon actuator body temperature which went from 72°F to 120°F; V58T0294A, the right outboard elevon hydraulic system 2 temperature which went from 127°F to 171°F; V58T0194A, the right outboard elevon hydraulic system 1 temperature which remained at a constant 28°F; V58T0983A, the right outboard elevon hydraulic system 3 temperature which went from 42°F to 70°F; and V58T0980A, the right outboard elevon actuator body temperature which went from 82°F to 134°F. All eight of these temperature measurements followed a smooth and uniform rise from EI to LOS and were completely within the expected patterns of prior flights of the vehicle.

While each of the elevons can be actuated by any one of the three redundant hydraulic systems, during normal flight, these hydraulic systems are selected in mixed sets. The primary system, which was operating during the re-entry flight, consists of hydraulic system 3, V58T0394A, for the left outboard elevon, hydraulic system 2, V58T0257A, for the left inboard elevon; hydraulic system 3, V58T0359A, for the right inboard elevon; and hydraulic system 2, V58T0294A, for the right outboard elevon. During the re-entry flight, there are two principal time periods when the elevons are being actuated to effect rolls of the vehicle. The first of these occurs over GMT 13:48:09 to 13:50:09 (EI + 240 to 360 sec), and each of these four hydraulic return line temperatures for the primary system showed some slightly erratic temperature readings during this period. The second period occurs over GMT 13:56:09 to 13:57:09 (EI + 720 to 780 sec), and both of the right hydraulic return line temperatures for the primary system showed similar erratic behavior. By this time, both of the cables to the other two primary hydraulic return line temperature sensors had burned through and were off line. For completeness, the secondary hydraulic system is composed of all four of the hydraulic system 1 lines, V58T0193A, V58T0157A, V58T0159A, and V58T0194A. The tertiary hydraulic system is composed of hydraulic system 2, V58T0883A, for the left outboard elevon; hydraulic system 3, V58T0833A, for the left inboard elevon; hydraulic system 2, V58T0933A, for the right inboard elevon; and hydraulic system 3, V58T0983A, for the right outboard elevon.

The temperatures of the three hydraulic system fluid reservoirs that are located inside the aft fuselage are also included with the OFI telemetry data. Each of these three sensors are RTD temperature sensors, part number ME449-0156-0003, and are calibrated to measure temperatures over the range of –75°F to +300°F. Sensor V58T0101A, on hydraulic system reservoir 1, showed a perfectly normal and smooth rise from 94°F at EI up to 178°F at the LOS. Sensor V58T0201A, on hydraulic system reservoir 2, measured a normal and smooth rise from 127°F at EI up to 169°F at LOS. Similarly, sensor V58T0301A, on hydraulic system reservoir 3, also showed a normal and smooth rise from 84°F at EI up to 141°F at LOS. All three of these temperature measurements were completely consistent with the expected patterns of past flights.

Skin Temperatures

The OFI telemetry data included a number of measurements of the orbiter skin temperatures. The V09T set included 23 temperature measurements over the wing and fuselage skin, the V34T set included 18 temperature measurements over the fuselage, primarily the mid-body section, and the V37T set included 4 temperature measurements over the payload bay doors. In each of these cases, a "skin" temperature refers to the temperature at the bond line where the heat tiles are bonded to the aluminum vehicle skin, and not the actual surface temperature of the heat tiles or friable surface insulation. Because of the lower temperatures experienced along the bond line, RTD temperature sensors were used for each of these measurements, using either part number ME449-0160-0001 or ME449-0160-0008. All of these were calibrated for the temperature range of –200°F to +450°F. The 8-bit telemetry data gave a bit quantization of 650°F / 256 = 2.45°F. From all of these temperature measurements, only six appeared to show any anomalous behavior from the trends of prior flights of the vehicle. There were also a total of 47 temperature mea-

surements within the engine compartments of the left and right OMS pods, set V43T, but all of these measurements, being inside the OMS pods, were completely consistent with the trends of prior flights of the vehicle.

Three of the skin temperature sensor readings involved clearly defined wiring burn through failure modes. Sensor V09T1006A, the left inboard elevon lower skin temperature, started at a reading of 11°F at EI, and then dropped by 1 bit to 8°F at GMT 13:52:56 (EI + 527 sec), at which point it exhibited a wire burn through failure mode which took it to an OSL value of –200°F at GMT 13:52:59 (EI + 530 sec). This burn through process took only 3 seconds and was thus comparatively quick. Sensor V09T1002A, the left lower wing skin temperature, began by reading 6°F at EI which increased slowly to 10°F at GMT 13:56:03 (EI + 714 sec), when it began to show a wire burn through failure mode. This was a very slow burn through process which finally reached an OSL value of –200°F at GMT 13:57:28 (EI + 799 sec). Similarly, the corresponding sensor at the same X-Y location on the left wing but on the upper surface, V09T1024A, the left upper wing skin temperature, began with a reading of 0°F at EI which then increased slowly to a value of 20°F at GMT 13:56:24 (EI + 735 sec), when it also began to show a wire burn through failure mode. This burn through process was also rather long in duration, with the reading finally going to an OSL value of –200°F at GMT 13:57:43 (EI + 814 sec). It is noteworthy that the wiring from each of these three temperature sensors was routed within the same harness which passed along the upper outside wall of the left wheel well, the point at which most of the sensor wiring burn throughs are thought to have taken place.

The other three anomalous skin temperature sensor readings each involved a change in the rate of the temperature rise, one of which was clear and drastic, while the other two were more subtle. Sensor V09T1724A, the left aft fuselage sidewall temperature, measured at section X1410, began at a reading of 31.5°F at EI and then started a normal rise at GMT 13:50:34 (EI + 385 sec). At GMT 13:54:22 (EI + 613 sec), the reading was 42°F and the rate of temperature rise approximately doubled, reaching a final value of 71.5°F at LOS, which was about 10-15°F hotter than what it would have reached if the original slope would have continued. Sensor V34T1106A, the left mid fuselage bond line side temperature at section X1215, started with a value of 20°F at EI and at GMT 13:54:22 (EI + 613 sec), the same timing as the preceding sensor, the reading increased rapidly from 20°F to 90°F at LOS. This was a 25 bit increase over this time period which was quite different from past flights in which the reading only increased by 6-7 bits. This V34T1106A sensor also exhibited an anomalous and abrupt spike up to 280°F over GMT 13:50:07 to 13:50:09 (EI + 358 to 360 sec), after which it appeared to react normally. This may have been a transient within the instrumentation or telemetry system, as there were a few other sensors which showed a similar abrupt spiking over the precise same three second time interval. Sensor V34T1118A, the mid fuselage left sill longeron temperature at section X1215, started at a value of 21.2°F at EI and at GMT 13:55:41 (EI + 692 sec), began a more rapid rise up to a value of 29.0°F at LOS. This was a fairly subtle off nominal rate of temperature rise, producing a 3 bit rise, whereas prior flights only produced 1-2 bits over the same period.

None of the other V09T, V34T, or V37T temperature measurements showed any anomalous behavior in comparison to prior flight data. Corresponding to V09T1002A and V09T1024A on the lower and upper left wing, were V09T1000A and V09T1004A on the lower and upper right wing, respectively. Sensor V09T1000A chattered between 1.0-3.5°F at EI and then at EI + 720 seconds started a smooth rise from 1.0°F to 7.5°F at LOS. Similarly, sensor V09T1004A also chattered between –2.0°F and –4.0°F at EI and then at EI + 300 seconds began a smooth rise from –2.0°F to +21°F at LOS. This was normal behavior for both sensors.

A variety of temperature measurements were made along the forward and mid sections of the fuselage, all of which also appeared to be completely consistent with prior flight data. These included V09T1008A, lower centerline front web temperature at X582; V09T1010A, front side cap temperature at X582; V09T1012A, forward fuselage left bond line temperature at X480; V09T1016A, mid fuselage bottom left bond line temperature at X620; V09T1018A, upper fuselage cap temperature at X576; V09T1020A, forward RCS upper skin temperature; V09T1022A, mid fuselage bottom left bond line temperature at X777; V09T1026A, lower center skin temperature; V09T1028A, right OMS pod skin temperature; V09T1030A, left OMS pod skin temperature; V09T1510A, right forward fuselage RCS skin temperature; V09T1514A, left forward fuselage RCS skin temperature; V09T1524A, forward fuselage upper skin centerline temperature; V09T1624A, forward fuselage lower skin bottom centerline temperature; V09T1702A, aft fuselage floor bottom centerline temperature; and V09T1720A, right aft fuselage sidewall temperature. The last of these, V09T1720A, is the right side equivalent of V09T1724A, which showed an anomalous rate of temperature rise. Sensor V09T1720A started at a reading of 19°F at EI and then rose smoothly to a value of 52°F over EI + 210 seconds to LOS. This pattern was also nominal for most of the sensors in the V09T set, that is, beginning at a fairly low temperature of 10-35°F at EI, staying constant for several minutes, and then slowly and smoothly climbing up to their peak value which occurred at LOS. Overall temperature rises were in the range of 10-30°F.

Similar behavior was found for most of the V34T set. These included: V34T1100A, lower right web temperature at X582; V34T1102A, mid fuselage left bond line temperature at X650; V34T1104A, mid fuselage right bond line temperature at X650; V34T1108A, mid fuselage right bond line temperature at X1215; V34T1110A, mid fuselage lower aft skin temperature; and V34T1112A, mid fuselage bottom center bond line temperature. Sensor V34T1108A is the right hand mate to sensor V34T1106A which exhibited an anomalous rate of temperature rise. Sensor V34T1108A recorded an initial temperature of 11°F at EI and this then rose to a value of 24°F over the period of EI + 420 seconds through LOS, all of which was completely nominal behavior.

Six temperature sensors were placed on the mid fuselage sill longerons: V34T1114A, on the left at X650; V34T1116A,

on the left at X1030; V34T1118A, on the left at X1215; V34T1120A, on the right at X650; V34T1122A, on the right at X1030; and V34T1124A, on the right at X1215. Except for V34T1118A, which showed the anomalous rate of temperature rise that resulted in an overall 3 bit rise, each of these other five showed a perfectly normal behavior in comparison to past flights, starting out in the range of 8-15°F, and rising up to a final value of 13-18°F at LOS. Sensor V34T1114A increased by 2 bits, while the other four increased by only 1 bit over the period from EI to LOS.

Five sensors were placed around the circumference of the fuselage structural frame at the X582 cross section. These included: V34T1126A, left side temperature; V34T1128A, left upper mid temperature; V34T1130A, right side temperature; V34T1132A, right upper mid temperature; and V34T1134A, right upper off center temperature. Because all five of these sensors were inside the skin of the fuselage, they only experienced an overall temperature increase of 1-2 bits over the period from EI to LOS. All five exhibited normal behavior.

Four sensors were placed on the payload bay doors on the top of the vehicle. These included: V37T1000A, payload left forward skin temperature; V37T1002A, payload right aft skin temperature; V37T1004A, payload left aft skin temperature; and V37T1006A, payload right forward skin temperature. Each of these exhibited normal behavior, starting out at –20°F to 0°F and rising by approximately 10°F to final values in the range of –10°F to +10°F at LOS.

Communications Drop Outs

One of the earliest indications of abnormal conditions during the re-entry, prior to the recovery of the OEX recorder data, was the series of communication drop outs that occurred while the orbiter was still over the Pacific Ocean. Many of these occurred close to the timing of various observed debris shedding events, suggesting that the shed debris could have blocked, attenuated, or scattered the S-band telemetry signal between the SSO and the TDRS. It is known, for example, that the fine metal particles in the plume from the solid rocket boosters (SRBs) strongly scatter and attenuate RF signals. Similarly, chaff that is used by the military consists of fine metal particles that are used to confuse enemy radars. An obvious speculation is that the vaporized aluminum spar materials might cause a similar effect on the communications links between the SSO and TDRS.

There are, however, numerous other physical mechanisms which could contribute to causing the communication links to drop out. First, the overall link margins during the re-entry flight are rather low to begin with. The received signal power is typically –112 to –114 dBm, and when the signal power falls to –122 to –124 dBm, bit errors in the transmission become frequent enough that valid data flow becomes interrupted. During the first six minutes past EI, the received bit energy to noise density ratio E_b/N_o for the SSO to TDRS-171 link typically varies from +13 to +19 dB, and then decays to +10 to +16 dB over the next ten minutes. After that, the link margins become sufficiently degraded that numerous communication link dropouts are commonplace. Angling off of the high gain direction of a given antenna can cause a reduction of 4 to 6 dB, and this in general occurs for look angles that have elevations greater than +80° (pointing straight ahead toward the nose of the vehicle would be +90°), or less than –70° (pointing directly aft toward the tail of the vehicle would be –90°). The plasma flow around the orbiter during re-entry is also a factor. This plasma sheath raises the ambient noise floor around the vehicle and thus reduces both the forward and return link margins. The much higher plasma density under the belly of the orbiter also renders the lower four antennas unusable during the re-entry flight. Since the orbiter flies through most of the re-entry path with a pitch of approximately 40°, the nose is pointed high into space and the best look angles for any of the S-band antennas are toward the rear which provides high gain looking toward the West horizon. This direction is also in the draft zone of the orbiter for which plasma accumulation is minimal. Radio frequency interference (RFI) arising from either ground or space sources can also corrupt the communication links. On the positive side, however, the S-band frequency of around 2.1 GHz incurs a particularly low atmospheric attenuation. Signal transmission from the surface of the Earth into low Earth orbit (LEO, typically 100 to 200 km altitudes, and farther out than what the shuttle ever reaches) incurs a signal loss of only 5 to 10 percent at frequencies in the range of 2.0-2.4 GHz, hence the popularity of this frequency range for satellite communications.

For a normal re-entry flight, as the orbiter executes various roll maneuvers, there are several switches that occur between different S-band antennas to maintain high gain signal reception from TDRS-171 which would be seen looking aft of the vehicle toward the West horizon. From entry interface (EI) up to about EI + 100 seconds, the upper right forward (URF) S-band antenna is active. From about EI + 100 seconds to EI + 350 seconds, the link is switched to the upper right aft (URA) antenna. From about EI + 350 seconds to EI + 650 seconds, the upper left aft (ULA) antenna is used, and then the upper right aft (URA) antenna again up until about EI + 800 seconds. Beyond this time, the link margins have degraded to the point where communication drop outs are frequent and actual two-way communication with the vehicle becomes spotty at best. For most of the prior flights, continuous communications were maintained up until this point where the link margins degraded. For STS-62, continuous communications remained up until EI + 840 seconds. For STS-73, communications remained up until EI + 940 seconds, although this flight did experience some 20 second long drop outs at approximately EI + 720 and EI + 840 seconds. For STS-78, communications were continuous up until EI + 830 seconds, and for STS-90, communications did not drop out until EI + 920 seconds. The orbiter's initial attitude at EI is a pitch up of approximately 40° with zero roll and zero yaw. Over approximately EI + 320 to EI + 350 seconds the orbiter executes a right roll to about +70° while maintaining the same pitch and yaw. This roll forces a switch over from the URA to the ULA antenna. After descending for several minutes, the orbiter then, over approximately EI + 740 to EI + 770 seconds, executes a reverse roll from right +70° to left –70° while still maintaining the same pitch and yaw. Just prior to initiating this roll reversal, the communications link is switched back from the ULA to the URA antenna for the duration of the re-entry. Several

minutes later, the communications links usually drop out as the link margin has degraded too far by that point.

For flight STS-107, the first 350 seconds past EI showed normal communications link behavior. The switch from the URF to the URA antenna occurred at GMT 13:46:16 (EI + 127 sec). Prior to and following this antenna switchover, the received signal strength of the forward link AGC showed a healthy signal, the return link frame counts were reading 100/100, and the return link E_b/N_o showed a healthy and nearly constant signal to noise ratio.

The anomalous communication drop outs began immediately after the completion of the first rightward roll when the S-band antenna was switched from URA to ULA at GMT 13:50:00 (EI + 351 sec). At this moment, the orbiter was a distance of 38,082 km away from TDRS-171 to the West. The major telemetry frame at this second had only 81 of its 100 minor frames lock on the primary integrated receiver (IR-A), and only 28/100 minor frames lock on the secondary integrated receiver (IR-B). The frame synchronization signal was present throughout on IR-A, but was lost on IR-B. This can be interpreted to mean that 81% of the telemetry data of that major frame was received on the primary receiver, and only 28% of the telemetry data was received on the secondary receiver. The MCC front end processor (FEP) rejects the entire frame of telemetry data as invalid whenever the frame lock count falls below 95/100 on either receiver. This is the definition of a communications drop out in this context. The antenna switchover is normally accomplished in only 5 ms, however this switching is not timed to match to any convenient point in the framed data. The antenna switchover should in principle corrupt only one minor frame, but if the switching took significantly longer, several minor frames could be corrupted. If more than five minor frames were to have been corrupted, implying an antenna switchover that took more than 50 ms to settle, then an official communication drop out would be declared by the MCC FEP. The antenna switching is accomplished using mechanical relays, and switch closure and opening times of 50 ms or longer could certainly be possible, particularly if the relay mechanism is old, dirty, or the solenoid pulser has become weak. On this basis NASA has explained this first communications drop out as being a direct result of the antenna switchover. However, in this instance, the two integrated receivers behaved quite differently, with IR-A losing only a few minor frames and IR-B losing most of them. An antenna switching issue would be thought to affect both integrated receivers in the same manner, while a decaying signal strength or increasing noise level could produce different effects within the two receivers.

The second communications drop out occurred over GMT 13:50:04 through 13:50:06 (EI + 355 through 357 sec). During the middle of this three second outage, both integrated receivers lost frame synchronization and the minor frame counts dropped to 9/100 and 5/100. Since the outage was greater than one second, the Doppler signal was lost for the last two of the three seconds, but it recovered without any noticeable jump in frequency. Similarly, the E_b/N_o estimators for both integrated receivers also fell to zero for the last two of the three second outage. NASA suggested that this second communications drop out could have been caused by a loss of the forward link which they say dropped out over GMT 13:50:03 through 13:50:06. However, if the forward link were to have been lost over this period, the transponder in the shuttle would have switched over to its local oscillator and then when the forward link returned, switched back to a frequency locked carrier at 240/221 times the received forward link frequency. This switchover in return carrier frequency would have created a jump in the Doppler signal which was not observed.

Communications drop out #3 occurred over GMT 13:50:16 through 13:50:22 (EI + 367 through 373 sec). Both receivers showed an immediate loss of frame synchronization and both showed minor frame counts that went essentially to zero for the middle 5 seconds of the seven second drop out. In this instance and in all subsequent ones, the responses of both integrated receivers were essentially identical.

Communications drop out #4 occurred over GMT 13:50:25 through 13:50:28 (EI + 376 through 379 sec). Both integrated receivers recorded exactly the same behavior, with zero minor frame counts and no frame synchronization over the middle two of the four second drop out.

Communications drop out #5 seems hardly a drop out at all. At GMT 13:50:42 (EI + 393 sec), both integrated receivers recorded a minor frame count of 94/100; one minor frame short of the 95 needed to constitute a valid frame. Neither receiver lost frame synchronization, nor had the E_b/N_o estimator fall. As minor as this drop out was in nature, there is very little of any consequence that can be associated with it.

Communications drop out #6 occurred over GMT 13:52:09 through 13:52:15 (EI + 480 through 486 sec). Both integrated receivers recorded exactly the same behavior, with the minor frame count dropping to zero over the middle five seconds, and the frame synchronization being lost over EI + 480 through 485 seconds. Doppler data and the E_b/N_o estimator also fell to zero for both receivers over EI + 480 through 485 seconds. Doppler data returned at EI + 487 seconds, without any major deviation from its prior readings, as would be expected if the forward link were to have remained intact over this drop out period.

Communications drop out #7 was by formal definition only two seconds in length and occurred over GMT 13:52:25 through 13:52:26 (EI + 496 through 497 sec). In this case, the primary integrated receiver IR-A lost the frame synchronization over EI + 496 through 498 seconds, while the secondary integrated receiver IR-B only lost the frame synchronization over the EI + 496 second alone. The IR-A thus lost Doppler data at EI + 497 while the IR-B kept continuous Doppler data. Both integrated receivers had their minor frame count fall to 32/100 at EI + 496, but at EI + 497, the IR-A frame count fell to zero while the IR-B frame count climbed back up to 79/100. At GMT 13:52:27 (EI + 498 sec), the IR-A frame synchronization and minor frame count were still both zero, but the IR-B frame synchronization was locked and a full 100/100 minor frames were counted, yielding a valid telemetry signal for the secondary (IR-B) receiver. Thus, this communication drop formally ended when the telemetry signal returned on the secondary integrated receiver, even

though the signal from the primary integrated receiver was completely dead. At GMT 13:52:28 (EI + 499 sec), the IR-A frame synchronization returned and it had a minor frame count of 25/100, an improving signal, although not yet good enough to produce valid telemetry.

Communications drop out #8 was only three seconds in duration and occurred over GMT 13:52:29 through 13:52:31 (EI + 500 through 502 sec). At EI + 500 seconds, both integrated receivers lost frame synchronization and both of their minor frame counts fell to 22/100. At EI + 501 seconds, both frame synchronizations and minor frame counts were zero. At EI + 502 seconds, the IR-B frame synchronization returned and its minor frame count went up to 25/100, while the IR-A was still zero on both scores. At EI + 503 seconds, both integrated receivers had frame synchronization, the IR-B minor frame count was back up to 100/100, but the IR-A minor frame count had only returned to 25/100. At EI + 504 seconds, both integrated receivers had frame synchronization and 100/100 minor frame counts. The period from GMT 13:52:25 through 13:52:31 (EI + 496 through 502 sec) is thus formally defined to be two communications drop outs, but clearly this period constitutes one overall event expressing the same effects on the communications links. The unusual feature of this particular pair of drop outs (#7 & #8) is that the two integrated receivers behaved quite differently, with the IR-A performance being significantly poorer than that of the IR-B. In so far as the IR-A receiver was concerned, this event would have been one continuous drop out from EI + 496 through 503 seconds. In nearly all of the other communications drop outs, the performance of both integrated receivers was nearly identical, with the only other slight exception being within drop out #2, where for one second the IR-A appeared to out perform the IR-B. This could be explainable by the two integrated receivers simply having closely matched, but slightly different, levels of signal lock range, whereby a small drop in the overall signal to noise ratio would loose lock and frame count in one receiver but not the other. The E_b/N_o estimators provide some evidence of this, with a fairly sharp threshold for which the frame synchronization is lost, typically between an E_b/N_o value of +10 to +11 dB. The minor frame counts begin to drop from 100/100 at E_b/N_o values in the range of +13 to +14 dB.

Communications drop out #9 occurred over GMT 13:52:49 through 13:52:55 (EI + 520 through 526 sec). At EI + 520 seconds, IR-A lost frame synchronization and its minor frame count fell to 42/100, while IR-B retained frame synchronization and recorded a minor frame count of 41/100. At EI + 521 seconds, both integrated receivers lost frame synchronization, IR-A counted zero minor frames and IR-B counted only 1/100. Over the next four second periods, both receivers have no frame synchronization and no minor frame counts. Then at EI + 526 seconds, both receivers regained frame synchronization and both had frame counts of 25/100. At GMT 13:52:56 (EI + 527 sec), the communications link was fully restored with both receivers in full frame synchronization and recording 100/100 minor frames. Although the secondary integrated receiver (IR-B) held on to the signal just slightly longer than the primary (IR-A), the two receivers were in large part tracking each other very closely over this drop out. At GMT 13:53:28 (EI + 559 sec), the ground track of the orbiter passed from over the Pacific Ocean into California.

Communications drop out #10 was only three seconds long and occurred over GMT 13:53:32 through 13:53:34 (EI + 563 through 565 sec). Both integrated receivers behaved exactly the same over this period, losing frame synchronization over EI + 563 to 564 seconds, and having their minor frame counts fall to 9/100 at EI + 563 sec, zero at EI + 564 sec, and the climb back up to 25/100 at EI + 565 seconds. Both the Doppler signal and the E_b/N_o estimator fell to zero over the last two seconds of the drop out, but returned immediately thereafter to nearly their original values without any noticeable jumps.

It is of note that following communications drop out #10, visual ground observations of debris shedding from the orbiter were made. Debris event #1 was sited at GMT 13:53:46 (EI + 577 sec); debris event #2 occurred at GMT 13:53:48 (EI + 579 sec); debris event #3 occurred at GMT 13:53:56 (EI + 587 sec); debris event #4 occurred at GMT 13:54:02 (EI + 593 sec); and debris event #5 occurred at GMT 13:54:09 (EI + 600 sec).

Communications drop out #11 was the longest at nine seconds and occurred over GMT 13:54:14 through 13:54:22 (EI + 605 through 613 sec). Both integrated receivers behaved in an identical fashion over this period. At EI + 605 seconds, the minor frame counts went to zero, although frame synchronization remained. At EI + 606 seconds, the frame synchronization was lost, and only one minor frame was counted on both receivers. Both frame synchronization and minor frame counts remained completely dead until EI + 613 seconds when the frame synchronization was restored and the minor frame count came back up to 25/100 on IR-A and 24/100 on IR-B. Communications were fully functional again at GMT 13:54:23 (EI + 614 sec). All eleven of these communications drop outs had thus far occurred while the upper left aft (ULA) S-band quad antenna was active. At GMT 13:54:26 (EI + 617) the antenna was switched from the ULA to the URA, coincident with the ground track of the vehicle passing from California into Nevada. While there might have been some question as to whether the ULA quad antenna might have been injured to cause these communications drop outs over the already fading re-entry link, the subsequent drops of precisely the same pattern in the URA antenna appear to rule out this possibility. There is no indication that either of the ULA or URA antennas were damaged. Damage to the antennas from any impacts during flight is also a remote possibility, as none of the S-band antennas are actually exposed to the outer surface. Each antenna is covered by heat tiles, and the RF signal propagates through the heat tiles with little attenuation. Foreign matter striking the orbiter over one of the antenna areas might damage the associated heat tiles, but would most likely not damage the antenna quad underneath.

At GMT 13:54:33 (EI + 624 sec), the first of the flashes around the envelope of the vehicle was observed from the ground. Following shortly thereafter, additional debris shedding was also observed. Debris #6 was sited at GMT 13:54:36 (EI + 627 sec); debris #7 occurred at GMT 13:55:07 (EI

+ 658 sec); debris #8 occurred at GMT 13:55:24 (EI + 675 sec); debris #9 occurred at GMT 13:55:27 (EI + 678 sec); and immediately following, debris #10 occurred at GMT 13:55:28 (EI + 679 sec).

Communications drop out #12 occurred 5 seconds after debris #10, and lasted for three seconds over GMT 13:55:33 through 13:55:35 (EI + 684 through 686 sec). This occurred just after the orbiter's ground track crossed into Utah at GMT 13:55:30 (EI + 681 sec). The second before the formal drop out at EI + 683 sec, the IR-A minor frame count fell to 97/100 and the IR-B minor frame count fell to 98/100. At EI + 684 sec, IR-A had lost frame synchronization and had a minor frame count of only 1/100, while IR-B still retained frame synchronization but had a zero minor frame count. At EI + 685 sec, both integrated receivers had lost frame synchronization, IR-A had a zero minor frame count, and IR-B had a minor frame count of only 1/100. At EI + 686 sec, both integrated receivers had reacquired frame synchronization and their minor frame counts had climbed back up to 25/100 and 24/100. At EI + 687 sec, full communications were restored on both integrated receivers. Although this drop out was now while the URA antenna quad was in use, it had precisely the same behavior as the drop outs from the ULA antenna quad.

In between communications drop outs #12 and #13, several more debris shedding events were observed from the ground. Debris #11 was observed at GMT 13:55:39 (EI + 690 sec); debris #12 occurred at GMT 13:55:47 (EI + 698 sec); debris #13 occurred at GMT 13:55:57 (EI + 708 sec), one second after the ground track crossed into Arizona; and debris #14 occurred two seconds later at GMT 13:55:59 (EI + 710 sec).

Communications drop out #13 occurred immediately following debris #14 and was four seconds long, occurring over GMT 13:56:00 through 13:56:03 (EI + 711 through 714 sec). Both integrated receivers behaved in an identical fashion, to within a minor frame count of one another. At EI + 711 sec, frame synchronization was lost and minor frame counts fell to 34/100 and 35/100. The frame synchronization and minor frame counts were zero for both integrated receivers for the middle two seconds of the drop out, and then at EI + 714 sec, frame synchronization was restored and the minor frame counts climbed back up to 26/100 and 24/100. At EI + 715 sec, both integrated receivers had fully restored communications links.

Shortly following communications drop out #13, debris shedding event #15 was seen from the ground at GMT 13:56:11 (EI + 722 sec).

Communications drop out #14 was three seconds in duration and occurred over GMT 13:56:55 through 13:56:57 (EI + 766 through 768 sec). Just prior to this drop out, the orbiter executed a roll reversal from the right to the left over GMT 13:56:30 through 13:56:55 (EI + 741 through 766 sec) which caused the URA quad antenna look angle to become slightly closer to the vertical stabilizer with an elevation of less than –60°. This is known to reduce the communication link margins and could be a contributing cause to communications drop out #14.

At this point, immediately following drop out #14, the forward link AGC signal strength level dropped out for an extended period of 30-40 seconds and then only returned sporadically for the remainder of the recorded re-entry flight. At this phase of the re-entry flight, the communication link margins have degraded to the point where further communication drop outs are common and considered normal in comparison to prior flight history. Between approximately GMT 13:57:30 to the formal loss of signal (LOS) at 13:59:32, another ten distinct communications drop outs were recorded as a period where one or the other of the integrated receivers recorded less than 95/100 valid minor frames. NASA categorized all ten of the communications drop outs within this time frame as "in family."

Over the period of GMT 13:59:31 through 13:59:38 (EI + 922 through 929 sec), just following the formal LOS, a brief and weak S-band communication signal was picked up through TDRS-047 to the East. The minor frame count on IR-A only climbed up to a maximum of 91/100 at GMT 13:59:36 (EI + 927 sec), and this was close, but still not sufficient, for any data validation by the MCC. This at first appeared unexpected, because the URA quad antenna was active during this time, and thus looking aft, not forward to where TDRS-047 would have been located. However, the radiation patterns of the upper aft S-band quad antennas do exhibit a side lobe towards the nose of the vehicle. The line of sight to TDRS-047 at this time would have been an elevation of +55° (pointing straight ahead toward the nose of the vehicle would be +90°), and an azimuth of 140° (pointing to the right of the vehicle would be +90° and pointing straight up out of the payload bay would be 0°). The calculated antenna gain for the URA quad would be only –6.00 dB or less, as this particular orientation does not catch much if any of the forward looking side lobe. The maximum gain of the side lobe is between –2.00 and 0.00 dB, and occurs at an elevation of +85° and an azimuth of 35° to 105°. Thus, the side lobe gain itself cannot account for pulling in the TDRS-047 signal. NASA calculations on the antenna gain to TDRS-047 show that it began at –14.8 dB at GMT 13:58:00 and steadily rose to approximately –7.5 dB at GMT 13:59:35. NASA also calculated that the required antenna gain to produce the measured frame synchronization values would be –6.9 dB. It is thus quite possible that the necessary link margin was present to have produced the observed minor frame counts via TDRS-047 over this period. These calculations did not include any attenuation from the plasma sheath, but this effect would seem likely since the pointing angle would have been forward. The plasma attenuation is known to behave in an unsteady fashion, so it still remains quite possible that a brief opening in the plasma sheath could have allowed the TDRS-047 link to be marginally connected. Regardless, the computed link margins and antenna gains are very close to fully explaining this event.

Shortly following the official LOS point, the orbiter S-band antenna was switched from the URA to the URF quad antenna. Within the period of GMT 14:00:05 through 14:00:10 (EI + 956 through 961 sec), the minor frame count climbed up to approximately 60/100, but this was insufficient to provide valid telemetry data to the MCC, so the LOS signal represents the last point of any valid data, although not actu-

ally the point of no signal whatsoever. Only one second of any data was received, by way of TDRS-171 to the West, and this was only sufficient to validate the OI talk-back, part of which indicated that the orbiter had in fact made this antenna switchover. Due to the diminishing information at this point in the re-entry flight, very little can be concluded from this brief communications reconnection. The antenna pattern from the URF quad would have given a lower gain of –6.00 dB or less for look angles to TDRS-171 to the West, and this could have occurred over a very wide range of possible orientations. Analysis of the communications margins shows that only –6.9 dB of antenna gain would be needed to account for the measured minor frame counts. In this instance like the previous one, the event can be fairly well explained by the computed link margins and antenna gains present at that point in the re-entry flight.

Although not discussed by NASA, there were a few other trends in the communication link performance measures which indicated a gradual degradation of the links over time into the re-entry flight. The formal communication drop outs are defined as where both of the integrated receiver minor frame counts fall to less than 95/100. However, there are several other occasions in which these minor frame counts fall, but not below the 95/100 threshold that would invalidate their data and define an additional communications drop out. Following drop out #4, over GMT 13:50:34 to 13:50:35 (EI + 385 to 386 sec), the IR-A first counts an anomalous 101/100 minor frames, and then immediately afterward 99/100 frames. While the running total number of minor frames remained correct, one minor frame apparently was counted amongst the wrong major frame. This type of major/minor frame lock count mishap occurred in several, but differently timed, groupings for the two integrated receivers. Over GMT 13:50:34 to 13:51:22 (EI + 385 to 433 sec), the IR-A recorded four of these frame mis-registrations at widely spaced times, while the IR-B saw none. After several minutes of none of this behavior, then over GMT 13:54:52 to 13:55:55 (EI + 613 to 706 sec), the IR-B recorded sixteen of these frame mis-registrations of the pattern 99-100-101, or 101-99. Finally, over GMT 13:56:21 to 13:56:47, both integrated receivers began acting up, with IR-A recording five and IR-B recording seven frame mis-registrations. Because these events only affected one of the 100 minor frames, they did not have any impact on the validity of the data used by the MCC. However, their increase in frequency toward the final moments of the re-entry flight further suggests a continuing degradation of the communication link margins.

At GMT 13:54:27 (EI + 618 sec), both integrated receivers recorded a minor frame count of only 97/100. This small drop is insufficient to be classified as a formal communication drop by the MCC. However, this event occurred immediately after the switch from the ULA to the URA quad antennas, and a drop in the minor frame count of this magnitude is completely consistent with the antenna switchover time. This small drop in the minor frame count over this one second of telemetry appears completely consistent with the expected behavior of a fully functioning communications system.

In summary, over the period from GMT 13:50:00 to 13:56:57 (EI + 351 to 768 sec), there were 14 distinct and formally defined communications drop outs which NASA considers to be out-of-family (OOF). Of these, #1 appears to clearly be associated with an antenna switchover at the end of the first roll maneuver, #5 was too minor to have had any consequence, #7 and #8 were really part of the same drop out event, and #14 simply marked the beginning of the time period for which communications drop outs were expected and considered "in-family" for the re-entry flight. The drop outs of a long duration and significant interruption were #3 (7 seconds long), #6 (7 seconds long), #9 (7 seconds long), and #11 (9 seconds long). While the one second sampling period for the minor frame counts does not provide any detail on a finer time scale than this, in each of these four major outages, both the frame synchronization and minor frame counts fell to zero within the span of approximately one second (and perhaps faster), indicating a rather abrupt loss of the signal. While the communications drop outs cannot be conclusively linked to the specific shedding of orbiter hardware, their timing does support the hypotheses drawn from other sensor and debris data. The hypothesized loss of the upper part of a leading edge T-seal at GMT 13:49:59 would have just preceded drop out #1. The hypothesized loss of the lower part of RCC panel #9 at GMT 13:52:21 would have occurred in between drop outs #6 and #7-8. The fairly well substantiated breach of the left wing leading edge spar at 5-15 seconds prior to the sensor wiring failure window of GMT 13:52:16 to 13:52:26 (EI + 487 to 497 sec) is simultaneous with the start of drop outs #7 and #8. The structural integrity of the wing spar was hypothesized to have been lost at GMT 13:52:54 (EI + 525 sec), and this is just at the end of the rather significant drop out #9. RCC panel #10 is hypothesized to have been lost at GMT 13:54:20 (EI + 611 sec), and this would have occurred toward the end of drop out #11. The longest duration drop out #11 also occurred only a few seconds after the first wave of debris shedding events (debris #1 through #5), and just prior the first observed flash around the orbiter's envelope. The shedding of RCC panel #10 could have thus accounted for the observed debris #6.

Orbiter Experimental Instrumentation (OEX) – Recorded Data

Four Key Sensors Behind RCC Panel #9

The four key sensors that were located behind RCC panel #9 were: V12G9921A, a strain gauge on the inside of the spar; V09T9895A, an RTD temperature sensor on the inside of the spar; V09T9910A, a high temperature RTD temperature sensor attached to the RCC clevis between RCC panels #9 and #10; and V07T9666A, a thermal protection system (TPS) thermocouple mounted on the outer surface of a heat tile, located two heat tiles aft of the closure panels and directly behind RCC panel #9. These sensors have turned out to be of greatest importance, because of their location on the aluminum honeycomb spar immediately behind RCC panel #9, and because their signals indicate clearly when the breach in the left wing leading edge broke through, breaching the spar and allowing hot gas to begin entering the interior of the wing box. These sensors also signaled unusual conditions far earlier than any of the OFI (telemetry) data, when the orbiter was out over the Pacific Ocean. Not only the response of the sensors themselves, but also the wiring

burn through patterns evident in the recorded signals help to identify both the time and location of the burn through of the left wing leading edge spar. This event is important, since it represents the time mark at which the destruction process of the left wing reached the interior frame of the wing box, and the fate of the orbiter was, at that point, irreversible.

The MSID # V12G9921A strain gauge has reference designation 65V12M331 and is installed as sensor part number ME449-0141-022 according to installation drawing M072-756106. The wiring is shown in installation drawing V070-786651 and appears in harness number (wire list) V070-776807. Wire lists were obtained from the Boeing Electronic Wire List of their P51 KSC on-line database. The strain gauge is taped down against the inside wall of the aluminum honeycomb left wing leading edge spar, immediately behind RCC panel #9, at coordinates (X1106.0, Y–231.5, ZMS), midway up on the spar. The type ME449-0141-0022 strain gauge contains two serpentine metal patterns, each with their sensitive axes at 45° to the edges of the substrate. The substrate is adhesively mounted to the spar surface and oriented so that the two sensitive axes point forward and down, and forward and up. The four contacts on the substrate are brought back to a connector strip, V070-780221, which ties the common center point of the half bridge together and reduce the wiring to three leads that get routed to a SGSC. From the connector strip, the sensor is spliced into harness V070-776807 which runs to interconnect panel 65P, connector P119. The three wires are named EXC, SIG, and RTN, and are wired as pins 69, 80, and 81, respectively, on connector 65V77W107P119. Integrated schematic V428-780122 shows the EXC+, SIG+, and SIG– leads as coming from pins 1, 2, and 3 (B, C, and A) of the strain gauge and going to pins 69, 80, and 81 of P119, with the shield connected to pin 114. J119 carries these same pin numbers to J503. P503 takes these three leads to P892 on the strain gauge signal conditioner (SGSC) 40V78A208A20 that is located on shelf 7, with the shield connected to the connector shell. The output SIG and RTN leads from P891 of the SGSC then go to pins 56 and 45 on J10 (channel 109) of PCM-2, 40V78A200, with the shield connected to the case. The interconnections and power feed to this strain gauge were handled entirely by its own dedicated SGSC that was located well within the protected part of the fuselage; thus, any failure of this sensor would not have had any effect on any other sensors in the vehicle.

The MSID # V09T9895A RTD temperature sensor has reference designation 65V09MT423 and is installed as sensor part number ME449-0160-0008 according to installation drawing V070-756114. The wiring is shown on installation drawing V070-786611 as harness number V070-776807. The sensor is adhesively fixed to the inside wall of the spar, halfway up, and behind RCC #9 where the strut line intersects it. The sensor is located at coordinates (X1102.2, Y–239.0, Z310.0). Drawing V070-786611 shows the wiring as running up and then forward along the spar, while drawing V070-756114 show the same wiring as running down and then forward along the spar. Close-out photographs show that the latter case is correct, with the wiring running down and then forward along the spar. Following splices, the three leads from the RTD sensor are routed into harness V070-776807 which leads forward along the spar to interconnect panel 65P. The EXC, COMMON, and SIG leads are connected to pins 111, 112, and 114, respectively, of connector 65V77W107P117. Integrated schematic V428-780082 shows the EXC, COM, and SIG leads coming from pins 1, 3, and 2 of the RTD temperature sensor and going to pins 111, 112, and 114 of P119/J119, with the cable shield is connected to pin 115. The leads are then routed to pins 117, 115, and 119 of J504/P504 with the shield connected to pin 120. On shelf 8, the leads then go pins 105, 115, and 1?6 on J9 (channel ?) of PCM-1, 40V78A199, with the shield connected to the case. Since this sensor was wired directly and independently to PCM1, any failure mode it may have taken would not have affected any other sensors in the vehicle.

The MSID # V09T9910A high temperature RTD temperature sensor has reference designation 65V09MT371 and is installed as sensor part number ME449-0160-0006 according to installation drawing V070-786142. The wiring is shown on installation drawing V070-786611 as harness number V070-776807. This sensor installation is unusual, as it is the only active OEX measurement in which the sensor is located in front of the leading edge spar. The purpose of the sensor was to measure the temperature of the RCC attachment clevis, and to implement this, the RTD is affixed to a metal tab that is installed underneath the head of the lower forward RCC #10 attachment bolt, much like a washer. This places the sensor close to the lower part of the T-seal between RCC panels #9 and #10. The sensor is located at coordinates (X1112.0, Y–239.0, Z289.0). The three leads from the RTD are spliced to a connector plug, whose mating receptacle is installed into the spar fitting. The wires from the receptacle pass through a penetration in the spar where they are in turn spliced into harness V070-776807. The EXC, SIG, and COMMON leads from the sensor are connected to pins 93, 102, and 103, respectively, of connector 65V77W105P113. Integrated schematic VS72-978099 differs from this description in some respects. It shows the EXC, SIG, and RTN leads as coming from pins 1, 2, and 3 of the RTD sensor and going to pins 5, 6, and 4 of 65P305/65J305 located on the spar attachment hardware. From here, the leads go to pins 87, 78, and 75 of 65P103/40J103 with the shield connected to pin 79. The cable then runs to pins 70, 69, and 81 of 40J502/40P502 which takes it into shelf 8. The leads then run to pins 17, 16, and 27 of J11 on PCM1, 40V78A199, with the shield connected to the case. No resolution was found to the discrepancies between the installation drawing and the integrated schematic. Regardless, this sensor was also wired directly to PCM-1, and any failure mode that it may have experienced would not have affected any other sensors in the vehicle.

The MSID # V07T9666A thermocouple temperature sensor has reference designation 65V07TC113 and is installed as sensor part number ME449-0204-0002 (Type R, Pt:Rh/Pt) according to installation drawing V070-192131. The wiring is shown on installation drawing V070-786611 as harness number V070-776803 (different from the other three sensors above). This particular thermocouple measures the left wing lower surface temperature at a point two rows of tile aft of the junction between RCC panels #9 and #10. The coordinates for the sensor are (X1121.7, Y–236.7, Z102.0), and it

is installed in heat tile number 192158-099, as detailed in the James A. Smith document, "OV-102 Modular Auxiliary Data System Measurement Locations," (revised Jan. 1992). This type of thermocouple installation penetrates the heat tile by means of a slot and after the thermocouple bead is threaded through, the tile is glazed over to seal the thermocouple bead into the outer surface layer. The thermocouple wires extend through the tile to a pair of recesses cut into the back of the tile. The SIP tile mounting material has a hole cut into it where the wing penetration occurs, and this is an inch or two laterally offset from where the thermocouple bead is located. The thermocouple wires are spliced to the thermocouple extension wires (type SX) underneath the tile before the tile is bonded to the orbiter skin. After passing through the wing penetration, the thermocouple extension wires are then routed to the thermocouple reference junction (TRJ) box that is mounted on to the surface of the leading edge spar. This TRJ is a 10-channel unit with part number MC476-0133-0050. The signal and power leads from the TRJ unit then run forward along the leading edge spar to interconnect panel 65P. The thermocouple bead is located at the coordinates (X1121.7, Y–236.7, Z102.0). The SIG and SIG RTN leads are connected to pins 19 and 20 of connector 65V77W103P101. Integrated schematic V428-780372 shows the + and – leads from the thermocouple going to TRJ box 65V78Z121-6 (channel 6 of 10). The EXC+ and EXC– leads from the TRJ box then go to pins 91 and 92 on P113/J113 with the shield connected to pin 113. Similarly, the SIG+ and SIG– leads from the TRJ box go to pins 19 and 20 on P101/J101 with the shield connected to pin 21. Two parallel, independent, 2-conductor shielded cables are used for the full length of this run. The excitation cable leads then go to pins 50 and 61 on J546/P546, and the signal cable leads go to pins 51 and 62 on J546/P546, with both shields connected to pin 67. Once on shelf 8, the excitation cable leads go to pins 89 and 101 of J5 (channel ?) of PCM-1, 40V78A199, and the signal cable leads go to pins 119 and 126 on J12 (channel ?). Both shields are connected to the case. Because the power to the TRJ box was obtained from PCM-1 PPS-17,18,89,90 which also supplied several temperature sensors on the lower fuselage surface, a failure in V07T9666A which took down the power supply voltage would also kill the output of these sensors as well.

The V12G9921A strain gauge was the only strain gauge to register any significant anomalous behavior prior to EI + 500 seconds, and its response started to climb away from those of past flights as early as GMT 13:48:39 (EI + 270 sec). From GMT 13:48:39 to 13:50:09 (EI + 270 to 360 sec), the recorded strain climbs anomalously, reaching at peak of +180 μin/in. At GMT 13:51:39 (EI + 450 sec), the strain reverses sign, and then peaks in the opposite direction at GMT 13:52:04 (EI + 475 sec) to a value of –140 μin/in. At GMT 13:52:04 (EI + 475 sec), the strain abruptly reduces by a small amount, and then remains constant and negative up until GMT 13:52:24 (EI + 495 sec), at which point the signal bounces up and down in a completely unphysical manner, continuing on through GMT 13:52:59 (EI + 530 sec), when it flatlines at a bias value slightly above zero. The non-physical behavior beginning at GMT 13:52:24 (EI + 495 sec) is presumed to result from the burn through of the left wing leading edge spar at a point somewhere along the length of the cable to this sensor. The out of family strains that were recorded prior to this are presumed to indicate some significant thermal bowing or buckling of the aluminum honeycomb spar. In particular, reversals in the sign of a strain are rather unusual and indicate either a complete reversal in the direction of loading, which is highly unlikely, or a buckling of the structural element. There was some initial speculation that the erratic behavior over the time span of EI + 495 to 530 seconds was actually a damped mechanical vibration, resulting from some mechanical impact or sudden loading change in the spar. However, the damping rate and the oscillation frequency that would be represented by this response are not consistent with the expected mechanical response from a honeycomb spar which would normally be quite rigid and oscillate at a much higher acoustic frequency. The erratic behavior is also characteristic of the burning or tearing of a cable, and this interpretation aligns better with the observed responses of the other sensors in the vicinity. The strain that is recorded prior to EI + 495 sec is considered valid data, but any response beyond this time is considered invalid. Since the strain gauge is temperature compensated by having both elements of the half bridge attached to the spar, the recorded signal should represent real strain, and not the temperature sensitivity of the gauge. High temperatures acting upon the spar could cause it to bow or deflect, and this deflection would certainly produce strains; however, the strain gauge should have been largely insensitive to the temperature of the spar itself. In several charts NASA labeled this sensor as having gone off scale. In point of fact this is not true. The range of strains that V12G9921A can measure extends from –1500 to +1000 μin/in. The recorded signal came close to these limits during its erratic behavior, but actually never reached them.

The V09T9910A temperature sensor on the RCC attachment clevis recorded a gradual, abnormal rise in temperature, beginning as early as GMT 13:48:59 (EI + 290 sec) and climbing steadily from a nominal 30°F to 65°F at GMT 13:52:22 (EI + 493 sec), after which it fell straight to OSL. This was one of the first sensors in the vehicle to fail during the re-entry flight, and it did so with extreme abruptness. Its data appears valid right up until the abrupt fall to OSL, and the data indicates only a gentle warming of the RCC attachment clevis at that point. This was also the only sensor that was located on the front side of the left wing leading edge spar. Although clearly abnormal, the temperature rise was slow and small in comparison to the temperatures that would be expected if it was exposed to the raw blast from a breach in the RCC panels. This is, however, consistent with the location of the sensor being buried deep beneath layers of inconel and cerachrome insulation that were installed around the spar fitting. The abruptness of the fall in the reading to OSL also suggests that the failure of the sensor could have just as easily been caused by a severe and sharp event, such a mechanical break in part of the leading edge structure which could have either clipped the wires, or otherwise mechanically destroyed the sensor. One possibility is that a piece of T-seal or RCC panel fell away at that time and took the sensor with it. The location of the sensor is actually several inches ahead of the spar surface, and the installation diagram shows its wiring as extending even further forward, offering an easy target to be torn off by any rapid loss of RCC panel or T-seal.

The V09T9895A temperature sensor on the inside of the left wing leading edge spar also recorded a rise in temperature that ended in an abrupt fall to OSL. The anomalous temperature rise began as early as GMT 13:51:14 (EI + 425 sec) and then abruptly fell at GMT 13:52:54 (EI + 525 sec). Unlike V09T9910A, the temperature rise was extreme, going from a nominal 20°F at GMT 13:51:14 (EI + 425 sec), to 40°F at GMT 13:52:14 (EI + 485 sec), and then rising much faster to 120°F at GMT 13:52:44 (EI + 515 sec), and then finally to an OSH at 450°F at GMT 13:52:51 (EI + 522 sec). Although the subsequent fall to OSL at GMT 13:52:55 (EI + 526 sec) was abrupt, the failure signature of this sensor clearly indicates a destruction due to direct thermal causes, which could include any of several processes by which one or more of the three leads of the device became open circuited. The rapid rise of the readings from this sensor, as compared to V09T9910A, are consistent with its location which is directly behind the part of the spar which had the least thermal insulation and obscuring RCC mounting hardware. Burn through of the spar would be expected to occur though this less protected zone first. The readings of this sensor appear to be valid up to the point where they went to an OSH. While all of the sensors with locations or wiring along the leading edge spar failed within the time span of GMT 13:52:16 to 13:52:26 (EI + 487 to 497 sec), this sensor failed at a comparatively later time, GMT 13:52:51 (EI + 522 sec).

The V07T9666A lower wing surface thermocouple showed a reading which had several important aspects. First, the readings starting becoming abnormally high and somewhat erratic as early as GMT 13:50:19 (EI + 370 sec), with several brief high temperature spikes climbing to 2500°F, significantly higher than the nominal 2000°F peak temperatures within a normal flight. Then, at GMT 13:52:25 (EI + 496 sec), the reading began an abrupt chatter between OSH and OSL, and then at GMT 13:52:35 (EI + 506 sec), essentially falling to OSL with some residual erratic noise up until GMT 13:52:52 (EI + 523 sec). This failure signature is indicative of a slower burning or tearing process. Because this thermocouple was located on the wing lower surface directly behind the junction between RCC panels #9 and #10, the high temperatures that it recorded were almost certainly a result of the initial gas jetting through the RCC panel damage area and the subsequent heating of the left wing around that zone. It is important to note that this sensor provided an external temperature measurement, while V09T9910A and V09T9895A both provided internal temperature measurements. Also of note is that this sensor fed immediately into a thermocouple reference junction (TRJ) box that was located on the spar as well. Both the power feed to the TRJ box and the signal conditioned output cables then ran along the spar in the forward direction with the other sensor wiring. Thus, both the sensor signal cable and the power supply feed cable were susceptible to damage from a burn through of the spar.

The timing of the failures of these four sensors and the path of their cable routing lends important information to determining both the timing and location of the breach of the leading edge spar. All of the cables from these sensors, as well as many others, were routed into wiring harnesses that traveled forward along the spar, up to the X1040 cross spar, where they passed through the service opening and then ran along in front of the left wheel well before reaching interconnect panel 65P, where they then entered the fuselage. All of the sensors with wiring in this set of harnesses had failure times within a rather narrow window of EI + 487 to 497 seconds, except for V09T9895A, which lasted up until EI + 522 sec. The diversity of sensor locations and types indicates that their common failure time was caused by their wiring being destroyed as part of the spar burn through, rather than the sensors themselves being destroyed by direct heating at their placement points. Close examination of the close out photographs and the engineering drawings for the wiring installation show that there were five main wiring harnesses running forward along the spar, labeled top-down as A-E in most charts. The upper four, A-D, are spaced within a few inches of each other, while the fifth, E, is routed about 6-8 inches below the rest. While the harness path taken by most of the sensors was fairly clear from the close out photographs, installation drawings, and wire lists, the routing of the wires for sensor V09T9895A was not immediately obvious. Closer inspection of the close out photographs and the geometry of the cable spot ties around the splice area showed that, indeed, this sensor was routed forward as part of the lowermost harness E. The physical separation between harness E and the other four is consistent with the later failure time of V09T9895A by 25-29 seconds, and thereby indicates that the breach of the leading edge spar began within the upper two-thirds of the spar, causing three of the sensors with their cables in this area to fail over EI + 493 to 497 seconds, and then progressed downward, causing the V09T9895A sensor to fail at EI + 522 seconds. This is also quite consistent with the fact that thick layers of inconel and cerachrome insulation protect the spar fitting hardware on the upper third and lower third of the spar. The center third of the spar, which is far less protected on the front, is where the initial breach most likely occurred and also where the upper four wiring harnesses were routed. The relevant close out photographs which show the sensor placement and wire harness routing are A950318L-I06G-jpg, A950318L-J08C-jpg, A950318L-K04C-jpg, A950318L-A03C-jpg within left wing cavity 1, and A950309J-55C.jpg and A950309J-54C.jpg within the left wing glove.

The failure times for these four key sensors behind RCC panel #9 each indicate the timing for which their response was no longer trustworthy by virtue of displaying an impossible physical behavior, rising or falling faster than known thermal time constants would allow. The characteristics of those behaviors were indicative of a wiring fault in their cables at that moment, most likely short circuits, since these occur before open circuits and at lower degrees of applied external stress. The rapid rise in the spar temperature sensor V09T9895A just prior to this sequence of sensor failures clearly indicates that high temperature was the source of the external stress. Comparisons between temperature sensors on the outside of the wing (V07T9666A) versus those on the inside (V09T9910A and V09T9895A) also clearly indicate that the abnormal heating began first on the outside and worked its way inward. As noted previously, while the timing of the electrical anomalies is known and recorded to within one second precision, the initiation of the physical events that caused them is known with far less precision because of the variability in the burn through speed of the sensor cables. Since the aluminum spar would have to burn through before

any of the cable harnesses on the inside would begin their burn through process, the breach of the spar must have occurred some time prior to the first of the sensor failures. The first sensor failure was V09T9910A at EI + 493 seconds, but the sensor and some of its wiring were located on the outside of the spar; therefore, this particular sensor failure cannot be used to conclusively indicate that the spar was breached. The next sensor failures were V12G9921A and V07T9666A at EI + 495 and 496 seconds, respectively. Both of these sensors had all of their wiring within the inside of the wing box and therefore provided a conclusive indication of when the hot gas had actually breached the spar. The shortest recorded burn through times were 2 seconds, and the longest 200 seconds, for any of the sensors in the system. The most conservative assertion is therefore that the breach of the leading edge spar occurred between 2 and 200 seconds prior to the first conclusive sensor wiring burn through failure on the inside of the spar at EI + 495 seconds.

As will be discussed in the next section, there were eleven pressure sensors on the left wing which also had their cable harnesses routed along the leading edge spar. The range of times over which these failed with a cable burn through signature was EI + 487 to 497 seconds and overlaps very closely with the failure times of V09T9910A, V12G9921A, and V07T9666A. The earliest failure among these was V07P8038A out on the wing tip, which NASA reported failing at EI + 487 seconds, but it also had some of its wiring on the outside of the spar and thus cannot be considered a conclusive indicator for a breach of the spar. The next pressure sensor failing with a burn through signature was V07P8023A, which had a clearly defined failure point at EI + 489 seconds. All of its wiring was routed within the inside of the wing box and this provides a conclusive indication of a spar breach that occurred a few seconds prior to those of the V12G9921A and V07T9666A. Thus, the pressure sensor data allows the breach of the leading edge spar to be placed between 2 and 200 seconds prior to the first conclusive sensor wiring burn through failure on the inside of the spar at EI + 489 seconds.

The number of sensors is, however, large enough to make valid use of statistics. The three large cable harnesses that pass above the outboard wall of the left wheel well happen to create a nicely controlled experiment in their own right. These provide a statistically significant test of the average burn through speed of typical sensor cable harnesses under virtually the same conditions as those on the left wing leading edge spar behind RCC panel #9. Bundle #3 contained the cables for 138 sensors of which 134 failed in the time span of EI + 487 to 600 seconds. Bundle #1 contained the cables for 11 out of 11 sensors that failed in the time span of EI + 493 to 560 seconds. And bundle #4 contained the cables for 25 out of 25 sensors which failed during the time span of EI + 516 to 738 seconds. There were actually far more cables in bundles #1 and #4, but they were associated with sensors that were operating in the snap-shot mode, and whose precise failure times could thus not be determined. Overall, it is remarkable that bundles of around 100 or more cables could be burnt through in their entirety within only about two minutes. These larger bundles of 100 or more cables had approximately 8-10 radial layers to them. If one supposes that one layer must burn through before the next begins, the overall burn through process becomes sequential, and the overall burn through time of approximately 100 seconds on the average might actually represent the sequential burn throughs of 10 layers of cables, each roughly 10 seconds in length on the average. Taking this argument as the basis for a more aggressive assertion, the left wing leading edge spar breach could have occurred as late as 10±5 seconds (5 to 15 sec) before the first sensor wiring failure at EI + 489 seconds.

Even within these vagaries, the precise definition of what constitutes a specific breach of the spar remains. The breach could have been defined by a pin hole, a series of pin holes, or a hole greater than some threshold diameter to start admitting gas at a significant flow rate, or several such sufficiently large holes. NASA placed the breach of the leading edge spar as falling within the range of EI + 425 to 487 seconds, with a higher probability toward the EI + 487 second mark, thus taking the wiring failure of pressure sensor V07P8038A at EI + 487 seconds as the indicator and allowing for a burn through time period of 0-62 seconds. Nonetheless, NASA's conclusion and the above analysis are ultimately in fairly close agreement, differing only by a few seconds.

Left Wing Aerodynamic Pressures

From the MADS/OEX recorded data, NASA plotted 97 different aerodynamic pressures for the left wing and 84 for the right. The pressure readings were all MSIDs beginning with V07P, and 91 came from PCM-1, and 90 from PCM-2. Of these, a certain few were of greater importance than the rest because their wiring, like the that of the four key sensors discussed previously, also ran along the inside wall of the left wing leading edge spar. Lying directly behind RCC panel #8 are V07P8010A and V07P8058A on the upper and lower surfaces, respectively, of the left wing. A large number of pressure sensors are also clustered along the length of the Y = –256 plane on both the upper and lower surfaces of the left wing. Proceeding aft from the leading edge of the wing, V07P8022A, V07P8023A, and V07P8024A were on the upper surface, and V07P8071A, V07P8072A, and V07P8073A were on the lower surface. The wiring for all six of these was routed forward along the Y = –256 strut line of the wing and then along the leading edge spar as part of the larger cable harnesses. Out near the tip of the left wing at Y = –448 are V07P8037A, V07P8038A, and V07P8044A, each measuring pressures on the upper surface of the wing. The wiring for each of these three pressure sensors was routed along the full length of the left wing leading edge spar, although the wiring was uncharacteristically routed on the outside of the leading edge spar until it went through a penetration at X = 1164 and then continued along the inside of the leading edge spar along with the other sensor cable harnesses behind RCC panels # 7-10.

Sensor MSIDs V07P8010A and V07P8058A have reference designators 65V07MT310 and 65V07MT358, respectively, and are both sensor part number ME449-0177-2108, manufactured by Statham, with a 0 to +15 psia range. On the upper wing surface along Y = –256, sensor MSIDs V07P8022A, V07P8023A, and V07P8024A have reference designators 65V07MT322, 65V07MT323, and

65V07MT324, respectively, and all three are Kulite miniature pressure sensors with part number ME449-0219-0002 and a 0-16 psia pressure range. Matching to these same Y = –256 locations along the lower wing surface, sensor MSIDs V07P8071A, V07P8072A, and V07P8073A have reference designators 65V07MT371, 65V07MT372, and 65V07MT373, respectively, and are also miniature Kulite pressure sensors with a 0-16 psia range, part number ME449-0219-0002. Finally, out on the left wing tip upper surface, sensor MSIDs V07P8037A, V07P8038A, and V07P8044A have reference designators of 65V07MT337, 65V07MT338, and 65V07MT344, respectively, and these three are also miniature Kulite pressure sensors with a 0-16 psia range, part number ME449-0219-0002. Both of the Statham pressure sensors, V07P8010A and V07P8058A, were installed according to drawing M072-756106, and all nine of the Kulite miniature pressure sensors were installed according to drawing V070-192146. The Statham pressure sensors, because of their larger transducer housing, were typically mounted against a spar and a stainless steel tubing was routed from the transducer to the pressure sensing port fitting on the wing skin. The stainless steel tubing runs were usually routed along the wing strut frames (tube trusses). Sensor wiring was typically run along the spars. The Kulite pressure sensors, because of their smaller bodies, were mounted directly on the wing skin.

Sensor V07P8010A on the upper wing surface was reading essentially zero from EI up to GMT 13:52:26 (EI + 497 sec) at which point it abruptly shot to OSH at 15 psia and then chattered between OSH and OSL until GMT 13:52:34 (EI + 505 sec), after which is remained at a zero reading with occasionally small transient spikes. The failure at EI + 497 sec is both abrupt and clearly defined. The essentially zero pressure reading from the upper wing surface is normal for this phase of the re-entry flight, because most of the pressure is building up on the lower surface of the wing which is facing into the direction of motion due to the pitch of the vehicle. The companion sensor V07P8058A on the lower wing surface was reading a normal rise in pressure starting from a systematic offset value of about 0.2 psia at EI and gradually climbing to about 0.4 psia at GMT 13:52:29 (EI + 500 sec), completely normal with comparison to previous flights. At around GMT 13:52:34 to 13:52:39 (EI + 505 to 510 sec), the reading begins to gradually fall, and hits an absolute zero at GMT 13:53:04 (EI + 535 sec), without any remainder of the original offset. Over EI + 547 to 575 sec, the reading chatters between OSL and OSH, and then remains at zero thereafter. NASA claimed that this sensor failed around EI + 495 sec, but this is only vaguely supported by the plotted data. Because the sensor reading transitioned downward to an absolute level that no longer had the systematic offset, this downward trend, although smooth, is indicative of a soft short wiring failure mode for this sensor. This failure mode is somewhat more subtle than those of other sensors, but still uncharacteristic of the normal operation of an absolute pressure sensor. The disappearance of the systematic offset beyond EI + 535 sec indicates either an open or short circuit in the pressure sensor bridge power, or an open or short circuit in the sensing leads from the two arms of the bridge. A conclusive failure time of GMT 13:52:34 (EI + 505 sec) can be validly claimed from the data, behaving similarly to the soft shorts produced in the Kapton insulated wiring of other sensors. NASA still prefers to claim the failure time as GMT 13:52:24 (EI + 495 sec), 10 seconds earlier. The sensor behavior at EI + 495 sec appears suggestive of a possible failure, but not conclusive. By the slightly later time of EI + 505 sec, the failure signature is clearly evident and conclusive.

NASA claimed that sensors V07P8022A, V07P8023A, and V07P8024A on the upper surface of the left wing along Y = –256 failed at times of EI + 492, 489, and 490 seconds, respectively. The plot for V07P8022A was not among the data provided to the CAIB by NASA, so there was no means by which to verify the behavior of that sensor. Both V07P8023A and V07P8024A indeed showed clearly defined failures at EI + 489 and 490 seconds with the output showing an abrupt onset of erratic signal noise, in many cases approaching OSL and OSH. By EI + 530 sec, both of these outputs had settled down to a zero reading. Both of these sensors also showed a significant offset error over the full re-entry time span for previous flights of about –0.2 psia for V07P8023A and –0.7 psia for V07P8024A. Neither of these offsets appear to have altered the functioning of the sensor, however.

NASA also stated that the matching sensors V07P8071A, V07P8072A, and V07P8073A on the lower surface of the left wing had failure times of EI + 491, 490, and 492 seconds, respectively, and indeed this is shown clearly in the plotted data with each of these showing a very normal slowly rising pressure that had smoothly climbed by about 0.1-0.2 psia over the time period from EI to EI + 490 sec. At the various times of EI + 491, 490, and 492 sec, each sensor reading abruptly shot up with an erratic spiking, occasionally hitting the OSH value of 16 psia, and then quieting down to a zero reading by EI + 530 seconds. Sensor V07P8071A also showed a systematic offset of –0.5 psia over the full time span and for previous flights. Similarly, V07P8072A may have had a systematic offset of +0.4 psia, its value at EI for all previous flights.

For the three sensors in the left wing tip, V07P8037A, V07P8038A, and V07P8044A, NASA claimed failure times of EI + 492, 487, and 495 seconds. This is shown clearly in the plotted data, although the failure time for V07P8038A appears to be closer to EI + 492 than EI + 487 seconds. These sensors show exactly the same failure modes as the preceding six, with an abrupt onset of erratic spiking that occurs at their failure time and which ceases around EI + 530 seconds. Beyond this point, the reading remains at zero with minimal noise transients.

The nine aerodynamic pressure sensors V07P8022A, V07P8023A, V07P8024A, V07P8071A, V07P8072A, V07P8073A, V07P8037A, V07P8038A, and V07P8044A, have nearly simultaneous failures within the range of EI + 489 to 497 seconds and a common wiring route along the middle of the leading edge spar, thereby corroborating the time of the spar burn through. Close-out photographs and engineering blackline drawings confirm the wiring routes from the sensors. There was considerable confusion at first in identifying these wiring runs, but the key to properly identifying their placement is the fact that the larger Statham pressure sensors each have a sizeable stainless steel

tubing that routes the transducer to the sampling port on the wing, while the miniature Kulite pressure sensors were small enough to be mounted on the wing surface directly over their sensing port. The routing of the wiring to sensors V07P8037A, V07P8038A, and V07P8044A out on the left wing tip along the outside of the leading edge spar is very unexpected, but this is confirmed by the wiring penetrations shown in close-out photograph A950318L-G11C.jpg. This wire routing has also been confirmed in the engineering blackline drawings, and the recovered debris from this area of the left wing indeed had wire fragments on the front surface of the spar.

Close-out photograph A950318L-K04C.jpg shows sensors V07P8010A and V07P8058A, which were both the larger Statham type, the stainless steel tubing to their ports, and their wiring as it enters the cable harnesses leading forward along the leading edge spar. The wiring from V07P8010A runs vertically down from the top of the wing and meets the uppermost harness A, and then runs forward along the leading edge spar as part of harness A. Similarly, the wiring from V07P8058A runs vertically upward from the bottom of the wing and also meets the uppermost harness A, and then continues forward along with it. From the wiring routing path, it appears that sensor V07P8010A on the upper wing surface had its wiring damaged at EI + 497 sec, immediately following the first of the key sensors located behind RCC panel #9. Sensor V07P8058A on the lower wing surface was somewhat more protected and failed at a slightly later time. The earliest conclusive failure timing for this sensor is at EI + 505 to 510 seconds, although NASA cites a slightly earlier time of EI + 495 seconds. Because these two sensors were located forward of the four key sensors behind RCC panel #9, the burn through of the leading edge spar must have occurred at least this far forward to support the observed failure timing.

Within the broader picture, all of the aerodynamic pressure sensors were only beginning to record any significant rise in the absolute pressure during this phase of the re-entry flight. Pressure sensors on the upper wing surface experience essentially zero pressure until much further into the re-entry because they are not exposed to the oncoming dynamic pressure of the incident air stream. Only the pressure sensors on the lower surface of the wing experience any observable rise in their readings, typically less than 1.0 psia over this phase of the flight. Boeing engineers in several of their briefings also pointed out that the aerodynamic pressure instrumentation was designed for much lower altitude phases of the vehicle's flight. Because most of these pressure sensors were only beginning to come off of zero, their readings are already near to the OSL points, and thus somewhat more difficult to interpret than a mid-scale reading.

Fuselage Lower Surface Temperatures

Twelve temperature measurements were recorded by the MADS/OEX system along the lower surface of the fuselage. All but one of these were type R thermocouples that were mounted on the outside of the heat tiles, part number ME449-0204-0002. These were calibrated for ranges of either 500-2700°F or 0-2400°F, depending upon the specific location. The remaining sensor (V09T9731A) was a structural skin measurement, taken at the bond line between the heat tiles and the aluminum skin, and used an RTD, part number ME449-0160-0001, that was calibrated for the range of –200 to +450°F. Five of these were placed successively along the centerline of the vehicle (Y = 0.0), one was placed slightly off center 50 inches to the left (Y = –50.0), and the remaining six were placed along the left fuselage edge (Y = –100.0 to –117.0).

Sensor V07T9468A was a surface thermocouple mounted at (X618.9, Y0.0, ZBOT), just below the front of the payload bay area on the vehicle's centerline. This measurement behaved very much like that of prior flights until it momentarily spiked up to nearly OSH of 2650°F at GMT 13:58:31 (EI + 862 sec) and then returned to read within normal limits until it spiked up again at GMT 14:00:09 (EI + 960 sec), just a few seconds before the end of the OEX recorded data. The overall trend of this measurement was for a smoothly increasing temperature from an OSL value of 500°F at EI to approximately 1700°F at EI + 360 seconds, and finally leveling off to a value of approximately 1800°F for the remaining recorded re-entry flight.

Sensor V07T9478A was a surface thermocouple mounted at (X1006.0, Y0.0, Z267.3) below the middle of the payload bay area on the vehicle's centerline. This measurement behaved within normal family limits, also smoothly increasing from an OSL of 500°F at EI up to 1700°F at EI + 360 seconds. It then leveled off to a value of 1800°F until GMT 13:59:44 (EI + 935 sec) after which it started behaving erratically and then started chattering between OSL and OSH at GMT 13:59:59 (EI + 950 sec) and continued this until the last recorded OEX data point.

Sensor V07T9489A was a surface thermocouple mounted at (X1391.5, Y0.0, Z264.0) beneath the front of the main engine compartment and also on the vehicle's centerline. This measurement read an OSL value of 500°F from EI up to GMT 13:46:54 (EI + 165 sec), smoothly climbed to 1230°F at EI + 360 seconds, and then leveled off at 1300°F by EI + 480 seconds, and this was all well within the limits of past flight behavior. At GMT 13:52:22 (EI + 493.33 sec), the recorded data jumped abruptly up by 32 bits, or 250°F, and retained this offset for the remainder of the recorded data. At approximately GMT 13:59:09 (EI + 900 sec), the gently decreasing temperature reversed direction and began climbing upwards and at GMT 13:59:54 (EI + 935 sec) shot up to OSH and then chattered between OSL and OSH until the end of the recorded data.

Sensor V07T9492A was a surface thermocouple mounted at (X1511.1, Y1.3, Z275.6) beneath the rear of the main engine compartment and nearly on the vehicle's centerline. This measurement read an OSL value of 500°F from EI up to GMT 13:47:34 (EI + 205 sec), smoothly climbed to 1150°F at EI + 360 seconds, and then leveled off at 1200°F by EI + 480 seconds, and this was similarly well within the limits of the behavior of prior flights. At GMT 13:52:22 (EI + 493.33 sec), the recorded data from this sensor also abruptly jumped up by nearly exactly the same amount as the previous one, 32 bits, or 250°F, and similarly retained this offset for the

remainder of the recorded data. At GMT 13:59:49 (EI + 940 sec), the temperature shot upwards and continued to behave erratically with drastic chattering up and down (although not hitting OSL or OSH) until the end of the recorded data.

Sensor V07T9502A was a surface thermocouple mounted at (X1561.0, Y0.0, ZBOT) and centered on the lower surface of the body flap. The recorded data smoothly increased from 50°F at EI to 1150°F at EI + 360 seconds, and then leveled off at a maximum of 1250°F. At GMT 13:57:09 (EI + 780 sec), the temperature began to fall slightly, dropping to 1170°F at GMT 13:59:44 (EI + 935 sec), after which it rose sharply and then chattered between OSL and OSH values from EI + 960 seconds through to the end of the recorded data. The dropping temperature reading over EI + 780-935 seconds is out of family behavior, and this cooling trend could potentially be of a similar origin as that which affected the left OMS pod around this same time period.

Sensor V07T9470A was a surface thermocouple that was mounted at (X620.5, Y–50.0, Z278.8) underneath the front of the payload bay and offset 50 inches to the left side of the centerline. This measurement started at an OSL value of 500°F at EI and smoothly rose to 1750°F by EI + 360 seconds. The temperature then more slowly reached a maximum of 1920°F at EI + 780 seconds, mirroring the contour of the aerothermal peak heating curve for the re-entry flight, as did most of these surface temperature sensors on the lower surface of the orbiter. The heating was greater toward the nose as compared to the tail of the vehicle, as would be intuitively expected for its 40° pitch and descent vector, and each of the lower surface temperature sensors placed successively along the centerline showed progressively increasing temperature profiles going from tail to nose. At GMT 13:59:44 (EI + 935 sec), the reading began to rise rapidly and it continued to behave erratically until the end of the recorded data.

Sensor V07T9480A was a surface thermocouple mounted at (X1004.1, Y–99.8, ZBOT) under the middle of the payload bay and offset to the left to roughly match the side of the fuselage. This measurement began with an OSL reading of 500°F at EI, began to rise at GMT 13:46:29 (EI + 140 sec), and reached 1500°F at EI + 360 seconds. At GMT 13:52:22 (EI + 493.33 sec), the recorded data from this sensor also abruptly jumped up by 32 bits, or 250°F, and similarly to V07T9489A and V07T9492A retained this offset for the remainder of the recorded data. At GMT 13:59:09 (EI + 900 sec) the temperature reversed it gentle decrease and began to rise again, then at GMT 13:59:44 (EI + 935 sec), it rose dramatically and began chattering between the OSL and OSH limiting values until the end of the recorded data. As a note, the installation drawings also show a sensor V09T9493A to be installed at nearly the same location as V07T9480A; however, the signal from this sensor was not included in the OEX recorder data, and it is likely that this sensor was broken or simply no longer used.

Three more surface thermocouples were mounted on the fuselage lower surface along the Y–110 left side edge. Sensors V07T9784A, V07T9787A, and V07T9788A were placed toward the rear of the vehicle, midway back underneath the main engine compartment, underneath the aft end of the main engine compartment, and on the lower outboard forward edge of the body flap, respectively. All three of these sensors differed from the rest by having their signals channeled through the MADS PCM-2 unit. The available documentation did not provide any precise coordinates for any of these three. All three of these sensors behaved in essentially the same manner, remaining well within the normal family limits of behavior up until GMT 13:59:44 (EI + 935 sec), when their readings began to rise sharply, fluctuate erratically up and down, and then chatter between OSH and OSL limiting values up until the end of the recorded data. All three started at a value of approximately 75°F at EI, smoothly rose to a knee value at EI + 360 seconds of 1300°F for V07T9784A and V07T9787A and 1150°F for V07T9788A, and then leveled out to a maximum heating temperature of 1450°F for V07T9784A and V07T9787A and 1250°F for V07T9788A. The measurement on the body flap, V07T9788A, showed somewhat more structured variations of temperature over certain periods; however, this was also observed in prior flights and most likely due to the more complex aerothermal dynamics existing around the edges of this unusual control structure.

Sensor V09T9731A as also different from the rest and was a structural RTD temperature sensor that was placed on the bond line between the heat tiles and the aluminum skin of the orbiter at the coordinates (X1443.0, Y–117.0, ZBOT), very close to V07T9784A on the lower fuselage. This reading began at a value of 30°F at EI and very smoothly and gently climbed to 80°F at GMT 14:00:04 (EI + 955 sec), after which it rose sharply to a final value of 180°F as the last recorded value in the OEX data. The behavior over the entire time from EI to EI + 955 seconds was completely normal.
Finally, sensor V07T9508A was a surface thermocouple mounted at (X1558.5, Y–105.0, Z281.3) midway back on the lower left edge of the body flap. This reading began at an OSL value of 500°F at EI and smoothly climbed to a knee value of 1300°F at EI + 360 seconds, and finally leveled out to a maximum temperature of 1400°F. At GMT 13:57:09 (EI + 780 sec), the temperature began an uncharacteristic decrease, falling to 1350°F at GMT 13:59:44 (EI + 935 sec). Beyond this point, the temperature rose abruptly to 2100-2300°F and then chattered between OSL and OSH limiting values until the end of the recorded data. Similar to V07T9502A, this uncharacteristic cooling trend over EI + 780 to 935 seconds could be related to the same origins as the cooling seen on the left OMS pod around the same time.

The fuselage lower surface temperatures thus behaved very much according to their prior flight patterns from EI up until a few seconds before the last recorded MADS/OEX data. In addition, three of these sensors (V07T9480A, V07T9489A, and V07T9492A) each showed an abrupt upward step of very nearly the same magnitude (+32 bits) at precisely the same time of GMT 13:52:22 (EI + 493.33 sec). Boeing and NASA identified that these three sensors, in addition to being of the same type R, using the same type of thermocouple reference junction (TRJ) of part number MC476-0133-0070, being sampled at ten times per second, and using the same second order calibration curve, that they each shared the same +5.0 V precision power supply (PPS) output from the

MADS PCM-1 unit, namely PPS output 89. Besides these three thermocouple sensors, it was also found that sensor V07T9522A on the left side surface of the fuselage jumped down by –5 bits at precisely the same time of EI + 493.33 seconds. Further, sensor V07T9636A, a thermocouple surface temperature sensor on the upper left wing had its reading jump down by –7 bits at the same time of EI + 493.33 seconds. Both sensors V07T9522A and V07T9636A were type K thermocouples, both used a TRJ of type ME476-0133-0001, both were sampled once per second, both used the same first order calibration curve, and notably, both TRJ units were supplied +5.0 V DC power from the same PPS output 89 of PCM-1 unit as the other three measurements. The commonality of these five measurements is electrically traceable to a single terminal junction bar which takes the output from PPS-89 and distributes it to each of the five TRJ units for these thermocouples.

For a Wheatstone bridge-type signal conditioner, as is used for all of the temperature, pressure, and strain sensors on the orbiter, most of the wiring failure modes (open or short circuits between various combinations of the wires) result in a measurement output that is either off scale low (OSL), off scale high (OSH), or zero. There are a few, less probable combinations of faults which can introduce an abrupt and persistent offset in the reading. These would be associated with the power supply leads to the Wheatstone bridge, which, in the case of the thermocouples, is located within the TRJ unit. NASA performed testing and analysis of the ME476-0133-0001 thermocouple reference junction units and found that there were three wiring failures which could produce this offset in the output: an open circuit in the +EXC lead, an open circuit in the –EXC lead, or a short circuit between the +EXC and –EXC leads, each of which has the effect of removing power from the Wheatstone bridge and allowing the bridge to float to whatever common-mode potential exists between the +SIG and –SIG output leads.

While NASA and Boeing identified the electrical commonality of these five thermocouple measurements, they did not identify the cause. They noted that in addition to these five thermocouples, that thermocouple sensor V07T9666A was also powered by this same PPS output from PCM-1, although it did not use the common terminal junction bar. They incorrectly stated that V07T9666A responded nominally all the way through to the terminal period of the re-entry flight, and that the cause for the jump in the other five thermocouple readings was therefore an vaguely defined "terminal block anomaly." In point of fact, thermocouple sensor V07T9666A was one of the four key sensors located behind RCC panel #9, and it failed to OSL at GMT 13:52:24 (EI + 495 sec), only two seconds behind the jump in the other 5 thermocouple sensors. While the burn-through of V07T9666A happens two seconds later than the jumps in the other five thermocouples, this does not discount their connection, since a given burn-through will create several faults within a sensor cable, and it is perfectly conceivable that the power supply fault which caused the jumps occurred a few seconds prior to the signal wire fault which caused V07T9666A to transition to an OSL value. A much better explanation for the abrupt jumps in these five thermocouple readings is offered simply by noting that a burn-through induced short between the power supply wires for the TRJ unit that supplied V07T9666A would pull the overall PCM-1 PPS outputs 17, 18, 89, and 90 to zero, and this effect would propagate to the other five thermocouple reference junction units as well. The jumps seen the these five thermocouples are in all likelihood the propagating electrical effects of the burn through of the left wing leading edge spar behind RCC panel #9.

Fuselage Left Side Surface Temperatures

Seven thermocouple temperature sensors on the left side surface of the fuselage recorded measurements in the MADS/OEX data. These were all instrumented through the MADS PCM-1 unit, and the thermocouples were listed in the Boeing integrated part and component locator (IPCL) as part numbers ME449-0204-0001, -0002, and -0003. The -0003 is probably a typographical error in the locator, since thermocouples only come in the -0001 type K and -0002 type R forms. In general, the thermocouples closer to the nose recorded largely normal behavior up until the last few seconds of the OEX data, while those toward the tail recorded anomalous temperature variations which indicated some unusual aerodynamic flow and heating trends that was most likely the result of damage to the left wing leading edge farther forward.

Starting from the nose of the vehicle and working towards the tail, sensor V07T9880A was the most forward located of all of the thermocouple surface temperature sensors, and it was mounted at (X322.5, Y–56.6, Z340.9), about six feet back from the tip of the nose on the left hand side of the vehicle. The reading from this sensor started at an OSL value of 0°F at EI, smoothly rose to a knee temperature of 960°F at EI + 360 seconds, and then steadily climbed at a much slower rate to 1100°F at GMT 13:59:44 (EI + 935 sec). At this point, it abruptly shot up towards an OSH limit of 1750°F and varied about this level until the end of the recorded data. Prior to this point, the behavior was well within the usual patterns of past flights.

Sensor V07T9522A is a surface thermocouple that is mounted at (X650.0, Y–105.0, Z354.7), about eight feet behind the crew door on the left side of the vehicle. The reading from this sensor began at an OSL value of 0°F at EI, climbed smoothly to 640°F over GMT 13:46:09 to 13:50:09 (EI + 120 to 360 sec), and then more slowly climbed to 940°F at GMT 13:59:44 (EI + 935 sec). At this point, the reading went straight up to an OSH value of 1300°F and remained there until the end of the recorded data. As noted previously, this sensor also exhibited an abrupt jump downward by –5 bits at EI + 493 seconds, and the origin of this was traced to a common power supply feed to its TRJ signal conditioner that was shared with other thermocouples on the lower surface of the fuselage. The cause of these jumps is most likely the wiring burn through of thermocouple sensor V07T9666A which occurred precisely at this time and which also shared this common power supply feed from PCM-1.

Sensor V07T9253A is a surface thermocouple mounted at (X1006.0, Y–105.0, Z355.5), on the left side of the midbody, just below the payload bay door and above the left wing. The reading from this sensor started at an OSL value

of 0°F at EI, and rose smoothly from 0°F to 200°F over GMT 13:47:24 to 13:53:24 (EI + 195 to 555 sec). At this point the behavior deviated sharply from that of prior flights and the temperature soared up to 400°F at GMT 13:54:39 (EI + 630 sec), steadily decreased back down to 240°F at GMT 13:57:49 (EI + 820 sec), and then rose steadily up to 450°F at GMT 13:59:44 (EI + 935 sec). Following this, the reading went up to an OSH limit of 880°F at GMT 13:59:51 (EI + 942 sec) and chattered between this and OSL until the end of the recorded data. Although the heating and cooling rates are large, this thermocouple appears to be measuring accurate data over the time period from EI through EI + 942 seconds where it reached its OSH limit.

Sensor V07T9903A is a surface thermocouple mounted at (X1006.0, Y–105.0, Z399.0), directly above V07T9253A and just below the left payload bay door. The reading from this sensor began at an OSL value of 0°F at EI, rose from 0°F to 480°F over GMT 13:46:09 to 13:53:09 (EI + 120 to 540 sec), and then continued to rise in a somewhat more erratic manner to 520°F at GMT 13:59:27 (EI + 918 sec). From this point, the temperature rapidly climbed to 630°F at GMT 13:59:41 (EI + 932 sec), after which it shot up to an OSH limit of 1300°F and remained there until the end of the recorded data, aside from one subsequent transition to OSL and back.

Sensor V07T9913A is a surface thermocouple mounted at (X1003.8, Y–105.0, Z441.4), directly above V07T9253A and V07T9903A on the payload bay door. The reading from this sensor started at an OSL value of 0°F at EI, rose from 0°F to 730°F over GMT 13:46:39 to 13:53:09 (EI + 150 to 540 sec), and then climbed more slowly and more erratically up to 840°F at GMT 13:59:41 (EI + 932 sec). At this point the reading shot straight up to an OSH value of 1300°F and then subsequently chattered between the OSL and OSH limits until the end of the recorded data. These reading appear accurate up until the failure point at EI + 932 seconds, and show a more erratic than normal heating trend over EI + 540 to 932 seconds, consistent with the timing of the anomalous readings from V07T9253A located just below it.

Sensor V07T9925A is a surface thermocouple mounted at (X1138.4, Y–105.0, Z441.4), also located on the left payload bay door at the same elevation as V07T9913A, but approximately eight feet further back. The reading from this sensor began at an OSL value of 0°F, rose from 0°F to 260°F over GMT 13:47:09 to 13:50:09 (EI + 180 to 360 sec), at which point the heating rate abruptly decreased and the temperature fell below the trend shown by prior flights. This sensor showed an abrupt jump downward by approximately 20°F at EI + 505 seconds, after which the heating rate began to increase again, reaching the normal value of 500°F at GMT 13:53:39 (EI + 570 sec), and continuing up to a peak of 830°F at GMT 13:54:34 (EI + 625 sec). The temperature then fell back to normal trends and values over EI + 780 to 900 seconds, and then it rapidly rose to an OSH limit of 1740°F at GMT 13:59:44 (EI + 935 sec), where it remained until a drop to OSL near the end of the recorded data. Sensor V07T9925A was the first of the left side fuselage temperature readings to show an anomalous behavior, and this occurred at GMT 13:50:09 (EI + 360 sec).

Sensor V07T9270A is a surface thermocouple mounted at (X1486.1, Y–124.8, Z307.1), located at the far tail end of the vehicle, and low on the fuselage to be directly behind the trailing edge of the left wing. The readings began at an OSL value of 0°F at EI, rose from 0°F to a knee temperature of 600°F over GMT 13:47:49 to 13:52:09 (EI + 220 to 480 sec), and then climbed more slowly to 650°F at GMT 13:57:09 (EI + 780 sec). Beyond this point, the temperatures still rose but with significantly more variations than normal and then shot up from 850°F to an OSH value of 1740°F at GMT 13:59:44 (EI + 935 sec), where they remained aside from one brief transition to OSL and back.

While not located on the fuselage left side surface per se, sensor V07T9749A was a surface thermocouple mounted on fuselage upper surface canopy at (X474.2, Y–24.0, Z482.4) and exhibited a similar behavior as the others. The response from this sensor began at an OSL value of 0°F at EI, rose smoothly from 0°F to a plateau at 360°F over GMT 13:46:39 to 13:53:09 (EI + 150 to 540 sec), and then rose smoothly again to 570°F at GMT 13:59:47 (EI + 938 sec), when it abruptly shot up to 990°F and then fell back to 800°F at GMT 14:00:09 (EI + 960 sec).

Collectively, all eight of these surface thermocouple sensors appeared to record valid data up until their failure points at around EI + 935 seconds. The two surface thermocouples with the most severe departures from normal flight behavior were V07T9253A and V07T9925A. Both of these happen to form a straight line that extends forward to the damaged area of the left wing leading edge, and this straight line also extends aft to pass very close to the front of the left OMS pod and the left side tip of the vertical stabilizer, both of which were heavily damaged by hot gas and particulate flow from the damaged left wing. The anomalous variation from normal heating trends over the period of EI + 560 seconds onward is indicative of a significant disruption in the normal air flow patterns across this part of the vehicle, and point to these as being downstream effects of the damage zone on the left wing leading edge.

Left Wing Lower Surface Temperatures

Twelve surface thermocouple measurements were recorded in the MADS/OEX data for the lower left wing. Each was a type R thermocouple that was mounted into the outer surface of the heat tiles, part number ME449-0204-0002, and were calibrated over a range of either 0-2400°F or 0-3000°F. In addition, one surface thermocouple measurement was recorded for the upper surface of the left wing, and this was a type K thermocouple, part number ME449-0204-0001, that was calibrated over a range of 0-900°F. These surface thermocouples were located along lines of constant Y coordinate, primarily Y = –235 and Y = –370, of the left wing.

Sensor V07T9636A was the only surface thermocouple located on the upper surface of the left wing at coordinates (X1352.3, Y–361.3, Z119.4). The reading from this sensor began at an OSL value of 0°F at EI and rose from 0°F to 90°F over GMT 13:47:49 to 13:52:22 (EI + 220 to 493 sec) following the normal behavior of past flights. At GMT 13:52:22 (EI + 493 sec), the reading took an abrupt jump downward by –7

bits or about 15°F. As noted previously, this can be attributed to its thermocouple reference junction sharing a PCM-1 precision power supply output with several other sensors which also showed an abrupt jump at the same instant. The originating cause is most likely the burn through of the wiring to the TRJ unit for thermocouple V07T9666A on the lower surface of the left wing, just behind RCC panel #9. Following this –7 bit jump, the reading then climbed briefly until GMT 13:52:59 (EI + 530 sec), at which point it shot up unphysically to 320°F and then back to 0°F at GMT 13:53:14 (EI + 545 sec). From this point onward, the reading stayed at the OSL level, aside for a few occasional and short lived jumps up from this value. This failure mode is characteristic of a wire burn through and indeed, the wiring for V07T9636A was routed along the X1307 cross spar of the left wing until it reached the access panels and there it joined other cables in forming harness #4 that was routed along the upper outboard surface of the left wheel well along Y = –167.0. From there, the cable went to connector 65P107 on the interconnect panel before passing through into the fuselage.

Sensor V07T9666A was a surface thermocouple on the lower surface of the left wing, located at coordinates (X1121.7, Y–236.7, Z102.0), close to the leading edge of the left wing. This was one of the four key sensors behind RCC panel #9 that provides the strongest evidence for establishing the burn through time of the left wing leading edge spar. The reading from this thermocouple began at 120°F at EI, rose smoothly up to 2000°F at GMT 13:50:09 (EI + 360 sec), and then began to behave anomalously with a higher rate of heating and an erratic spiking up until GMT 13:52:25 (EI + 496 sec), when it started to chatter between OSH and OSL limiting values. Three seconds prior at GMT 13:52:22 (EI + 493 sec) is when the jumps in the readings of V07T9480A, V07T9489A, V07T9492A, V07T9522A, and V07T9636A occurred, and as noted previously, it is wholly possible for the power supply fault which caused these jumps to have preceded the burn-through fault which caused the response of V07T9666A to transition to OSL. Yet, these events could not have been separated by too much time, either, and the three second difference between the two appears well within the range of reasonable time delay for these sequential events. Close inspection of the readings from V07T9666A show that there was a small downward transition in its data at EI + 493, too, which could be the result of the power supply fault. Sensor V07T9666A is also a sensor that NASA has not understood very well. Its position on the leading edge makes it subject to some unusual features of the air flow boundary layers during re-entry. For some flights the overall profile of the response from V07T9666A follows the normal, symmetrical heating curve. For other flights, the response shows portions where the response drops abruptly from 2000°F to 1500°F. The best explanation that NASA has for this phenomenon is that the boundary layer associated with the air flow over the wing surface experiences somewhat randomly timed attachments and releases which cause the heat transfer to the wing to vary greatly and produce the observed effects.

Three other sensors are located on the left wing lower surface and lie close to the Y = –235 plane. Sensor V07T9674A is a surface thermocouple located on the trailing edge of the left wing at coordinates (X1351.1, Y–237.0, Z96.1). The response of this sensor followed normal trends, rising from an OSL limit of 500°F to 1500°F over GMT 13:46:59 to 13:52:29 (EI + 170 to 500 sec). Immediately following this, it took a small dip down to 1450°F over EI + 520 to 550 seconds, and then returned to 1500°F. At GMT 13:53:44 (EI + 575 sec), the sensor exhibited a wire burn through failure mode consistent with a soft short burn-through process of the Kapton insulation. From EI + 595 seconds onward, the reading remained largely at the OSL limit. Sensor V07T9786A is a thermocouple on the left inboard elevon lower forward surface. Its response climbed smoothly from 80°F to 1600°F over EI to GMT 13:52:41 (EI + 512 sec), and the response then shot up briefly to over 3000°F and then plummeted to OSL where it largely remained. Sensor V09T9231A is a thermocouple mounted on the left inboard elevon lower middle surface at the coordinates (X1441.9, Y–234.5, Z101.9). The response of this sensor climbed smoothly from 80°F to 1250°F over EI to GMT 13:52:49 (EI + 520 sec) where it then fell abruptly to OSL. All three of these sensors had their cables routed among the four harnesses that followed Y = –167 forward through the access ports and along the upper outboard wall of the left wheel well.

Two surface temperature thermocouple sensors were located on the inboard edge of the outboard left elevon at approximately Y = –320. Sensor V09T9845A is mounted at mid-gap in the middle of the inboard edge. The response of this sensor climbs smoothly from 50°F to 1800°F over the time from EI to GMT 13:53:04 (EI + 535 sec), when its response drops abruptly, reaching OSL at GMT 13:53:19 (EI + 550 sec). Sensor V09T9849A is mounted on the lower surface edge of the outboard elevon. The response of this sensor climbs smoothly from 100°F to 1900°F over the time from EI to GMT 13:52:51 (EI + 522 sec), after which it falls abruptly to OSL. The wiring from both of these sensors follows nearly the same route, traveling inboard along the cross spar at X1307 and then heading forward along the access ports and upper outboard wall of the left wheel well at Y = –167.

Three other surface thermocouples were located close to the left outboard elevon along the Y = –370 plane. Sensor V07T9711A was mounted on the lower surface of the trailing edge of the left wing at the coordinates (X1363.0, Y–369.0, ZBOT). Sensor V07T9713A was mounted on the lower middle surface of the left outboard elevon at the coordinates (X1402.0, Y–375.3, Z98.2). Sensor V07T9785A was mounted on the lower forward surface of the left outboard elevon. All three of these sensors had essentially the same characteristic behavior, beginning at approximately 100°F at EI and climbing smoothly to a maximum heating value of 1700°F. Close to their normal maximum, each abruptly fell to OSL with a failure signature that is once more typical of a soft-short wiring burn through. The burn through occurred at GMT 13:52:59 (EI + 530 sec) for V07T9711A; at GMT 13:53:09 (EI + 540 sec) for V07T9713A; and at GMT 13:52:59 (EI + 530 sec) for V07T9785A. The wiring for all three of the thermocouples runs inboard along the X1307 cross spar and then forward along Y = –167.

The last three remaining surface thermocouples are located further out on the left outboard elevon. Sensor V09T9893A measures the lower surface temperature of the left outboard

elevon cove, while sensor V09T9894A measures the upper surface temperature at nearly the same location. The lower surface temperature of the elevon cove rose from 50°F at EI up to 1150°F at GMT 13:52:32 (EI + 503 sec), after which it spiked up and then fell to OSL. The upper surface temperature of the elevon cove rose from 70°F at EI up to 300°F at GMT 13:52:32 (EI + 503 sec) also, after which it also spiked up and then fell to OSL. Sensor V09T9860A is another thermocouple that measures the elevon cove insulation surface temperature at the coordinates (X1382.0, Y–422.0, Z289.0). The response of this sensor rose from 50°F at EI up to 780°F at GMT 13:52:32 (EI + 503 sec), after which it, too, spiked up and fell to OSL. The wiring for V09T9893A and V09T9894A is routed identically and first inboard along the X1307 cross spar, and then forward along Y = –167. The wiring for V09T9860A is routed somewhat differently, first traveling inboard along the elevon hinge line, then forward along Y = –254, then inboard along the X1307 cross spar, and then forward along Y = –167.

All thirteen of these left wing surface temperatures experienced an abrupt burn through failure within the rather narrow time frame of EI + 496 to 540 seconds. The one exception to this is V07T9674A, which exhibited an anomalous and inexplicable drop of 50°F at EI + 505 seconds prior to its transition to OSL that began at EI + 575 seconds. Sensor V07T9666A was the earliest to burn through at EI + 496 seconds, since its wiring was routed along the leading edge spar of the left wing. The burn through the aluminum honeycomb spar itself and the time for which hot gases began to enter the wing box falls within the range of EI + 492 to 497 seconds, based upon the four key sensor behind RCC panel #9, for which V07T9666A is one. The other twelve surface temperature sensors all had their wiring routed along the opposite side of the wing box cavity, along the upper outboard wall of the left wheel well. The data shows that these underwent burn through wiring failures as early as EI + 503 seconds, only 6 to 10 seconds after the hot gas breached the wing box cavity. While the observed ordering of the events makes logical sense, the short time delay between the spar breach and the burn through of wires on the opposite wall of the wing box indicates an extremely intense internal heating rate and/or directionality to the intruding flow.

Orbital Maneuvering System (OMS) Pod Temperatures

The MADS/OEX system recorded 8 temperatures on the left OMS pod and 1 on the right OMS pod. All 9 of these were instrumented through PCM-1 of the MADS system. All of these but one were thermocouple temperature sensors with part numbers ME449-0204-0001 or ME449-0204-0003, and the remaining one (V07T9221A) was an RTD temperature sensor of part number ME449-0106-0001. The interesting feature of this set of sensors is that they began to deviate from the normal re-entry pattern at an early time of approximately GMT 13:49:49 (EI + 340 sec), during the execution of the first rightward roll of the vehicle, and just prior to the first set of anomalous communications drop outs. Another interesting feature of these sensors is that most of them recorded a drop in the outside temperature of the left OMS pod during a period of the re-entry flight for which these surface temperatures are normally slowly rising. The sensors will be described in an order going from the rear of the OMS pods forward.

Sensor V07T9219A is a thermocouple mounted into the high temperature reusable surface insulation (HRSI) heat tiles at the most rearward position on the left OMS pod, located toward the bottom of the pod where it meets the fuselage of the orbiter. The recorded temperature from this sensor followed normal re-entry behavior until GMT 13:52:59 (EI + 530 sec), when its previously smooth rising behavior changed directions and started downward. It then followed an approximately constant 800°F until GMT 13:53:44 (EI + 575 sec) at which point it took a more rapid drop in temperature, bouncing up and down between 600-800°F up until its apparent failure at GMT 13:59:48 (EI + 939 sec). The normal pattern for this sensor on re-entry is to continue rising from about 800°F to about 1000°F over the same period. After this, it chattered between an OSH value of 1740°F and an OSL value of 0°F up until the end of the OEX recorded data at GMT 14:00:14 (EI + 965 sec).

Sensor V07T9222A is another thermocouple mounted into the HRSI heat tiles, also toward the bottom of the pod where it meets the fuselage, but a few feet forward of V07T9219A. This sensor recorded a normal heating trend up to 680°F at GMT 13:52:34 (EI + 505 sec), after which it dropped sharply and abnormally to roughly 500°F where it largely remained until its apparent failure at GMT 13:59:48 (EI + 939 sec). The normal trend for this sensor would be for it to continue smoothly climbing up to about 900°F by roughly EI + 850 seconds. After its failure, V07T9222A chattered between its OSH value of 1740°F and its OSL value of 0°F.

Sensor V07T9223A is also a thermocouple that is mounted into the HRSI heat tiles, also toward the bottom of the pod where it meets the fuselage, and a few more feet further forward than the previous two. This sensor similarly recorded a fairly normal rise in temperature up to about 300°F at GMT 13:52:34 (EI + 505 sec), when it abruptly fell by 40°F for 20 seconds, and then started climbing at an abnormally fast rate, recording temperatures much higher than normal. By GMT 13:59:19 (EI + 910 sec), this sensor was reading well above 600°F, whereas normal behavior would have only reached about 400°F by the same time. At this point, the temperature rose extremely rapidly to 1140°F at GMT 13:59:48 (EI + 939 sec), when it failed by starting a chattering behavior between an OSH of 1740°F and OSL of 0°F. The interesting feature, of course, is that two sensors, V07T9222A and V07T9223A, located within only a few feet of each other, could record such drastically different trends, one recording temperatures up to 400°F lower than normal and the other recording temperatures up to 250°F higher than normal.

Sensor V07T9978A is a surface thermocouple that is mounted into the heat tiles at an approximately mid elevation on the pod and approximately six feet back from the front. This is considerably further forward than the previous three sensors. This sensor recorded a normal heating trend up to 520°F at GMT 13:49:49 (EI + 340 sec), when its rate of rise reduced and it began recording cooler than normal temperatures for this time during the re-entry. This temperature then stayed lower than normal by 50-100°F up until GMT 13:52:

29 (EI + 500 sec), after which it rapidly rose to higher than normal temperatures, reaching at first peak at 820°F at GMT 13:53:10 (EI + 541 sec). The temperature then fell rapidly to 670°F at GMT 13:54:09 (EI + 600 sec), and then rose rapidly to 1175°F at GMT 13:56:59 (EI + 770 sec). Normal temperatures at this time would have been only 600-650°F. Over the period from EI + 840-900 seconds, the temperature dipped down by about 200°F, and then soared up to its OSH value of 1300°F at GMT 13:59:30 (EI + 921), just two seconds before the telemetry loss of signal. After this, the recorded temperature chattered between its OSH and OSL limits.

Sensor V07T9976A is also a surface thermocouple that is mounted at approximately mid elevation on the pod and approximately four feet back from the front. This sensor behaved very similarly to V07T9978A, following normal trends up to 550°F at GMT 13:49:49 (EI + 340 sec), when its rate of rise dropped off prematurely and it then followed below the normal temperatures by about 50°F. Over GMT 13:52:54 to 13:53:14 (EI + 525 to 545 sec), the temperature then rapidly rose to 1030°F, and the plummeted to 750°F at GMT 13:54:09 (EI + 600 sec). Following this sharp dip in temperature, which was also recorded by most of the sensors on the forward part of the left OMS pod, the temperature then rapidly climbed up to vary about within the 1100-1300°F range until it dropped by about 300°F over EI + 840-900 seconds, another characteristic that was shared by most of the sensors on the front of the left OMS pods. After this, the temperature very rapidly rose to its OSH value of 1740°F at GMT 13:59:28 (EI + 919), where it failed and began chattering between its OSH and OSL limits.

Sensor V07T9972A is another surface thermocouple that is mounted high on the left OMS pod, approximately two feet back from the front. Its response was also very similar to that of V07T9976A and V07T9978A. It recorded a normal temperature up to 440°F at GMT 13:49:52 (EI + 343 sec), after which its rate of rise fell below normal. It slowly caught back up to a normal temperature of about 640°F at GMT 13:52:49 (EI + 520 sec), and then over GMT 13:53:09 to 13:53:49 (EI + 540 to 580 sec), it rapidly rose to 870°F. It then reached 1000°F at GMT 13:55:44 (EI + 695 sec), and stayed around this value until it dropped by about 150°F over EI + 840-900 seconds. At GMT 13:59:44 (EI + 935 sec), the temperature hit the OSH value of 1300°F and then chattered between the OSH and OSL limits until the end of the recorded MADS/OEX data.

Sensor V07T9220A is a thermocouple that was placed on the outside surface of the low temperature reusable surface insulation (LRSI) heat tiles at approximately mid elevation and approximately two feet back from the front of the pod. This sensor responded normally up to 310°F at GMT 13:49:59 (EI + 350 sec), when its rate of temperature rise fell below normal and its temperature fell about 100°F below the normal values for this time. The temperature began climbing faster at GMT 13:52:39 (EI + 510 sec), reaching a normal value of 500°F at GMT 13:53:14 (EI + 545 sec), and continuing up to around 1000°F at GMT 13:55:39 (EI + 690 sec). At GMT 13:59:37 (EI + 928 sec), it peaked up to 1200°F, and then failed at its OSH value of 1740°F at GMT 13:59:47 (EI + 938 sec), chattering between OSH and OSL limits.

Sensor V07T9221A is an RTD temperature sensor that was placed at the same location as V07T9220A, but on the underside of the LRSI heat tile, on the skin-to-tile bond line of the left OMS pod. This sensor, in contrast to its mate on the outer surface of the LRSI heat tile, recorded a perfectly normal temperature versus time profile over the entire re-entry period, up until it abruptly failed at GMT 13:59:49 (EI + 940 sec). At EI, it read 5°F, and this very slowly and smoothly rose to 12°F at its point of failure, when it then began to chatter between its OSH limit of +450°F and its OSL limit of –200°F. This RTD sensor mounted on the aluminum skin of the bond line shows rather clearly that the abnormal heating that was seen on the other left OMS pod sensors was coming from conditions outside the pod, rather than from within, as could have possibly been the case if, for example, an OMS pod or RCS hydrazine or oxygen cell might have ruptured and/or exploded.

Finally, sensor V07T9224A is a thermocouple that was placed on the outside surface of the LRSI heat tiles at the same location as V07T9220A and V07T9221A, but on the right OMS pod. This was one of the few temperature sensors that was on the right side of the vehicle. While the normal behavior for this sensor involves several gradual variations between 500-700°F over the course of the re-entry flight, the behavior on STS-107 fell largely within the range of these variations. The only substantive departure from normal behavior occurred at GMT 13:59:59 (EI + 950 sec) where the temperature shot up rapidly to 870°F just prior to the end of the MADS/OEX recorded data. This sensor never hit either its OSH limit of 1740°F or its OSL limit of 0°F, and its failure mode was a simple abrupt rise at the end of its data, rather than the characteristic chattering between OSL and OSH that the temperature sensors on the left OMS pod all exhibited.

The collected debris of the *Columbia* included a large section of the front of the left OMS pod which shows quite clearly that it was impacted by an abnormally intense stream of hot gas and particulates. The front of the left OMS pod was also directly downstream from the damaged area of the left wing leading edge, and thus, any material eroded away from that part of the left wing could easily be carried back to impact the front of the OMS pod. The temperatures on the front of the left OMS pod (V07T9220A, V07T9972A, V07T9976A, and V07T9978A) all dropped below normal after EI + 340 seconds, and then rose well above normal after EI + 540 seconds. Each also recorded distinct drops in their elevated temperatures at EI + 600 and over EI + 840-900 seconds. The two most rearward located temperatures (V07T9219A and V07T9222A) both showed normal behavior up to EI + 540 seconds and then significantly lower than normal temperatures. Sensor V07T9223A which was located roughly midway between these two groups, although closer to the rear group, showed only the higher than normal temperatures beyond EI + 540 seconds. If aerodynamic heating is correlated with suspended particulates which could cause surface damage to the front tiles of the left OMS pod, then this damage must have occurred during the post EI + 540 period. Since the temperatures and rate of heating on the front of the left OMS pod were actually lower than normal during EI + 340-540 seconds, it is unlikely that they were receiving any intensified flow or particulate flux from the left wing

damage zone during this time. The drastic difference in the temperature variations between two sensors that were located fairly close together (V07T9222A and V07T92232A) suggests that the air flow over the left OMS pod was either turbulent, unstable, or broken into segments in which the boundary layer was attached in some places, but not in others. Any of these circumstances would be consistent with a drastic disruption in the vehicle's airflow patterns originating from damage to the left wing leading edge.

Chin Panel Temperatures

The chin panel is a rather unusual piece of bodywork that covers the area between the nose cap and the nose wheel door on the underside of the vehicle. It is also constructed of reinforced carbon – carbon (RCC), the same material as the leading edge of the wings, and it also makes use of a T-seal piece for the joint between it and the nose cap. The T-seal and the chin panel itself are attached to the vehicle with a clevis pin assembly, similar to the mounting of the RCC panels for the wings. The location of the temperature sensors is detailed in drawing JSC-ES3-33189, which shows five temperature sensors in cross sectional view C-C. Two are located on the clevis just behind the nose cap, V09T9888A at Y0 (on the vehicle's centerline) and V09T9889A at Y-23 (23 inches to the left of the centerline). One sensor was located on the inside of the aluminum skin behind the chin panel, V09T9890A at Y-8. The two others were located on the inside surface of the RCC chin panel material, V09T9891A at Y-8 and V09T9892A at Y+8. The latter of these, V09T9892A was an unused spare; hence, there were only four measurements recorded for the chin panel area, all on PCM-1 of the MADS/OEX system. The other sensor on the inside surface of the RCC chin panel material, V09T9891A, was know to have been bad as a pre-existing condition to the flight. Its output reads a constant and erroneous 2500°F for all of the recorded re-entry period.

Of the three chin panel temperature sensors that recorded valid data, two of these were perfectly normal in their behavior in comparison to past flight data. Sensor V09T9888A, also described as the "RCC attachment lower clevis temperature," recorded 40°F at EI which then rose slowly and smoothly to 680°F over the period from EI + 260 to 965 seconds, which was the end of the recorded OEX data. Similarly, sensor V09T9890A, also known as the "RCC aluminum structure temperature," toggled between 47.0-49.5°F at EI and then over EI + 700 to 965 seconds rose by 4 bits to a final recorded value of 59.5°F. Neither of these sensors showed any spikes or abnormal transients in their recorded data.

The chin panel temperature sensor with the anomalous behavior was V09T9889A, also known as the "RCC attachment outboard clevis temperature." This sensor recorded a temperature of 20-30°F at EI which began a normal rise starting at EI + 300 seconds. However, at from GMT 13:52:19 to 13:52:34 (EI + 490 to 505 sec) the temperature rose abnormally from 105°F to 180°F, and then somewhat more slowly fell to 155°F at GMT 13:53:04 (EI + 535 sec). From this point onward, the temperature followed a smooth and gradual to climb to 605°F at GMT 14:00:14 (EI + 965 sec) which was the end of the recorded data, although the rate of rise was slightly higher than normal.

While the overall departure of this sensor away from normal behavior is rather minor, the spiking up of the temperature over EI + 490 to 535 seconds is quite distinct. And while there were other significant events occurring within the left wing damage zone within this time frame, this signature is puzzling, because of its very forward location and the lack of any common interconnections or power feeds which could have coupled disruptive signals into this measurement. These events are, however, simultaneous with the OFI telemetry measurements of the fuselage water dump and vacuum vent nozzle temperatures, both of which are also located well forward on the vehicle. The V09T9889A chin panel temperature also has in common with the water dump and vacuum vent nozzle temperatures a location toward the left side of the vehicle and the same relative magnitude of the recorded temperature anomalies. It is reasonable to suspect that the chin panel and the water dump and vacuum vent nozzle temperatures were all responding to the same set of external environmental conditions over the critical time frame of EI + 490 to 535 seconds.

Structural Strain Gauge Measurements

The MADS/OEX strain gauge structural measurements are voluminous, but not as revealing as the temperature and pressure measurements. This is due largely to the more difficult interpretation of structural strain data, often requiring both a strong background in structural mechanics and a detailed model of the structure. Typically, many different strain gauge measurements must be compiled and compared against a computer model to determine the originating forces that would be responsible for such strains, anomalous or normal. Because strain is a vector quantity with six principal components (three axial strains and three shear strains), several different strain gauge measurement combinations must usually be used to resolve the desired strain vector components. Strains also vary strongly with location, much more so than temperatures and pressures, and this is why such a large number of strain gauges are typically used to instrument a given structure. However, the burn through timing and failure modes of the strain gauge wiring further validate the overall sequence of events, and this is generally where the more valuable data lies within this group of measurements.

A total of 422 strain gauge measurements were active when STS-107 lifted off, and these were recorded by the MADS/OEX system on PCM-1, PCM-2, and PCM-3. All of the 184 strain gauge measurements that were recorded on PCM-3 were done in a "snap-shot" mode, in which data is taken for a one minute period, followed by four minutes during which no data is taken. The snap-shot mode is typically used for those sensors whose readings change sufficiently slowly as to not require the faster once or ten times per second rates that the MADS system supports. With a few exceptions, the strain gauge measurements on PCM-1 and PCM-2 were continuous over the recorded time period. Because the snap-shot mode only samples for 20% of the running time, it is considerably less useful for picking out critical timing of events, unless those events just happen to fall within a one minute period that the data is being taken. As such, the PCM-3 data was far less useful than that from PCM-1 and PCM-2.

Within the left wing, 121 strain gauge measurements were made on the wing box structure itself and having MSIDs starting with V12G, with 45 on PCM-2 in continuous mode and 76 on PCM-3 in snap-shot mode. There were 26 strain gauge measurements made on the left elevon hinges in the V13G group, all on PCM-2, with 10 made continuously and 16 made in snap-shot mode. By far the most common pattern for these measurements is a sudden off-scale event occurring in the time period of EI + 500 to 580 seconds, after which the measurement returns to a nearly zero reading. This pattern was evident in 41 of the 45 left wing strain gauges on PCM-2, and in all 10 of the 10 left elevon hinge strain gauges on PCM-2 that were in continuous mode.

A few of the left wing strain gauges deserve particular comment. Sensor V12G9921A was one of the four key sensors on the aluminum honeycomb spar behind RCC panel #9. As discussed previously, this gauge recorded an anomalous reading as early as GMT 13:48:29 (EI + 260 sec) when its recorded strain began to rise above normal behavior, peaking up to a value of +180 μin/in at GMT 13:50:09 (EI + 360 sec), then falling and crossing zero at GMT 13:51:39 (EI + 450 sec), reaching a negative peak of –140 μin/in at GMT 13:52:04 (EI + 475 sec), and then shooting up and down drastically at GMT 13:52:24 (EI + 495 sec). This last event is the failure signature for the wires of this strain gauge and provides a timing mark for the burn through of the spar itself. Following the failure signature, the recorded strain falls to a flat, unresponsive reading which results from the residual offset trim of the strain gauge signal conditioner, in this case about +35 μin/in. Prior to GMT 13:52:24 (EI + 495 sec), the strain readings were well within the range of measurement for the system, and within the range that would be expected for actual strains in the leading edge spar, given that it was being subjected to destructive forces from the broken RCC materials of the left wing leading edge. Thus, the data from this strain gauge appears perfectly valid prior to EI + 495 seconds.

In addition to V12G9921A, sensor V12G9056A is a strain gauge mounted on the top of the spar cap at coordinates (X1365.0, Y–238.0, ZUPR) that Boeing identified as another which showed an anomalous response well before EI + 500 seconds, however this characterization is somewhat debatable. The normal trend for this sensor has been to remain at a constant value of –65 μin/in for the period of EI to EI + 800 seconds, varying up and down by only a bit or two. For STS-107, the reading from this sensor went down by one bit at GMT 13:48:29 (EI + 260 sec), and then down by another bit at GMT 13:49:20 (EI + 311 sec) to a value of about –105 μin/in. At GMT 13:53:29 (EI + 560 sec), the reading shot downward to OSL, and then immediately return back to a flat and unresponsive reading of nearly zero for the remainder of the recorded data. This behavior of falling by two bits over the period of EI + 260 to 311 seconds is different from past flights only in that previously the maximum drop was one bit during the same period. The location of this strain gauge is also far back toward the trailing edge of the left wing, and quite some distance from the damage zone of the leading edge. It is difficult to conceive of any physical means by which a sensor this far back would be responding this early to the left wing damage. This time frame is also earlier than the earliest identified wire burn through, so the additional bit changes during this time cannot be attributed to instrumentation system damage. In any event, the departure from prior flights of the reading from this strain gauge is quite small and can be largely dismissed as a random bit flip that had no conclusive relation to the left wing damage effects. Of the 45 strain gauges on the left wing that were in continuous recording mode, only V12G9921A showed a significant and conclusive departure from normal behavior prior to EI + 500 seconds. The so-called anomalous reading from V12G9056A is very subtle, if present at all, and far from conclusive. Given the large number of structural strain gauges distributed throughout the left wing frame, the fact that only one of these showed any significantly anomalous behavior prior to EI + 500 seconds gives fairly conclusive evidence that the entry of the damage path into the wingbox did in fact occur only at the leading edge spar behind RCC panel #9.

Of the remaining 43 of the 45 left wing strain gauges in continuous recording mode, all but two showed a wiring burn through failure mode within the time span from GMT 13:52:29 to 13:53:49 (EI + 500 to 580 sec). A typical response was like that from V12G9055A, in which the data followed the past flight history perfectly until GMT 13:52:29 (EI + 500 sec) where it started to anomalously decrease, and then at GMT 13:52:54 (EI + 525 sec) it rapidly shot up to OSH and then fell back to a zero, unresponsive level at GMT 13:53:05 (EI + 536 sec) for the remainder of the recorded data. Another typical response was like that from V12G9911A, where the data again followed the prior flight history up until a time of GMT 13:52:44 (EI + 515 sec), after which it chattered back and forth between OSH and OSL until falling permanently to a zero unresponsive state at GMT 13:55:09 (EI + 660 sec). The response from V12G9063A was generally of a similar nature, but appeared to record several sudden events within its wiring burn through failure signature. The response first fell abruptly from past trends at GMT 13:52:34 (EI + 505 sec), going from +150 μin/in to –200 μin/in. It held roughly this value for quite some time, until a series of off-scale spikes that occurred over GMT 13:53:49 to 13:54:39 (EI + 580 to 630 sec), after which it decayed back to the –200 μin/in level until it abruptly dropped to zero at GMT 13:57:59 (EI + 830 sec). The V12G9063A strain gauge is located at coordinates (X1191.0, Y–244.0, ZLW), which is about seven feet directly aft of V12G9921A on the leading edge spar. Its wiring also gets routed along the inside of the leading edge spar, and this can account for a large share of the unusualness of its response.

Two of the 45 left wing strain gauges that were in continuous recording mode also recorded an anomalous event around EI + 500 to 580 seconds, but their readings did not go off-scale, nor behave erratically until the terminal phase at EI + 930 seconds. Both of these strain gauges were located far forward on the left wing X1040 spar. Strain gauge V12G9048A was located at the coordinates (X1040.0, Y–135.0, ZLWR) on the lower spar cap, and strain gauge V12G9049A was located at coordinates (X1040.0, Y–135.0, ZUPR) on the upper spar cap. At GMT 13:52:19 (EI + 490 sec), the reading from V12G9048A began to smoothly rise from +50 μin/in to a peak at +350 μin/in at GMT 13:54:39 (EI + 630 sec), and then smoothly decayed back to a normal value of +150

μin/in at GMT 13:57:49 (EI + 820 sec), with only a minor upward jump of 30 μin/in at GMT 13:55:34 (EI + 685 sec). At GMT 13:59:44 (EI + 935 sec) the response then began spiking up to off-scale values, typical of a wire burn through failure at that point. The reading from V12G9049A followed normal trends until GMT 13:53:39 (EI + 570 sec), when it began to rise smoothly from −40 μin/in to +240 μin/in at GMT 13:55:34 (EI + 685 sec). At this point, the same time as when V12G9048A took a slight jump upward, strain gauge V12G9049A took a larger jump downward to a value of +80 μin/in. From there, the response increased smoothly again to a value of +250 μin/in at GMT 13:59:44 (EI + 935 sec), after which it, too, began spiking up to off-scale values as it began a wire burn through failure signature. The simultaneous jumps in both of these strain gauge readings appears to be the result of a common power supply connection. The responses from both of these two strain gauges on the X1040 spar appears to be the actual strain at that location up until their failures at EI + 935 seconds. Because the X1040 spar crosses in front of the left wheel well, and the exposed wiring for most of the sensors in the left wing runs along the front of this spar, the fact that both of these strain gauges remained operational until EI + 935 seconds indicates that no left wing damage propagated into the wing cavity area in front of the wheel well until at least EI + 935 seconds. This is significant, because it implies that the route that the hot gases must have taken to cause the damage inside the left wheel well must have occurred by way of burning through the outboard wall of the wheel well, rather than snaking around forward and then back through the access panel at the front of the wheel well, as was originally hypothesized. Further, both of these strain gauges record some significant and anomalous strains prior to their failure, indicating strong twisting distortions that were occurring within the wing frame near to the front of the left wheel well.

Within the right wing, 126 strain gauge measurements were made on the wing box structure itself in the V12G group, with 65 on PCM-1 in continuous mode, 21 on PCM-2 in continuous mode, and 40 on PCM-3 in snap-shot mode. There were also 26 strain gauge measurements on the right elevon hinges in the V13G group, all on PCM-1, with 10 made continuously and 16 made in snap-shot mode. One of the right wing upper skin strain gauges, V12G9653A, recorded ascent data, but did not respond for re-entry data, presumably failing somewhere in between the two periods. Thus, there were only 125 recorded measurements for the right wing during the re-entry flight. The most common measurement pattern for the right wing was a completely normal response, matching to the trends and values of past flights, up until the terminal phase that began around EI + 930 seconds. Of the 85 continuous mode right wing strain measurements on PCM-1 and PCM-2, 51 showed this behavior, as did 8 of the 10 continuous mode right elevon strain measurements. The remaining 34 continuous right wing strain measurements and 2 continuous right elevon strain measurements exhibited an anomalous event near EI + 500 seconds, but this did not cause off-scale readings or erratic behavior. One example of this is strain gauge V12G9068A, whose reading at GMT 13:52:29 (EI + 500 sec) reversed its rising trend and fell continuously below its normal trend by about 100 μin/in until its failure at GMT 13:59:44 (EI + 935 sec). Another example is strain gauge V12G9815A, whose reading rose and fell by 3 bits over the time span of GMT 13:52:24 to 13:53:04 (EI + 495 to 535 sec) before returning to normal values and then ultimately failing at GMT 13:59:44 (EI + 935 sec).

A variety of other strain gauges were measured during the re-entry flight, but these were all done completely in snap-shot mode and did not provide much relevant information. There were 15 strain gauge measurements made on the payload bay door hinge lines in the V37G group, and all of these were made on PCM-2 in the snap-shot mode. There were 40 strain gauge measurements made on the midbody fuselage in the V34G group, 28 on PCM-1 and 12 on PCM-2, all in the snap-shot mode. There were 38 strain gauge measurements made on the vertical stabilizer in the V22G group and 12 rudder hinge moment strains in the V23G group, all made in snap-shot mode. Finally, there were 2 aft fuselage strain measurements in the V08G group and 16 aft fuselage OMS deck strains in the V35G group, again, all made in snap-shot mode. Many of these exhibited completely normal behavior over the 1 minute sampled time windows, such as V13G9834A located on the right outboard elevon hinge, while a few showed anomalous behavior during their 1 minute sampled time windows, such as V13G9818A located on the left outboard elevon hinge. However, the lack of any recorded data for this sensor and ones like it over the 4 minute blank time windows makes further investigation of their anomalous behavior difficult at best and rather nonconclusive.

Wide Band FDM Data

The two frequency division multiplex (FDM) units were programmed to interleave a total of 104 different wide bandwidth measurements. Each of the two FMD units can interleave 15 channels on each of their 4 multiplexers for a total of 120 measurements. For STS-107, 16 channels were unused. For FDM-1, multiplexers M1A, M1B, M1C, and M1D were recorded on tracks 6, 8, 10, and 12, respectively, of the OEX recorder during the re-entry flight; for FMD-2, multiplexers M2A, M2B, M2C, and M2D were recorded on tracks 22, 24, 26, and 28, respectively. The ascent and deorbit flight segments were recorded on a different selection of OEX recorder tracks.

The wideband data included two MSIDs which are reserved for FDM timing synchronization, V75W9006D and V75W9016D, filling channel 1 of M1A and M2A, respectively. The main body measurements included 17 vibration sensors with MSIDs beginning with V08D, 4 acoustic measurements with MSIDs beginning with V08Y, and two wideband strain measurements with MSIDs beginning with V08G. The tall vertical stabilizer had 6 wideband strains recorded with MSIDs beginning with V22G, and the rudder had 12 wideband strains with MSIDs beginning with V23G. The midbody fuselage had 9 accelerometer measurements recorded with MSIDs beginning with V34A, and 16 additional wideband strains with MSIDs beginning with V35G. In addition, 12 wideband strains and 24 vibrations were recorded for the main engines with MSIDs beginning with E41G and E41D, respectively. Since the main engines are off, the 36 measurements associated with them do not pro-

vide any useful information for the re-entry flight. Analysis of the FDM data was accomplished rather late in the analysis because the raw OEX recorder data had to be sent to Boeing at Huntington Beach for them to perform the power spectral density (PSD) analyses. The results of that analysis were presented to NASA and the CAIB on May 23.

For the re-entry flight, the primary wideband sensor of interest was V08D9729A, which is an accelerometer that measures the Z-axis motion of the left outboard elevon at the coordinates (X1429.4, Y–435.0, Z). It has a matching counterpart on the right outboard elevon, V08D9737A, located at the coordinates (X1429.4, Y+435.0, Z). The Z-coordinate for both was not specified in the available documentation. Both accelerometers are part number ME449-0163-0002, and measure accelerations of up to 20 G, peak-to-peak. These two accelerometer readings were recorded on the 16 kHz center frequency channel #2 of FDM-1, with V08D9729A on the M1B multiplexer and V08D9737A on the M1C multiplexer. Since both of these accelerometers measure Z-axis motion of the wing tips, they are sensitive to symmetrical or anti-symmetrical "flapping" modes on both wings.

The recorded data for both of these accelerometers showed a normal behavior up through approximately GMT 13:52:19 (EI + 490 sec), which included a normal transient response to the activation of the elevons at GMT 13:47:52 to 13:47:53 (EI + 233 to 234 sec). This transient matched to the known activation of the elevons at this time, and consisted of 6-7 cycles of a damped oscillation with a peak acceleration of slightly less than 1 g in both directions. Two sharp transients then occurred on the left outboard elevon at GMT 13:52:25 (EI + 496 sec) and GMT 13:52:31 (EI + 502 sec), with peaks close to 2.0 g for the first and nearly 2.5 g for the second. The right outboard elevon did not record any significant disturbances during these periods, and its data remained at a fairly normal rms noise level of approximately 0.2 g. The power spectral density (PSD) showed no significant changes before and after these transient events, as all of the expected frequency components that are associated with known vibrational modes of the wings and elevons were present. These included a primary 5.7 Hz mode associated with symmetrical bending of the wings, akin to flapping motion, a 13 Hz mode associated with the first rotational mode of the elevon itself, 19 Hz and 22 Hz modes associated with the second bending mode of the wings, and a 30 Hz mode associated with a torsional mode of the outboard elevon. At GMT 13:53:03 (EI + 534 sec), the left outboard elevon accelerometer recorded a transient which saturated the measurement range at greater than ±10 g. Over EI + 534 to 537 seconds, a displacement grew within the recorded measurement that was unphysical and most likely indicated a failure mode of this type of linear, low-frequency accelerometer. After the displacement caused a saturated output, the 6 Hz wing mode was no longer recognized in the PSD, and this is another indication that the accelerometer or its wiring had been damaged by the event at EI + 534 seconds. Beyond this point, the recorded data shows numerous chattering between OSH and OSL limits of ±10 g, all of the way out to the end of the recorded data. The right outboard elevon accelerometers begins to pick up this activity also from about GMT 13:58:19 (EI + 850 sec) onward.

Among the other wideband re-entry data, there were several other accelerometers which were placed along the longeron of the orbiter, but none of these recorded any significant transient vibrations or displacements. The wideband strain gauges also recorded essentially nominal strain values over the re-entry flight. The PSD of the wideband sensors on STS-107 generally matched well to those of STS-109 in the frequency domain; however, STS-107 exhibited a large number of transient spikes in the time domain that STS-109 did not. Overall, the wideband FDM data did not add any significant new information about the orbiter's damage extent or propagation, but simply reinforced the timing of around EI + 495 seconds onward, during which the damage began to cause wiring burn throughs and other internal structural damage to the left wing that was recorded on many of the different instrumentation systems.

Ascent Data

Ascent data from both the OEX and OFI instrumentation systems is largely unremarkable. Particular interest is in the time frame around 82 seconds Mission Elapsed Time (MET), around which the foam debris strike from the external tank (ET) is best centered. As detailed below, none of the sensors in the PCM OEX suite recorded any significant disturbance which could be linked to a debris strike around this period of time.

The temperature sensors are divided into two systems: the aerothermal sensors on the outer skin of the left wing, left fuselage, and left OMS pod (35 sensors in the V07T set), and the internal structural sensors on the elevon coves, spars, and RCC clevises (14 sensors in the V09T set). Several temperature sensors showed some differences from prior flight histories; however, these deviations are in general not very significant. V07T9222A showed a slight rise at 330 sec MET on the left OMS pod, but this was still well within family. V07T9224A showed widely disparate data on all past flights, but STS-107 was still within this overall band. V07T9468A showed a slightly warmer lower fuselage surface temperature over 120-360 sec MET. V07T9470A showed some transient spiking over 90-120 sec MET, although this was also seen on prior flights. V07T9478A showed a 2-bit higher temperature on the fuselage surface, and this is very faint, if significant at all. V07T9522A showed a slightly warmer fuselage aft penetration area over 120-360 sec MET. Several temperature sensors recorded a slight fall in the fuselage surface temperatures at 380 sec MET, and these included V07T9880A, V07T9903A, V07T9913A, and V07T9925A.

NASA had called attention to temperature sensor V09T9895A, the wing front spar panel 9 temperature, which decreased by 5 bits over 30-180 sec MET, and then slowly rose by 3 bits over 300-900 sec MET. Other prior flights showed a 4 bit drop and then a 1 bit rise over the same periods. Each bit corresponds to approximately 2.5°F. The only substantive difference from prior flights was the 3-bit rise which occurs over a 10 minute span that was well past the event timing for the debris strike; thus, this sensor does not appear to indicate any direct correlation to the ET foam strike.

Aerodynamic pressure readings from both the left and right wings were similar. V07P8026A read 2.5 psi lower than previous flights, and this appeared to be a simple case of the sensor becoming uncalibrated. The overall shape of the response versus time was the same as all previous flights, but simply offset downward by 2.5 psi over the recording period. Similarly, V07P8092A was offset downward by 2.5 psi, and was also erratic prior to launch. Several pressure sensors gave unphysical readings over the recording period, starting at around 1 psia before launch and then flatlining at 0 psi immediately after launch. These were assumed to be dead measurement channels and included V07P8181A, V07P8182A, V07P8188A, V07P8189A, and V07P8190A. V07P8013A only recorded a pressure fall from 15 psia to 2.5 psia over the ascent, indicating a gain and/or offset error in its calibration. V07P8088A recorded readings which bounced up to OSH at 16 psia immediately after launch. V07P8103A only fell from 15 psia to 1.8 psia during ascent, again indicating a loss of calibration. V07P8144A failed and went to OSL at 30 sec MET. V07P8175A started out reading only 1.8 psia, indicating a sensor grossly out of calibration or beginning to fail completely. V07P8191A recorded some spikes at 480 and 670 sec MET. Overall, the aerodynamic pressure sensors showed no deviations from prior flight history aside from the above noted ones for which the behavior was indicative of a loss of calibration in the sensor or a completely dead measurement channel. None of the anomalous events appeared to have any time correlation to the foam debris strike at 82 sec MET.

Aerodynamic pressure sensor V07P8073A deserves special comment, as it was also noted by NASA as having an unusual response near to the 82 sec MET foam debris impact time. This was the only sensor within the OEX suite which had any unusual behavior near to 82 sec MET. This sensor first showed some erratic behavior at 61 sec MET when it recorded an abrupt 2 psi drop for half a second. Up until 84.5 sec MET, its response was fully consistent with prior flight history, when it fell to OSL and largely remained there at 0 psia for the rest of the recorded ascent period. Over 85-88 sec MET, the sensor recorded a parabolic burst, peaking at 2.5 psia at 86.5 sec MET. Shortly thereafter, it recorded an abrupt transition from OSL to OSH which then decayed back to OSL over 93-96 sec MET. This second transient is clearly non-physical and can be attributed to an instrumentation fault or interference pickup. The fast rise and exponential decay are typical for a system impulse response to any sudden charge injection. The first parabolic transient, because of its nearness to the 82 sec MET foam strike, could possibly be interpreted as a piece of foam debris either flying past the pressure sensing port or perhaps becoming temporarily lodged in the port orifice. Neither of these events is likely, because the port is flush with the surface of the heat tile and not prone to trap flying debris, and the duration of the parabolic pulse is too long (3 seconds) to match to any reasonable size piece of foam debris flying past a 3 mm diameter port at 150 mph. Similarly the time of the pulse, starting at 84.5 sec MET, is too far past the debris strike at 82 sec MET to match to the transit time between the wing leading edge and the location of the pressure port in the middle of the left wing. Also notable is the fact this was only one of eight sensors in the $Y_o = -250$ forward band of the left wing, which should have also recorded a similar event. The other 7 sensors in this zone showed completely normal ascent data, and include V07P8071A, V07P8072A, V07P8074A, V07P9186A, V07P9188A, V07P9189A, and V07P9190A. Pressure sensor V07P9186A is located within a few inches of V07P8073A, and it recorded data that was nearly identical to V07P8073A except for those time periods where V07P8073A was behaving erratically. The behavior of pressure sensor V07P8073A can thus be largely attributed to a "normal" failure mode of the sensor, most likely caused by a loss of its vacuum reference chamber. Any leaking in this chamber would cause the sensor to read low, and ultimately go OSL, which is what is observed. Several other pressure sensors in this suite show similar behavior before launch, and it should also be noted that leaking of the vacuum reference chamber on an absolute pressure sensor is the primary failure mode and shelf-life limit for these devices. Of the 181 aerodynamic pressure sensors installed on OV-102, 55 were already known to be bad or producing untrustworthy readings prior to launch.

A small fraction of the strain gauges showed differences with prior flight history, but in most cases this was a systematic offset that merely shifted the response up or down without changing its shape or features. These offset errors were typically small, on the order of 20-30 μin/in. For the 131 strain gauges on the left and right wing structural elements, 13 on the right wing showed some offset errors, including V12G9081A, V12G9442A, V12G9452A, V12G9641A, V12G9642A, V12G9648A, V12G9649A, V12G9651A, V12G9656A, V12G9629A, V12G9635A, V12G9636A, and V12G9637A. By contrast, only 2 strain gauges on the left wing showed any offset errors between STS-107 and prior flights, and these were V12G9058A and V12G9921A. The latter of these, V12G9921A, is one of the key sensors located on the spar panel immediately behind RCC panel #9. Even on the expanded time scale plots covering 50-150 sec MET, there is no evidence of any significant event around the ET foam debris impact at 82 sec MET. There were a total of 52 strain gauges on the right and left elevons, and all of these but one, V13G9749A which showed a slight offset error, responded similar to prior flight history. The middle fuselage area had 40 strain gauges, and of these a few recorded data that contained offset errors: V34G9503A, V34G9934A, V34G9935A, V34G9936A, V34G9937A, V34G9938A, V34G9941A, and V34G9952A. Some of these offsets were more apparent over 80-500 sec MET, but may exist over a wider time span. The 15 strain gauges on the payload bay door hinges (V37GxxxxA) each recorded data that was completely consistent with the behavior of prior flights.

The wideband FDM data, which because of its more complex encoding took longer to extract from the OEX recorder tape, also showed some signatures which are indicative of a debris strike near to 82 sec MET. One of the accelerometers on the left wing elevons, V08D9729A, showed a single cycle sinusoidal pulse at 81.9 sec MET that was approximately ±2 g in amplitude, as compared to a background vibration level which generally stayed well below ±1 g. This is a fairly significant pulse which could easily represent a strike of foam debris upon ascent. The timing and amplitude of this pulse were taken from a preliminary assessment of the wideband

FDM data that was printed out on a strip chart recorder by NASA at JSC.

Boeing of Huntington Beach performed a more thorough analysis of the remainder of the wideband FDM ascent data and in general did not find much that was anomalous. They found that the overall noise levels and power spectral density (PSD) matched very closely to the data from the previous flight, STS-109. They noticed that at approximately 40 sec MET, the vertical stabilizer had some of its higher order modes growing slightly larger than normal, and this was attributed to some wind buffeting that was thought to occur around this time. These modes then decayed shortly thereafter, indicating that the so-called flutter instability was not becoming excited, as can occur when the wing bending modes and the fuselage vertical modes coalesce into a single coupled oscillation. Boeing's analysis also pointed out that the recorded accelerations along the longeron were normal. Detailed analysis of the wideband FDM data over the time frame around 80-85 sec MET was performed. For the left outboard elevon accelerometer, V08D9729A, several wing and elevon oscillation modes were found to be excited during this time, with the strongest being a second order wing bending mode that matched best to the fundamental component of the single cycle sinusoidal pulse at 81.9 sec MET. Boeing's more detailed time scale showed the period of the single sinusoidal pulse to extend over 81.70 to 81.74 sec MET, reaching +3.0 g on the positive peak at 81.71 sec MET, and –2.6 g on the negative peak at 81.72 sec MET.

In addition, another accelerometer on the right wing, V08D9766A, showed a 1.5 cycle sinusoidal pulse response at a slightly earlier time of around 80 sec MET. This accelerometer was located at the coordinates (X1367.0, Y+312.0, Z) towards the middle of the right wing and was sensitive to Z-axis motion. This accelerometer recorded an anomalous pulse beginning at 80.22 sec MET, growing to a first positive peak of +1.5 g at 80.23 sec MET, reaching a negative peak of –1.9 g at 80.24 sec MET, then another positive peak of +2.0 g at 80.26 sec MET, before dying away beyond 80.27 sec MET. The best fit to these peaks was a combination of outboard elevon torsion and the first wing bending mode. There have not been any explanations offered for the cause of this right wing accelerometer response.

Findings and Recommendations

Clearly Defined Features within the Sensor Data Evidence

The vast number of sensors in place in both the OFI and MADS/OEX instrumentation systems of *Columbia* have provided a wealth of information about the circumstances of the accident. Physical sensors that were originally placed to monitor the vehicle as it passed through the harsh environments of ascent and re-entry have provided critical real-time measurements of vehicle temperature, pressure, and strain as the integrity of its left wing deteriorated. In many cases several sensors of the same type recorded different views of the same events, and this redundancy in the measurements provides an even higher degree of confidence in the interpretations. Correlations between different types of physical sensors, for example temperature and strain of the leading edge spar, together paint a more complete picture of the events than that provided by each sensor considered singly. Both the diversity of sensor types, the wide distribution of their placement, and the sheer numbers of them which were installed have provided rich information upon which to base hypotheses of the accident's chain of events and contributing causes, as well as to rule out other possibilities as being inconsistent with this voluminous amount of sensor data.

The fundamental design of the OFI and MADS/OEX instrumentation systems, which places a time stamp on each frame of telemetry or recorded data, inherently provides an extremely accurate, universal, and unambiguous time reference for each measurement, providing a time resolution on the events down to one second accuracy for most and to a tenth second accuracy for some. Since the time stamp is carried along with the measurement data itself, there is practically no uncertainty about when particular events occurred, at least in the electrical instrumentation sense. Any uncertainties in the timing of events are due to the random nature of the physical process which prompted the electrical instrumentation system reaction, for example, the speed at which sensor cables might burn through, or the thermal time constants that would be required for a sensor to reach its steady-state response to a fast changing stimulus.

While most instrumentation systems remain static and simply record unfolding events, the situation with the instrumentation systems on the *Columbia* is fundamentally different, because the instrumentation systems were themselves being injured by the left wing damage and were thus changing along with the rest of the vehicle that they were measuring. The most conservative approach is to simply disqualify any data beyond the time for which its readings imply a physically impossible event, for example, a temperature rising faster than what the thermal time constants of the material would allow. And indeed, after a sensor channel has obviously been damaged, the accuracy of its subsequent readings becomes wholly suspect. However, the manner in which the failures occur and the timing of these failures also provides important information about the events which have precipitated the failure. Considered in this manner, the cables of a given sensor now become a sensor, too. And similarly, drop outs within a barely connected communication link can become a sensitive indicator of obscuring matter or mis-orientation between the receiver and transmitter antennas.

The foremost feature in the accident's sequence of events that is clearly revealed by the sensor readings is the breach of the left wing leading edge spar at a time in the range of 5 to 15 seconds prior to GMT 13:52:18 (EI + 489 sec), when the first sensor whose cable was routed along the leading edge (V07P8023A) failed. The 10±5 second delay represents the best estimate for the burn through time of these sensor cables. Four key sensors were located within the damage zone of the leading edge spar, and included the RCC clevis temperature, V09T9910A, which was located on the outside of the leading edge spar, the spar strain gauge, V12G9921A, the wing lower surface thermocouple, V07T9666A, and the leading edge spar temperature, V09T9895A, which was located on the inside surface of the spar. Each of these four key

sensors recorded anomalous conditions very early into the re-entry flight, and each then failed with a cable burn through signature within a rather narrow span of time immediately following the breach of the leading edge spar. Specifically, the spar strain V12G9921A first recorded anomalous mechanical behavior of the spar at GMT 13:48:39 (EI + 270 sec) and it failed at GMT 13:52:24 (EI + 495 sec). The RCC clevis temperature V09T9910A first recorded anomalous temperatures on the outside of the spar at GMT 13:48:59 (EI + 290 sec) and it failed at GMT 13:52:22 (EI + 493 sec). The lower wing surface temperature V07T9666A first recorded anomalous heating on the bottom of the wing at GMT 13:50: 19 (EI + 370 sec) and it failed at GMT 13:52:23 (EI + 496 sec). The spar surface temperature V09T9895A first recorded an anomalous heating of the spar at GMT 13:51:14 (EI + 425 sec) and it failed at GMT 13:52:51 (EI + 522 sec), slightly later than the rest because of its cable harness lying farther away from the initial entry point of the spar breach. These four key sensor readings compile a very clear picture of abnormally high temperatures on the outside of the wing working their way through the RCC panels and then ultimately through the leading edge spar, accompanied by mechanical distortions and strains in the spar as this happened. These four key sensors, along with eleven other pressure sensors, each had their cable harnesses routed along the center backside of the leading edge spar. All fifteen of these sensors failed with a wiring burn through signature in the time span of GMT 13:52:18 to 13:52:26 (EI + 489 to 497 sec), except for V09T9895A, which failed at GMT 13:52:51 (EI + 522 sec) because of its different cable harness routing. Allowing an estimated 5 to 15 seconds for a cable to burn through on the average, the breach of the leading edge spar can then be placed at 10±5 seconds prior to GMT 13:52:18 (EI + 489 sec), which was the first failure of a sensor whose cable run was entirely behind the leading edge spar (V07P8023A).

An implicit assumption in the above reasoning is that the leading edge spar had to have been breached completely through before the sensor cabling began its burn through process, that is, the two processes were necessarily sequential. This appears well justified, because the melting point for the aluminum honeycomb spar is 1218ºF (659ºC), which is essentially the same the temperature needed to produce a soft short breakdown in the Kapton wiring insulation. In other words, it is unlikely that simple heating of the outside of the leading edge spar would have been sufficient to degrade the wiring insulation on the inside, since by the point at which the insulation would have degraded to failure, the spar itself would have melted.

The direction of the spar breach is also clearly evident, coming into the wing box from the outside, from behind the leading edge RCC panels. The RCC clevis temperature sensor V09T9910A, which was located behind the RCC panels and outside the wing box, was the first to register anomalous and significantly increasing temperatures at EI + 290 seconds, giving a clear picture that the temperature on the outside of the wing box was growing rapidly hotter than anything on the inside. The wing lower surface temperature V07T9666A began recording anomalously high temperatures on the bottom of the wing shortly thereafter at EI + 370 seconds. The inside surface temperature of the spar, V09T9895A, did not begin rising until significantly later, at EI + 425 seconds. The possibility that the left wing damage occurred by something blowing out from the inside of the wing box is not consistent with the timing or the observed temperatures of these sensor readings. Likewise, the timing for destructive events within the left wheel well occurs later than the leading edge spar breach, indicating also that the direction of substantive damage was from RCC leading edge, through the leading edge spar, through the wing box and the cabling it contained, and then finally into the left wheel well.

The locations of the various sensors which exhibited wiring burn through failures and the routing of their cable harnesses also provides fairly conclusive evidence of the location of the leading edge spar breach. In addition to the four key sensors behind RCC panel #9, eleven aerodynamic pressure sensors in the left wing had their sensor cables routed along the leading edge spar. All eleven of these exhibited a wiring burn through failure signature within the time range of GMT 13:52:16 to 13:52:26 (EI + 487 to 497 sec). These pressure sensors included V07P8010A, V07P8058A, V07P8022A, V07P8023A, V07P8024A, V07P8071A, V07P8072A, V07P8073A, V07P8037A, V07P8038A, and V07P8044A. There was also another strain gauge on the leading edge spar behind RCC panel #9, V12G9169A; however, this strain gauge was instrumented through PCM-3 in snap-shot mode and thus its precise time of failure cannot be determined, but it is nonetheless consistent with a burn through failure time in the range of EI + 487 to 497 seconds, too. The time span of EI + 487 to 497 seconds also brackets the burn through failure times of V09T9910A, V07T9666A, and V12G9921A on the leading edge spar behind RCC panel #9. The only sensor whose cable was routed along the leading edge spar whose failure time was different from this was V09T9895A, and is most likely because its cable was routed significantly lower on the spar than the rest.

The most noteworthy feature of the failed aerodynamic pressure sensor readings is that two of these, V07P8010A and V07P8058A, were located quite far forward on the left wing, just a few inches aft of the forward edge of RCC panel #8. The cables to these two pressure sensors did not extend any further aft than this point either, yet both sensors exhibited an unmistakable wire burn through failure signature at EI + 497 seconds for V07P8010A and EI + 495 to 505 seconds for V07P8058A. This implies that the leading edge spar breach must have occurred no farther aft than this point. Also of similar note are two strain gauges that were located on the X1040 cross spar which ran along the front wall of the wheel well. Sensors V12G9048A on the lower spar cap and V12G9049A on the upper spar cap recorded anomalous strain data around the time period of the lead edge spar breach, but neither failed until much later, at EI + 935 seconds, just before the end of the recorded OEX data. The cables to both of these strain gauges must therefore have remained intact until this point, and this implies that the leading edge spar breach must have occurred farther aft than the X1040 cross spar. Otherwise, the hot gas would have surely caused a wire burn through failure in the exposed cables of these two strain gauges. This then brackets the possible location of the leading edge spar breach to a fairly small area extending from the aft end of RCC panel #6 to the front end of RCC panel #8.

Besides the leading edge RCC panels, several other potential points of entry into the wing box could have existed, but these are each clearly refuted by the sensor data. A breach through either the upper or the lower wing surface acreage tiles in one of several areas was originally suggested, but none of these are consistent with the large number of pressure, temperature, and strain sensors on the left wing which did not record any anomalous behavior until nearly the end of the telemetry or recorded data. A breach through the upper or lower wing surfaces would also not explain the clearly evident rise in the V09T9910A RCC clevis temperature which was located outside of the wing box and back behind the RCC panels in what is termed the leading edge chunnel.

Prior to the recovery of the OEX recorder, attention was drawn to what was then the most dramatic events in the OFI telemetry data around the left wheel well, in which the tire pressure and wheel temperatures all exhibited failures within the time span of EI + 858 to 880 seconds. The possibility of a breach into the wing box by way of the wheel well was suggested, in addition to several other hypotheses which suggested that some other destructive event originating from the wheel well might have led to the breach of the wing box. However, the refuting evidence for these is that, within the wheel well, while one of the eight main landing gear hydraulic temperatures did record an anomalous rising temperature as early as EI + 488 seconds, only one actually failed outright, and this was not until EI + 913 seconds, just 10 seconds prior to the loss of the telemetry signal. Of equal importance, the temperature rises in these hydraulic system components were only a few tens of degrees for most, and the largest only rose to 172ºF. Before the OEX recorder data was available, these temperature rises may have been perceived as drastic, but within the larger perspective provided by the OEX sensors which recorded truly significant rises in temperatures near the damage zone of wing leading edge, rises of many hundreds of degrees, these temperature rises inside the wheel well are by comparison rather small, and occurred far too late in the time line to be seriously considered as the entry point for the breach into the wing box. The same sensors also provide rather conclusive evidence that the wheel well door did not open prematurely, that the tires did not explode, and that none of the pyrotechnic actuators fired, at least up until the loss of the telemetry signal. Further, the elevon hydraulic system temperatures, whose sensor cable harnesses were routed along the outboard wall of the wheel well, show wire burn through failures in the time span of EI + 533 to 567 seconds, consistent with and shortly following the timing of the leading edge spar breach. Of the eight main landing gear hydraulic system temperatures measured inside the left wheel well, five of these did not show any anomalous behavior until EI + 610 seconds.

Apart from the three which did show minor temperature rises prior to EI + 610 seconds, this suggests that a breach from the wing box into the wheel well could have occurred in the time frame of approximately EI + 550 to 600 seconds. Regardless of the precise timing of the wheel well breach, the time sequence of the anomalous sensor events shows clearly that the damage zone proceeded from the wing box into the wheel well and not from the opposite direction.

The combination of telemetry and recorded data also establishes the path and timing of several debris shedding events as the leading edge of the left wing began to come apart. Both increased and decreased heating patterns were shown in the temperature readings from sensors distributed across the left OMS pod and the left side of the fuselage, indicating a strongly altered aerodynamic flow pattern across these regions. The most dramatically affected sensors on both the side of the fuselage and the OMS pod lie almost perfectly along a straight line drawn from the supposed damage area of the left wing leading edge backwards along the direction of vehicle motion. This same straight line continues toward the left side of the vertical stabilizer, and this path of debris from the damage area on the leading edge of the wing is corroborated distinctly in the recovered wreckage which included large pieces from the front of the left OMS pod and the top of the vertical stabilizer. Both of these surfaces show an extreme amount of impact debris damage. Moreover, several of the longer communication drop outs that occurred earlier into the re-entry flight happened very close to the times at which the more significant debris shedding events were both observed from the ground and recorded as anomalous surface temperatures on the vehicle. While the debris shedding events cannot conclusively be identified as the actual cause of the anomalous, early communications drop outs, the relatively small and decreasing communications link margins suggest that even a small signal attenuation caused by some debris or vaporized metal could have produced the observed drop outs.

A number of temperature sensors on the lower surface of the fuselage and pressure sensors on the upper and lower surfaces of the right wing also showed anomalous readings during the re-entry flight. In almost all cases, these can be traced to common electrical power supplies within the instrumentation system which are shared between these sensors and ones which were more directly affected on the left wing. Thus, the anomalous readings given by these sensors on the lower fuselage and right wing surfaces do not contradict any of the other conclusions, but rather reinforce the explanations as being consistent with how the overall instrumentation systems of the orbiter should have reacted to the sensor wiring failures created within the left wing.

Remaining, Unexplained Inconsistencies

By far the most puzzling unexplained sensor anomalies are those readings from the sensors which were located forward of the damage area on the left wing leading edge. These are the slight temperature perturbations exhibited by the fuselage supply water dump and vacuum vent nozzles (V62T0439A, V62T0440A, and V62T0551A) and by the chin panel mounting clevis (V09T9889A). Each of these temperature sensors appeared to be working properly, and each recorded small, but still distinctly anomalous readings that began at EI + 499 ± 4 seconds. An explanation for how damage to the left wing leading edge could propagate forward to affect these locations, almost at the nose of the vehicle, has yet to be offered. The aerodynamic engineers have suggested that this was an instrumentation artifact, while the instrumentation engineers have likewise suggested that the cause was an aerodynamic artifact arising from the asym-

metrical vehicle profile that was produced by the left wing damage. The simultaneous occurrence of this unusual temperature rise on the water dump nozzles and vacuum vents, which were both OFI telemetry data, and on the chin panel mounting clevis, which was OEX recorded data, suggests that this was not a simple instrumentation glitch, as both instrumentation systems recorded the event independently. Changes in the overall aerodynamic profile could produce reaction vortices or turbulence further forward, and the thermal perturbations that were recorded in the fuselage nozzles and in the chin panel clevis both occurred around the time of the breach of the left wing leading edge spar.

Although they occurred comparatively late in comparison to the breach of the left wing leading edge spar, events within the left wheel well still raise some unanswered questions. First is the unexplained cause for the slight but distinctly abnormal rise in the temperature of the left hydraulic brake line point D, V58T1703A, located on the aft end of the inboard wheel well wall, at the early time of GMT 13:52:17 (EI + 488 sec). The left hydraulic brake line temperatures at points A and C, V58T1700A and V58T1702A, also recorded anomalous rises slightly thereafter at GMT 13:52:41 (EI + 512 sec). All three of these sensors inside the left wheel well responded anomalously prior to the failures of sensors with their cable harnesses routed on the upper outboard wheel well wall and thus presumably before the breach of the left wheel well wall. It has been hypothesized that the hot gas which began entering the wing box after the breach of the leading edge spar flowed around forward through the X1040 spar access panel and then backward into the wheel well through an approximately 5 inch diameter vent hole further inboard on the X1040 spar. This pathway for the hot gas does indeed exist, but the reason for the gas to take this tortuous path over other directions is not clear, nor is it understood why the heating effects would be registered by only a few sensors on the rear wall of the wheel well and not by others of a similar type and mounting located only inches away. For example, the brake switch return line temperatures V58T0841A and V58T0842A were only a few inches away from V58T1703A which recorded an anomalous rise first, but these other two hydraulic line temperature sensors did not record any anomalous behavior until several minutes later. Another unexplained feature is that every one of the tire pressure and wheel temperature sensors showed a clear wiring burn through failure within a narrow window of EI + 858 to 880 seconds, and this is quite well explained by all of these sensor cables being routed along a similar path on the backside of the left main landing gear strut. The inconsistency is that two of the hydraulic brake line temperatures V58T1700A and V58T1701A also had their cables routed along the same path and these two did not show any wiring burn through failures within any of the telemetry data. It is puzzling why the wiring burn throughs would completely destroy one type of system and leave an adjacent one untouched.

The communication drop outs occurred at times quite close to several major debris shedding events and to the breach of the left wing leading edge spar; however, a definitive link between these two is still largely conjectural. It is known that the link margins were decaying from EI onward, as was normal for the re-entry flight, and they would thus be increasingly sensitive to any events which would cause obscuration, attenuation, or scattering of the radio signal. Whether these events were the shedding of debris or vaporized metal from the damaged area of the left wing or simply some additional radio interference or multipath clutter caused the increasing heating and plasma envelope around the vehicle is unclear. The timing is suggestive of debris shedding events, but it is not conclusive.

A Few Recommendations

The MADS/OEX data has proven extremely valuable to the analysis of the accident and the validation of various scenarios. This, however, has been largely fortuitous. It was only pure happenstance that the *Columbia* (OV-102) was, by far, the most extensively instrumented of all the orbiter fleet and thus had the OEX sensor suite to record such detailed data. It was also fortunate that the orbiter broke up over a desolate area of the US mainland where the debris could be painstakingly and methodically collected. If the break up had occurred several minutes earlier or later, the debris would have been deposited into the Pacific Ocean or the Gulf of Mexico, where virtually none of it could have been collected. It was almost miraculous that the OEX data recorder was found, that it was intact, and that the data on it was in essentially perfect condition. No other avionics box besides the OEX recorder survived the re-entry. If the OEX recorder happened to have landed upside down, the weight of the capstan motors would have crushed the mylar tape spool upon impact. As luck had it, the OEX recorder landed right side up. Furthermore, it was also exceedingly fortunate that the damage occurred on the left wing rather than the right. The left wing contained 15 temperature sensors which recorded anomalous events, while the right wing contained none. The damaged area of the left wing also just happened to be at a place where the leading edge spar was most heavily instrumented with temperature, pressure, and strain sensors. It was also fortuitous that the orbiter flight instrumentation (OFI) telemetry data, that complements the OEX recorded data, was gathered. The communication systems on the orbiter were not originally designed to maintain radio contact during re-entry, but the link margins luckily happened to be sufficient to provide contact for most of the first half of the re-entry flight. Should the unthinkable occur and another space shuttle accident of a similar nature happen, there is only the slimmest of chances that all of these circumstances would occur once more to provide the fairly clear level of information that came from the *Columbia* accident.

Another notable feature is that the sensor suite installed on the *Columbia* was originally designed only for engineering development purposes during the first few flights of the orbiter to insure that it was following design specifications. This instrumentation remained on the vehicle as a historical legacy to the developmental process, but it has since been routinely used to provide vehicle flight data that has been of value to on-going flight analysis and vehicle engineering. Nearly all of the sensors used on the *Columbia* were specified to have only a 10 year shelf life, and in some cases a shorter service life. The *Columbia* was 22 years old in 2003, and thus, the majority of the instrumentation system was dated and was being used twice as long as its originally

designed service life. Many sensors, for example those for aerodynamic pressure, were already failing. Of the 181 active MADS/OEX pressure sensors on the wings, 55 had already failed or were producing questionable readings before the STS-107 mission was launched. The wiring and cabling was also becoming old and in need of repair and updating. In a general sense, the instrumentation systems on the vehicle were never updated from those which were originally installed, and the original systems were being used well beyond their intended length of service. It is a testament to the soundness of the original design that the instrumentation systems have lasted as long as they have and have provided reliable data up through the present.

Based upon the above, some rather obvious recommendations can be suggested to both improve the data gathering capability of the orbiter while in flight, as well as to provide improved vehicle safety by recognition of damaged components prior to their catastrophic failure. These recommendations include:

1. *The existing instrumentation systems which were designed only for developmental purposes should be changed over to instrumentation systems which are designed for assessing vehicle health and prompting preventative maintenance*. This is not to suggest that the existing operational flight instrumentation (OFI) system should be done away with, as it is quite crucial to the flight control of the vehicle. Rather, the large number of sensors in the OEX suite could be reduced to only those needed for critical monitoring of flight behavior, and made more symmetrical between the left and right sides of the vehicle. This OEX-like suite should also be added to each of the remaining orbiters so that vehicle-to-vehicle comparison data can be compiled in addition to flight-to-flight comparison data.
2. *Instrumental measurement and inspection techniques should be used which can detect injured or malfunctioning vehicle components prior to their being called into service, particularly in relation to the thermal protection system (TPS)*. Presently, most of the TPS components are qualified by visual inspection techniques which fail to probe the internal features. X-ray, acoustic, and radio frequency (RF) imaging techniques can provide penetrating examinations of vehicle components which can complement existing visual surface inspection. While this will undoubtedly add time and expense to the orbiter inspection process, it will however provide a more thorough screening and qualification process which should stand a higher probability of catching minute flaws before they become in-service component failures.
3. *The MADS instrumentation system and sensor suite on each of the orbiters should be updated to make use of current sensor and data acquisition technologies*. The temperature, pressure, and strain sensors on the *Columbia*, as well as the remaining orbiters, is a late 1970s vintage which does not take advantage of the revolutionary advances that have occurred in the sensors and instrumentation field since then. Notably absent on the orbiter are micromachined pressure, strain, and inertial sensors which are much more reliable, smaller, lower power, less expensive, and have in general displaced the older style units which were used on the *Columbia* and the rest of the fleet. Signal aggregation and sensor multiplexing can also be greatly improved and would produce improved signal fidelity and savings in wire weight. Wireless sensing systems can also be used to great advantage and could also help alleviate the cabling bird's nest on the orbiters. Similarly, many optical sensing techniques such as infrared thermometry and pyrometry could be used to great advantage to sense the high outer surface temperatures where direct placement of a contact temperature sensor is not possible.
4. *A more robust OEX-like flight data recorder should be developed which can be used analogously to the black boxes on commercial aircraft*. Flight data recorders should be packaged to survive a re-entry breakup and fitted with a homing beacon by which they can be located.
5. *The instrumentation system should be designed to be reconfigurable during flight, allowing certain data to be recorded or telemetered or both, as the needs change*. Reconfigurability in general imparts improved robustness and fault tolerance, and while this has been implemented in the original design of the orbiter to some degree, it can be further improved upon. Specifically, the OEX recorder data is not accessible until the vehicle has landed back on the Earth, yet it also records ascent data which could, in principle, have been examined for abnormalities which might be clues to latent problems.
6. *Instrumentation should be added which can both detect impacts to the vehicle and the extent of damage that was left as a result of such impacts*. One of the original problems with the space shuttle orbiters that has existed from the first flight up through the present, and which has yet to be satisfactorily solved, is that the belly of the vehicle cannot be inspected prior to de-orbit and re-entry. Robotic inspection cameras offer one of the most flexible solutions, but the problems with such robots potentially creating more damage than they discover needs to first be surmounted. Modern accelerometers and acoustic microphones could readily be used to detect sharp impact events and signal the need for closer inspection of the vehicle. Light weight optical fiber sensors could also be put to good use to monitor the conditions along critical sections of the structure.

The *Columbia* accident has been a regrettable tragedy which has set back the progress of manned spaceflight and briefly tarnished many of the truly outstanding aspects of the American space program. However, the aftermath of the accident provides a unique and valuable learning opportunity in view of the detailed information and analysis which has been compiled. While there may be some sentiment by the general public that space flight has become a routine business, akin to commercial air travel, it is important to bear in mind that space travel will always be a venture with significantly and necessarily higher risks for the given rewards. The only fatal error at this juncture would be to fail to learn from the events and circumstances of the *Columbia* accident. Improved instrumentation systems only provide the raw data; properly interpreting this data and making good judgments from it is an exclusively human endeavor.